



University
of Glasgow

Ferenczi, Gergely (2016) *Which-path problem for one and two particles with two degrees of freedom and a relation between transverse spatial structure and group velocity of light*. PhD thesis.

<http://theses.gla.ac.uk/7475/>

Copyright and moral rights for this thesis are retained by the author

A copy can be downloaded for personal non-commercial research or study

This thesis cannot be reproduced or quoted extensively from without first obtaining permission in writing from the Author

The content must not be changed in any way or sold commercially in any format or medium without the formal permission of the Author

When referring to this work, full bibliographic details including the author, title, awarding institution and date of the thesis must be given

WHICH-PATH PROBLEM FOR ONE AND TWO PARTICLES WITH
TWO DEGREES OF FREEDOM AND A RELATION BETWEEN
TRANSVERSE SPATIAL STRUCTURE AND GROUP VELOCITY OF
LIGHT

Gergely Ferenczi

Submitted in fulfilment of the requirements for the degree of Doctor of
Philosophy

School of Physics and Astronomy
College of Science and Engineering
Univeristy of Glasgow
July 2016

Declaration

The work presented here is the authors own except where otherwise indicated. In particular figure 4.6 is reproduced from [1] and figures 6.1, 6.2, 6.3 and 6.4 are reproduced from [2]. These figures have been removed from the electronic version due to copyright reasons. A reference to each figure is given instead.

Acknowledgements

I would like to thank:

- the members of the Quantum Theory group at the University of Glasgow and the Computational Nonlinear & Quantum Optics group at the University of Strathclyde (in reverse chronological order) for accepting me as one of their own. Thanks go out in particular to Václav Potoček for helping me *a lot* with the work contained herein and to Stephen Barnett and Thomas Brougham for supervising me.
- Daniel Giovannini, Jacqueline Romero and Miles Padgett from the Optics group at the University of Glasgow for the opportunity to collaborate on their wonderful experiment.
- Kirsteen Faulds for scanning in my diagrams produced by troglodyte methods.
- Balázs Szigeti and Áron Ferenczi in Edinburgh for periods of fun and relaxation.
- and of course my parents Erzsébet and Szabolcs Ferenczi for supporting me.

Publications

- Gergely Ferenczi, Václav Potoček, and Stephen M. Barnett. Two-particle multi-mode interference. *Journal of Optics*, 16(10):105710, 2014.
- Daniel Giovannini, Jacqueline Romero, Václav Potoček, Gergely Ferenczi, Fiona Speirits, Stephen M. Barnett, Daniele Faccio, and Miles J. Padgett. Spatially structured photons that travel in free space slower than the speed of light. *Science*, 347(6224):857-860, 2015.
- Václav Potoček and Gergely Ferenczi. Which-way information in a nested Mach-Zehnder interferometer. *Physical Review A*, 92:023829, Aug 2015.

Abstract

Quantum mechanics, optics and indeed any wave theory exhibits the phenomenon of interference. In this thesis we present two problems investigating interference due to indistinguishable alternatives and a mostly unrelated investigation into the free space propagation speed of light pulses in particular spatial modes.

In chapter 1 we introduce the basic properties of the electromagnetic field needed for the subsequent chapters. In chapter 2 we briefly review optical angular momentum, entanglement and spontaneous parametric down conversion. In chapter 3 we review the properties of interference using the beam splitter and the Mach-Zehnder interferometer. In particular we review what happens when one of the paths of the interferometer is marked in some way so that the particle having traversed it contains information as to which path it went down (to be followed up in chapter 4) and we review Hong-Ou-Mandel interference at a beam splitter (to be followed up in chapter 5).

In chapter 4 we present the first of the interference problems. This consists of a nested Mach-Zehnder interferometer in which each of the free space propagation segments are weakly marked by mirrors vibrating at different frequencies [1]. The original experiment drew the conclusions that the photons followed disconnected paths. We partition the description of the light in the interferometer according to the number of paths it contains which-way information about and reinterpret the results reported in [1] in terms of the interference of paths spatially connected from source to detector.

In chapter 5 we present the second of the interference problems namely Hong-Ou-Mandel interference with particles possessing two degrees of freedom. We analyse the problem in terms of exchange symmetry for both boson and fermion pairs and show that the particle statistics at a beam splitter can be controlled for suitably chosen states. We propose an experimental test of these ideas using orbital angular momentum entangled photons.

In chapter 6 we look at the effect that the transverse spatial structure of the mode that a pulse of light is excited in has on its group velocity. We show that the resulting group velocity is slower than the speed of light in vacuum for plane waves and that this reduction in the group velocity is related to the spread in the wave vectors required to create the transverse spatial structure. We present experimental results of the measurement of this slowing down using Hong-Ou-Mandel interference.

Contents

1	Light	13
1.1	Maxwell's and wave equations	13
1.1.1	Potentials	14
1.2	Paraxial wave equation	15
1.2.1	Paraxial modes	16
1.2.2	Higher order modes	17
1.3	Quantised amplitudes	18
1.3.1	Continuum treatment	18
1.3.2	Narrow bandwidth approximation	19
2	Angular momentum and spontaneous parametric down conversion	21
2.1	Optical angular momentum	21
2.1.1	Laguerre-Gaussian beams	22
2.1.2	Bessel beams	22
2.1.3	Experimental demonstration of optical angular momentum	22
2.2	Entanglement	23
2.2.1	Bell states	23
2.2.2	Partial Bell state analysis	26
2.3	Spontaneous parametric down conversion	26
2.3.1	Phase matching	27
2.3.2	Angular momentum conservation and entanglement	28
2.3.3	Experimental demonstration of optical angular momentum entanglement	29
3	Beam splitter and Mach-Zehnder interferometer	31
3.1	Beam splitter	31
3.1.1	Single particle inputs	34
3.1.2	Mode swap	37
3.1.3	Biparticle input states	37
3.1.4	Hong-Ou-Mandel dip	39
3.2	Mach-Zehnder interferometer	41
3.2.1	Interference of paths in the interferometer	41
3.2.2	Mach-Zehnder interferometer with marked paths	43
4	Nested Mach-Zehnder interferometer with weakly marked paths	47
4.1	Introduction	47
4.2	Production and detection of slightly tilted Gaussian beams	49

4.2.1	Mode structure	49
4.2.2	Detection	52
4.3	Contribution of the distinct paths	53
4.4	Analysis of the relevant cases	55
4.5	Tunability of the peak heights	56
4.6	Conclusions	57
5	Two-particle interference	59
5.1	Introduction	59
5.2	Indistinguishable particles with two degrees of freedom	60
5.2.1	Exchange operators	60
5.2.2	Biparticle excitations of modes	61
5.3	Beam splitter	62
5.4	General one particle per port input state	64
5.5	An example for photons	66
5.6	Conclusions	68
6	Slow light in free space	71
6.1	Introduction	71
6.2	Group velocity and wave vectors	72
6.2.1	Eikonal model	72
6.2.2	Wave model	73
6.3	Bessel beams	75
6.3.1	Experimental results	76
6.4	Gaussian beam	76
6.4.1	Experimental results	78
6.4.2	Truncated beam	78
6.5	Error analysis	78
6.6	Conclusions	79
7	Summary	81

Chapter 1

Light

This thesis deals with interference problems involving the propagation of light in free space. The most complicated matter interaction that we deal with is reflection off of a surface. The purpose of this chapter is to introduce the basic properties of electromagnetic waves and paraxial optics that later chapters will build on. The material contained in this chapter can be found in standard pedagogical texts. The material in the first part of this chapter is contained in (§4 of) [3, 4], the material in the second part is contained in [5, 6] and the third part relies on [7] in addition to [3, 4].

This chapter constitutes a review of the topics used in chapter 5 and is not based on the author's research. First the classical concept of optical angular momentum is described. The discussion is restricted to light beams and within that mostly to the paraxial domain. Then the main properties of the quantum mechanical phenomenon of entanglement are described before moving onto a semiclassical treatment of spontaneous parametric downconversion.

1.1 Maxwell's and wave equations

The behaviour of light in free space is governed by Maxwell's equations with no charges or currents

$$\nabla \cdot \mathbf{E} = 0 \quad (1.1) \quad \nabla \cdot \mathbf{B} = 0 \quad (1.3)$$

$$\nabla \times \mathbf{E} = -\frac{\partial \mathbf{B}}{\partial t} \quad (1.2) \quad \nabla \times \mathbf{B} = \mu_0 \epsilon_0 \frac{\partial \mathbf{E}}{\partial t} \quad (1.4)$$

where \mathbf{E} and \mathbf{B} are the electric and magnetic fields respectively and ϵ_0 and μ_0 are the permittivity and permeability of free space respectively. The electric and magnetic fields obey the wave equation

$$\frac{1}{c^2} \frac{\partial^2 \mathbf{E}}{\partial t^2} - \nabla^2 \mathbf{E} = 0 \quad (1.5)$$

where $\mu_0 \epsilon_0 = 1/c^2$, with the magnetic field \mathbf{B} satisfying an identical equation. These can be arrived at by taking the curl of equation (1.2) or (1.4) respectively and making use of the divergencelessness (1.1) and (1.3) of the respective fields. From these fields the Poynting vector can be constructed

$$\mathbf{S} = \frac{1}{\mu_0} \mathbf{E} \times \mathbf{B} \quad (1.6)$$

which describes the energy flux of the field.

1.1.1 Potentials

The physical fields \mathbf{E} and \mathbf{B} can be derived from a vector potential \mathbf{A} and a scalar potential Φ . Gauss's law for magnetism (1.3) means that the magnetic field can always be expressed as the curl of a vector potential

$$\mathbf{B} = \nabla \times \mathbf{A} \quad (1.7)$$

due to the identity

$$\nabla \cdot (\nabla \times \mathbf{A}) = 0 \quad (1.8)$$

that holds for any vector \mathbf{A} . By expressing the magnetic field in the Faraday-Lenz law (1.2) in terms of the vector potential one finds that due to the identity

$$\nabla \times (\nabla \Phi) = 0 \quad (1.9)$$

for any scalar Φ , the electric field can be expressed in terms of the vector and scalar potentials as

$$\mathbf{E} = -\nabla \Phi - \frac{\partial \mathbf{A}}{\partial t}. \quad (1.10)$$

By inserting the electric and magnetic fields expressed in terms of the potentials into Gauss's law (1.1) and the Ampère-Maxwell law (1.4) and in addition imposing the Lorenz gauge condition

$$\nabla \cdot \mathbf{A} + \frac{1}{c^2} \frac{\partial \Phi}{\partial t} = 0 \quad (1.11)$$

one obtains wave equations for the scalar and vector potentials respectively

$$\left(\nabla^2 - \frac{1}{c^2} \frac{\partial^2}{\partial t^2} \right) \Phi = 0, \quad (1.12)$$

$$\left(\nabla^2 - \frac{1}{c^2} \frac{\partial^2}{\partial t^2} \right) \mathbf{A} = 0. \quad (1.13)$$

Due to the Lorenz gauge condition (1.11) the scalar and vector potentials for a monochromatic wave are related by

$$\Phi = \frac{c^2}{i\omega} \nabla \cdot \mathbf{A}. \quad (1.14)$$

The vector potential is not purely transverse, as defined by having zero divergence [3, §4.1], but it does give rise to an electric field, given by (1.10), that satisfies (1.1). The scalar potential compensates for the longitudinal component of \mathbf{A} . This ensures that the electric field as given by (1.10) is divergenceless even for a linearly polarised plane wave. The general solution to (1.13) is given by

$$\mathbf{A}(\mathbf{r}, t) = \sum_{\mathbf{k}} \mathbf{a}_{\mathbf{k}} e^{i(\mathbf{k} \cdot \mathbf{r} - \omega t)} + \mathbf{c.c.} \quad (1.15)$$

where $\mathbf{c.c.}$ denotes the complex conjugate (the vectorial nature of the quantity is also indicated) ensuring that the expression describes a real valued vector potential. In the above a fictitious cubic cavity of volume \mathcal{V} has been assumed which allows for a discrete set of k -vectors. When a continuum of wavevectors can be supported by the physical system under consideration the sum in (1.15) turns into an integral. The component explicitly represented in (1.15) is the positive frequency component $\mathbf{A}^{(+)}(\mathbf{r}, t)$. The negative frequency component is obtained by complex conjugation $\mathbf{A}^{(-)}(\mathbf{r}, t) = [\mathbf{A}^{(+)}(\mathbf{r}, t)]^*$. The magnitude of the wave vector $|\mathbf{k}|$, denoted by k , and frequency satisfy the relationship

$$c^2 k^2 = \omega^2 \quad (1.16)$$

everywhere in free space as obtained by applying the wave operator (1.13) to the ansatz (1.15). Due to this relationship $\mathbf{a}_{\mathbf{k}}$ in (1.15) need not be additionally parametrised by ω as for any given wave vector \mathbf{k} the frequency $\omega = ck$ is uniquely determined. A monochromatic wave

$$i \frac{\partial}{\partial t} \mathbf{A}_{\omega}^{(+)}(\mathbf{r}, t) = \omega \mathbf{A}_{\omega}^{(+)}(\mathbf{r}, t) \quad (1.17)$$

is one for which the summation in (1.15) is only over those \mathbf{k} with a given magnitude ω/c . For such a wave the magnitude of its wave vectors are fixed however they may point in arbitrary directions

$$\mathbf{A}_{\omega}(\mathbf{r}, t) = e^{-i\omega t} \sum_{|\mathbf{k}|=\omega/c} \mathbf{a}_{\mathbf{k}} e^{i\mathbf{k}\cdot\mathbf{r}} + \text{c.c.} \quad (1.18)$$

(as allowed by the cavity). When applied to a monochromatic field the wave equation (1.13) with the use of the relation (1.16) reduces to the Helmholtz equation

$$(\nabla^2 + k^2) \mathbf{A}_{\omega}(\mathbf{r}, t) = \mathbf{0}. \quad (1.19)$$

At this point some simplifications are made. As polarisation is not of particular interest in this thesis the vector potential is assumed to be linearly polarised in an arbitrary direction in the transverse plane $\mathbf{A}(\mathbf{r}) = A(\mathbf{r})\mathbf{e}_{x \text{ or } y}$ (propagation is assumed to be in the z -direction). The trivial time dependence $e^{-i\omega t}$ also to be neglected and the subscript ω dropped as in the transition to the Helmholtz equation from the wave equation a monochromatic solution has been assumed.

Solutions corresponding to light beams are of interest. These are solutions that propagate in predominantly one direction (set to be the $+z$ direction) though some spreading of the light beam is unavoidable. To this end it is useful to take the ansatz

$$A(\mathbf{r}) = \psi(\mathbf{r})e^{ikz} \quad (1.20)$$

where $\psi(\mathbf{r})$ is some envelope function for the monochromatic wave e^{ikz} .

1.2 Paraxial wave equation

The form of the ansatz (1.20) in itself does not yet constitute a transition to paraxial optics [5]. The paraxial condition is imposed on the ansatz (1.20) by restricting to solutions where the envelope function $\psi(\mathbf{r})$ varies slowly in the z -direction as quantified by

$$\left| \frac{\partial^2 \psi}{\partial z^2} \right| \ll \left| k \frac{\partial \psi}{\partial z} \right|. \quad (1.21)$$

The paraxial wave equation is then the equation governing the spatial evolution of the envelope function

$$\left(\nabla_{\perp}^2 + 2ik \frac{\partial}{\partial z} \right) \psi(\mathbf{r}) = 0 \quad (1.22)$$

where ∇_{\perp}^2 is the transverse laplacian involving second derivatives only with respect to the x and y coordinates. This is formally identical to the Schrödinger equation for a free particle in two dimensions

$$\left(\nabla_{\perp}^2 + 2i \frac{m}{\hbar} \frac{\partial}{\partial t} \right) \psi(\mathbf{r}_{\perp}, t) = 0. \quad (1.23)$$

This equivalence will be exploited in chapter 6 where a quantum mechanical formalism will be used (mainly due to the notational simplicity of braket notation) to make classical optical calculations.

1.2.1 Paraxial modes

The form of the lowest order solution of the paraxial wave equation may be motivated by looking at the spherical solution to the Helmholtz equation

$$A(\mathbf{r}) = \frac{e^{ik|\mathbf{r}|}}{|\mathbf{r}|} \quad (1.24)$$

far away from its source (as embodied by the Fresnel approximation)

$$|\mathbf{r}| \approx (z - z_0) + \frac{(x - x_0)^2 + (y - y_0)^2}{2(z - z_0)} \quad (1.25)$$

as is done in [5, §16]. The coordinates (x_0, y_0, z_0) describe the source of the spherical wave. As the envelope function varies slowly in the z -direction longitudinal distances are in general appreciably larger than transverse distances between two arbitrary points of concern. The spherical wave in the paraxial regime is thus

$$A(\mathbf{r}) = \frac{A_0}{q(z)} \exp\left(ik \frac{(x - x_0)^2 + (y - y_0)^2}{2q(z)} + ikz\right) \quad (1.26)$$

where the function

$$q(z) = z - z_0 \quad (1.27)$$

describes the radius of curvature of the spherical wave. This source point is arbitrary and the coordinate system may be chosen so that it is $(0, 0, 0)$. However before doing so let z_0 be augmented with an imaginary part, iz_R , that will not be set to zero. The quantity z_R is known as the Rayleigh range hence the potentially confusing subscript. The function $q(z)$ in its new complex form

$$q(z) = z - iz_R \quad (1.28)$$

turns the paraxial spherical wave into a Gaussian wave and now describes two features of the wave namely its radius of curvature as before and the width of the beam. This is usually expressed in terms of its reciprocal

$$\frac{1}{q(z)} = \frac{1}{R(z)} + i \frac{2}{kw^2(z)}. \quad (1.29)$$

where $R(z)$ is the radius of curvature of the Gaussian beam and $w(z)$ is the beam width. By inserting this into the paraxial spherical wave it is apparent that the imaginary part of $1/q(z)$ is responsible for the Gaussian transverse spatial profile of the beam. Once this is done,

$$A(\mathbf{r}) = \frac{A_0}{z - iz_R} \exp\left(-\frac{x^2 + y^2}{w^2(z)} + ik \frac{x^2 + y^2}{2R(z)}\right), \quad (1.30)$$

the reason for the decomposition of $1/q(z)$ in (1.29) is apparent. By splitting $1/q(z)$ into its real and imaginary components and comparing the result with (1.29) one obtains the forms

$$R(z) = z \left(1 + \left(\frac{z_R}{z}\right)^2\right) \quad (1.31) \quad w^2(z) = w_0^2 \left(1 + \left(\frac{z}{z_R}\right)^2\right) \quad (1.32)$$

for the radius of curvature and the beam width respectively with $w_0 = w(0)$. The radius of curvature diverges as $z \rightarrow 0$ meaning that at the beam waist ($z = 0$) the Gaussian beam approximates a plane wave with parallel wavefronts of no curvature. By setting $z = 0$ in (1.29) the Rayleigh range can be expressed as

$$z_R = \frac{kw_0^2}{2}. \quad (1.33)$$

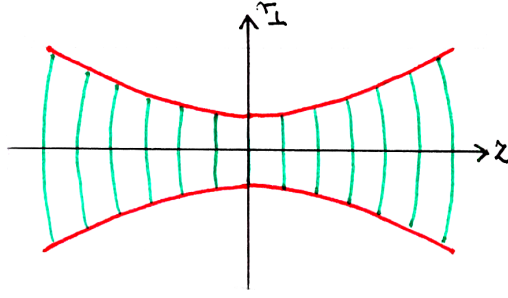


Figure 1.1: The width and phase fronts of the beam near the beam waist.

There is a z -dependent phase variation of the carrier wave e^{ikz} associated with propagation due to the $1/q(z)$ factor in (1.30) known as the Gouy phase

$$-i \frac{|q(z)|}{q(z)} = e^{i\zeta(z)}. \quad (1.34)$$

It takes the value

$$\zeta(z) = \arctan\left(\frac{z}{z_R}\right). \quad (1.35)$$

The Gaussian solution is generally normalised to have unit magnitude when integrated across the transverse plane

$$A(\mathbf{r}) = \sqrt{\frac{2}{\pi}} \frac{1}{w(z)} \exp\left(-\frac{x^2 + y^2}{w^2(z)} + ik \frac{x^2 + y^2}{2R(z)}\right). \quad (1.36)$$

1.2.2 Higher order modes

The two major classes of higher order modes arise by solving the paraxial wave equation in Cartesian and cylindrical coordinates. Working in a Cartesian coordinate system has the advantage that the ansatz $\psi_{nm}(x, y, z) = \psi_n(x, z)\psi_m(y, z)$ reduces the 2 + 1 dimensional paraxial wave equation to two 1 + 1 dimensional equations

$$\left(\frac{\partial^2}{\partial x^2} + 2ik \frac{\partial}{\partial z}\right) \psi_n(x, z) = 0 \quad (1.37)$$

with $\psi_m(y, z)$ satisfying an similar equation in the other transverse coordinate. Two dimensional solutions may then be constructed by simple multiplication $\text{HG}_{nm}(x, y, z) = \text{HG}_n(x, z)\text{HG}_m(y, z)$.

$$\text{HG}_{m,n}(x, y, z) = \sqrt{\frac{2}{\pi}} \frac{1}{w(z)\sqrt{2^{n+m}n!m!}} H_n\left(\frac{\sqrt{2}x}{w(z)}\right) H_m\left(\frac{\sqrt{2}y}{w(z)}\right) \exp\left(-\frac{x^2 + y^2}{w^2(z)} + ik \frac{x^2 + y^2}{2R(z)} + i(n+m+1)\zeta(z)\right). \quad (1.38)$$

The functions $H_n(x)$ are Hermite polynomials. The advantage of working in a cylindrical coordinate system is that it lends itself to solutions carrying a well defined value of angular momentum (c.f. chapter 4)

$$\text{LG}_{lp}(r, \varphi, z) = \sqrt{\frac{2n!}{\pi(l+p)}} \frac{1}{w(z)} \left(\frac{\sqrt{2}r}{w(z)}\right)^m L_p^{||l||}\left(\frac{2r^2}{w^2(z)}\right) \exp\left(-\frac{r^2}{w^2(z)} + ik \frac{r^2}{2R(z)} + il\varphi + i(2||l|| + p + 1)\zeta(z)\right) \quad (1.39)$$

though these are intrinsically two dimensional solutions. The functions $L_p^{||l||}(r)$ are associated Laguerre polynomials.

1.3 Quantised amplitudes

The transition to a quantum theory proceeds by replacing the components of the magnetic potential and its complex conjugate by the annihilation and creation operators

$$a_{\mathbf{k}} \mapsto \sqrt{\frac{\hbar}{2\epsilon_0\mathcal{V}\omega_k}} \hat{a}_{\mathbf{k}} \quad a_{\mathbf{k}}^* \mapsto \sqrt{\frac{\hbar}{2\epsilon_0\mathcal{V}\omega_k}} \hat{a}_{\mathbf{k}}^\dagger \quad (1.40)$$

where \mathcal{V} is the volume of the fictitious quantisation cavity that has been assumed in (1.15). They are hermitean conjugates of each other and obey the commutation relation

$$[\hat{a}_{\mathbf{k}}, \hat{a}_{\mathbf{l}}^\dagger] = \delta_{\mathbf{k}, \mathbf{l}} \quad (1.41)$$

where $\delta_{\mathbf{k}, \mathbf{l}}$ is unity only if all three components of the two vectors \mathbf{k} and \mathbf{l} are the same otherwise it is zero. The positive frequency part of the potential becomes

$$\hat{A}^{(+)}(\mathbf{r}, t) = \sqrt{\frac{\hbar}{2\epsilon_0\mathcal{V}}} \sum_{\mathbf{k}} \frac{1}{\sqrt{\omega_k}} \hat{a}_{\mathbf{k}} e^{i(\mathbf{k}\cdot\mathbf{r} - \omega_k t)} \quad (1.42)$$

(we stay in the scalar theory adopted for paraxial optics). In the quantum theory the negative frequency component is related to the positive frequency component by Hermitian conjugation $\hat{A}^{(-)}(\mathbf{r}, t) = [\hat{A}^{(+)}(\mathbf{r}, t)]^\dagger$. The scalar positive frequency electric and magnetic fields are in turn described by the operators

$$\hat{E}^{(+)}(\mathbf{r}, t) = i\sqrt{\frac{\hbar}{2\epsilon_0\mathcal{V}}} \sum_{\mathbf{k}} \sqrt{\omega_k} \hat{a}_{\mathbf{k}} e^{i(\mathbf{k}\cdot\mathbf{r} - \omega_k t)}, \quad \hat{B}^{(+)}(\mathbf{r}, t) = i\sqrt{\frac{\hbar}{2\epsilon_0 c^2 \mathcal{V}}} \sum_{\mathbf{k}} \sqrt{\omega_k} \hat{a}_{\mathbf{k}} e^{i(\mathbf{k}\cdot\mathbf{r} - \omega_k t)}. \quad (1.43)$$

1.3.1 Continuum treatment

In the case of unidirectional continuum modes instead of a quantisation volume a quantisation area \mathcal{A} is taken [7]. A unique propagation direction is typically found in optical experiments so that $a_{\mathbf{k}}$ can be represented in terms of frequency instead $a(\omega)$ with the commutation relations becoming

$$[\hat{a}(\omega), \hat{a}^\dagger(\omega')] = \delta(\omega - \omega'). \quad (1.44)$$

Correspondingly the summation over \mathbf{k} can be replaced with integration over ω/c .

$$\hat{A}_{mn}^{(+)}(z, t) = \sqrt{\frac{\hbar}{4\pi\epsilon_0\mathcal{A}c}} \int_0^{+\infty} \frac{1}{\sqrt{\omega}} \hat{a}_{mn}(\omega) e^{i\omega(z/c - t)} d\omega \quad (1.45)$$

with the corresponding electric and magnetic field operators

$$\hat{E}_{mn}^{(+)}(z, t) = i\sqrt{\frac{\hbar}{4\pi\epsilon_0\mathcal{A}c}} \int_0^{+\infty} \sqrt{\omega} \hat{a}_{mn}(\omega) e^{i\omega(z/c - t)} d\omega, \quad \hat{B}_{mn}^{(+)}(z, t) = i\sqrt{\frac{\hbar}{4\pi\epsilon_0\mathcal{A}c^3}} \int_0^{+\infty} \sqrt{\omega} \hat{a}_{mn}(\omega) e^{i\omega(z/c - t)} d\omega \quad (1.46)$$

where $\hat{a}_{mn}(\omega)$ are annihilation operators for the spatial mode labelled by n and m . The full description involving the transverse spatial profile is then

$$\hat{A}^{(+)}(\mathbf{r}, t) = \sum_{mn} \psi_{mn}(\mathbf{r}) \hat{A}_{mn}^{(+)}(z, t) \quad (1.47)$$

where $\psi_{nm}(\mathbf{r})$ are a set of orthonormal modes.

1.3.2 Narrow bandwidth approximation

Quantum optical experiments typically deal with pulses or at the very least are performed over a finite amount of time meaning that there is necessarily a spread of frequencies involved in their description straying from the assumption of monochromaticity. However in general the narrow bandwidth assumption is valid in these cases where the frequency spectrum

$$\exp\left(-\frac{(\omega - \omega_0)^2}{\sigma^2}\right) \quad (1.48)$$

is such that the bandwidth is much smaller than the central frequency of the experiment

$$\sigma \ll \omega_0. \quad (1.49)$$

One may extend the integration range to all negative frequencies so that the electric field can be rewritten as

$$\hat{E}_{mn}^{(+)}(\mathbf{r}, t) = i\sqrt{\frac{\hbar\omega_0}{4\pi\epsilon_0\mathcal{A}c}}\hat{a}_{mn}\left(t - \frac{z}{c}\right) \quad (1.50)$$

where $\hat{a}_{nm}(t)$ is the Fourier transform of the annihilation operator

$$\int_{-\infty}^{+\infty} \hat{a}_{mn}(\omega)e^{-i\omega t} d\omega. \quad (1.51)$$

Under these conditions the longitudinal component of the Poynting vector given in (1.6) takes the form

$$\hat{S}(x, y, z, t) = \hbar\omega_0 \sum_{m,n,m',n'=0}^{+\infty} \psi_{mn}^*(x, y, z)\psi_{m'n'}(x, y, z)\hat{a}_{mn}^\dagger\left(t - \frac{z}{c}\right)\hat{a}_{m'n'}\left(t - \frac{z}{c}\right) \quad (1.52)$$

which when integrated over the transverse plane gives

$$\iint_{x,y=-\infty}^{\infty} \hat{S}(x, y, z, t) dx dy = \hbar\omega_0 \sum_{m,n=0}^{\infty} \hat{a}_{mn}^\dagger\left(t - \frac{z}{c}\right)\hat{a}_{mn}\left(t - \frac{z}{c}\right). \quad (1.53)$$

This corresponds to the energy per unit time flowing through the transverse plane at z .

Chapter 2

Angular momentum and spontaneous parametric down conversion

This chapter constitutes a review of the topics used in chapter 5 and is not based on the author's research. First the classical concept of optical angular momentum is described. The discussion is restricted to light beams and within that mostly to the paraxial domain. Then the main properties of the quantum mechanical phenomenon of entanglement are described before moving onto a semiclassical treatment of spontaneous parametric downconversion.

2.1 Optical angular momentum

Light has associated with it a momentum density described by the quantity

$$\mathbf{p} = \frac{\epsilon_0}{2} (\mathbf{E}^* \times \mathbf{B} + \mathbf{E} \times \mathbf{B}^*) \quad (2.1)$$

where \mathbf{E} and \mathbf{B} are the complex electric and magnetic fields in free space respectively. The above momentum density integrated over a volume of the beam gives the momentum \mathbf{P} carried by that volume of the beam. Any light beam necessarily possesses angular momentum density about any point not on the beam axis

$$\mathbf{j} = \mathbf{r} \times \mathbf{p} \quad (2.2)$$

where \mathbf{r} is measured from the point of interest. The angular momentum \mathbf{J} obtained from (2.2) by integration over a volume is orthogonal to the direction of propagation of the beam. It is a recent realisation however that light beams can carry angular momentum in their direction of propagation [34] due to the momentum density twisting around the beam axis, heuristically speaking. Note that locally this angular momentum is everywhere orthogonal to the Poynting vector but due to the rotational symmetry of such beams each of these quantities integrated over a volume have dominant components along the direction of propagation and some radial component that need not be comparable in magnitude to the former.

The optical angular momentum can be separated into spin and orbital components which are themselves not true angular momenta [35, 36]. The spin component generates rotations of the polarisation but not the spatial distribution and conversely the the orbital component generates rotations of the spatial distribution of light but not its polarisation [37]. The angular momentum density obtained from (2.1) and (2.2) is in general subtly problematic and not the most natural way in which it can be expressed in that it is not the form one obtains from applying

Nöther's theorem to rotations of an electromagnetic field [37] but it does give the correct integrated quantities. In the following chapter angular momentum of photons will be used as a degree of freedom in particular due to the large state space it provides. We shall be interested in extending some results known for polarisation to this domain. For this reason the spin component, which can take only the values $\pm\hbar$ is not of particular interest hence in this review we focus on the orbital component of the angular momentum of light.

The required geometry for orbital angular momentum carrying beams is a helical phase structure $e^{il\phi}$ where ϕ is the azimuthal coordinate and l is an integer which is in principle unbounded [34, 38]. The angular momentum number l has to be an integer because azimuthal positions differing by integer multiples of 2π (at any given radius) represent the same point in space and thus must be assigned the same phase. For an $l = 1$ the surface of constant phase is the helicoid obtained by taking the half real line (from $r = 0$ to $r \rightarrow \infty$) and simultaneously translating it along and rotating it about the z -axis. For a general l the surface of constant phase are l intertwined such helicoids. For example for $l = 2$ the surface of constant phase when truncated at a radius r is the surface bounded by a double helix. The phase at $r = 0$ is not uniquely undefined so the amplitude of a helically phased beam must go to zero at the phase singularity so that the undefined phase has no physical consequence [38]. Note however that a dark spot in a beam does not automatically imply a helical phase structure.

2.1.1 Laguerre-Gaussian beams

Historically light has been established to carry angular momentum via the study of Laguerre-Gaussian beams [34]. For a cylindrically symmetric paraxial beam with spatial profile $v(r)e^{il\phi}$ it can be shown [34, 39] that the momentum density as given by the Poynting vector takes the form

$$\mathbf{p}(r, \phi, z) = \omega\epsilon_0 \left(-\text{Im} \left(v^* \frac{\partial v}{\partial r} \right) \mathbf{e}_r + \frac{l}{r} |v|^2 \mathbf{e}_\phi + k |v|^2 \mathbf{e}_z \right) \quad (2.3)$$

where $\mathbf{e}_r, \mathbf{e}_\phi, \mathbf{e}_z$ are the unit vectors in the r, ϕ, z directions. It has been shown in the original work [34] that the integrated angular momentum to integrated energy ratio for a Laguerre-Gaussian light beam is

$$\frac{\hbar l}{\hbar\omega} \quad (2.4)$$

where it has been put into a suggestive form by the superfluous use of \hbar . In this form this is to be interpreted as a single photon of energy $\hbar\omega$ in an l^{th} order Laguerre-Gaussian mode carries $\hbar l$ of angular momentum.

2.1.2 Bessel beams

Bessel beams

$$u_l(r, \phi, z) = J_l(\sqrt{k^2 - \kappa^2}r) e^{i\kappa z} e^{il\phi}, \quad (2.5)$$

where $J_l(x)$ are l^{th} order Bessel functions of the first kind [40], arise naturally from solving the full Helmholtz equation (1.19) in cylindrical coordinates. In a plane wave decomposition of a zeroth order Bessel beam all of the wave vectors lie on a cone parametrised by a single angle which results in an on axis bright spot. Higher order Bessel beams have a dark spot on axis as must be the case due to the undefined phase there. Bessel beams are non-paraxial beams that have a well defined value of angular momentum.

2.1.3 Experimental demonstration of optical angular momentum

It has been shown that an absorptive particle trapped in the centre of a Laguerre-Gaussian mode can be made to rotate [41]. It has also been shown for such trapped particles that by controlling the polarisation of the beam

the spin angular momentum can be made to add or to subtract from the rotation induced by the orbital angular momentum depending on whether the spin and orbital angular momenta point in the same or opposite directions confirming their mechanical equivalence [42, 43]. Beyond this the difference between spin and orbital angular momenta has also been demonstrated by trapping particles in the annulus of a Laguerre-Gaussian mode and transporting them along it thereby making the particles orbit a point external to them [44]. This is possible only for orbital angular momentum as spin angular momentum induces always rotation about the particles own axis.

2.2 Entanglement

In order to introduce the features of entanglement it is sufficient to consider qubits (2 dimensional quantum systems) in the computational basis $|0\rangle, |1\rangle$. The defining features of entanglement remain true for higher dimensional states. Superpositions of the computational basis that lie in the x - z plane of the Bloch sphere [45, §2.4] at an angle ξ to the z -axis will be denoted by

$$\begin{aligned} |\xi\rangle &= \cos\left(\frac{\xi}{2}\right)|0\rangle + \sin\left(\frac{\xi}{2}\right)|1\rangle \\ |\xi^\perp\rangle &= -\sin\left(\frac{\xi}{2}\right)|0\rangle + \cos\left(\frac{\xi}{2}\right)|1\rangle \end{aligned} \quad (2.6)$$

special cases of which are $|\pm\rangle$ for $\xi = \pi/2$.

An entangled state is defined negatively to be a state that is not a product state [45, §2.5]. A product state is a state that can be expressed as the tensor product of two states. For example the composite system composed of system A described by the state $\psi_0|0\rangle + \psi_1|1\rangle$ and of system B described by the state $\eta_0|0\rangle + \eta_1|1\rangle$ is described by the state

$$\psi_0\eta_0|00\rangle + \psi_0\eta_1|01\rangle + \psi_1\eta_0|10\rangle + \psi_1\eta_1|11\rangle \quad (2.7)$$

where the shorthand $|\psi\rangle|\eta\rangle = |\psi\eta\rangle$ for tensor products of states has been employed. Any state

$$\kappa_{00}|00\rangle + \kappa_{01}|01\rangle + \kappa_{10}|10\rangle + \kappa_{11}|11\rangle \quad (2.8)$$

where a consistent decomposition $\kappa_{ij} = \psi_i\eta_j$ is not possible in *any* basis is an entangled state. Entanglement encodes correlations between separated systems at the amplitude level rather than at the level of probabilities [46]. As a result in some cases entanglement can give rise to correlations stronger than is classically realisable. These are the famous violations of Bell's inequalities [47–51].

2.2.1 Bell states

The simplest (and possibly most notable) set of entangled states are the Bell states

$$|\Psi^\pm\rangle = \frac{|01\rangle \pm |10\rangle}{\sqrt{2}}, \quad |\Phi^\pm\rangle = \frac{|00\rangle \pm |11\rangle}{\sqrt{2}} \quad (2.9)$$

They form an orthonormal basis for a two-qubit system and are said to be maximally entangled, that is any protocol requiring entanglement works better (with higher probability of success) with (2.9) than with entangled states consisting of unbalanced superpositions.

Consider $|\Phi^+\rangle$ re-expressed in terms of the states $|\xi\rangle, |\xi^\perp\rangle$ of (2.6) in the x - z plane of the Bloch sphere

$$|\Phi^+\rangle = \frac{|\xi\xi\rangle + |\xi^\perp\xi^\perp\rangle}{\sqrt{2}}. \quad (2.10)$$

Alice can make a measurement on her qubit in any direction in the x - y plane and the state of Bob's qubit collapses to the same state that Alice obtained as a result of the measurement. This apparent *spooky action at a distance* [52] is not as omnipotent a property however as it may seem at first sight. For example without a classical communication channel between them Alice and Bob cannot send signals to each other using this property alone [53]. Bob does not know the state of his qubit without Alice communicating the result of her measurement to him because Alice could obtain either of the orthogonal outcomes with equal probability. Both before and after Alice's measurement the best Bob can say about his qubit is that it is in the maximally mixed state [45, §5]

$$\frac{1}{2}|\xi\rangle\langle\xi| + \frac{1}{2}|\xi^\perp\rangle\langle\xi^\perp|. \quad (2.11)$$

To illustrate the non-classical correlations possible consider the following game [54]. Alice and Bob are isolated from each other, they each flip a coin and for each outcome, heads (H) or tails (T), they respond with a value ± 1 . The victory condition of the game is for them to give the same response for the coin flip results HH , HT , TH but the opposite response for the coin flip outcome TT . Any strategy using classical means can win this game at most $3/4$ of the time.

Now suppose they share many copies of a pair of qubits (a copy for each time they play the game) in the $|\Phi^+\rangle_{AB}$ state and they each make measurements on their respective qubits. They each make a measurement in one of two basis determined by the coin flip. Alice measures along the $\pm\mathbf{a}_H, \pm\mathbf{a}_T$ directions (at angles $\alpha_H = 0$ and $\alpha_T = \pi/2$ to the z -axis on the Bloch sphere respectively) and Bob measures along the $\pm\mathbf{b}_H, \pm\mathbf{b}_T$ directions (at angles $\beta_H = \pi/4$ and $\beta_T = -\pi/4$ to the z -axis on the Bloch sphere respectively) as illustrated in figure 2.1. As Bob's state collapses conditionally on Alice's measurement to her measurement outcome it is reasonable to represent both their measurements on the same Bloch sphere.

When Alice measures in the $\pm\mathbf{a}$ on the Bloch sphere she can obtain the results \mathbf{a} or its antipodal vector $-\mathbf{a}$ as

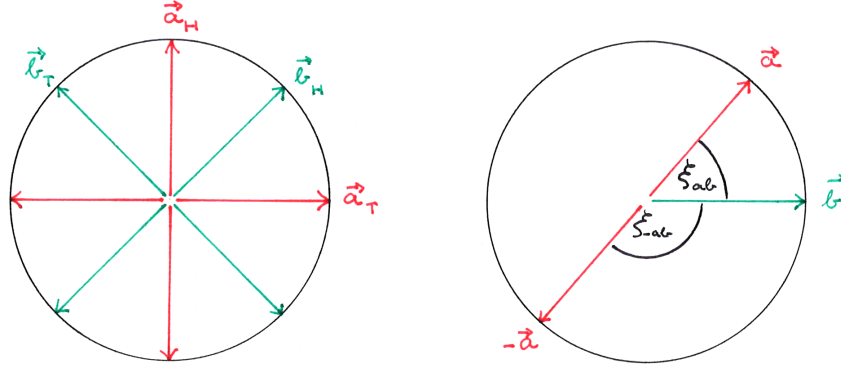


Figure 2.1: *Left*: The measurement basis used by Alice and Bob on the Bloch sphere. The angle between any neighbouring pair of arrows is $\pi/4$. The arrow which is labelled corresponds to the $+1$ outcome and its antipodal arrow corresponds to the -1 outcome. *Right*: The relationship of the angle subtended by \mathbf{a} and \mathbf{b} to the angle subtended by $-\mathbf{a}$ and \mathbf{b} . The angles subtended by $-\mathbf{a}$ and $-\mathbf{b}$ and by \mathbf{a} and $-\mathbf{b}$ are the same as that of the former two by symmetry.

results corresponding to the $+1$ and -1 outcomes of the measurement respectively. If Alice gets a measurement outcome corresponding to some Bloch vector \mathbf{a} then we know from (2.10) that the Bloch vector of Bob's qubit is also along \mathbf{a} . If Bob makes a measurement in some other basis then the probability that his outcome is that corresponding to some Bloch vector \mathbf{b} is given by

$$\frac{1 + \mathbf{a} \cdot \mathbf{b}}{2} = \cos^2\left(\frac{\xi_{\mathbf{a}\mathbf{b}}}{2}\right) \quad (2.12)$$

where $\xi_{\mathbf{ab}}$ is the angle subtended by the vectors \mathbf{a} and \mathbf{b} and use has been made of the fact that \mathbf{a} and \mathbf{b} are both unit vectors. However one must bear in mind that Alice obtains this result (or any other in the $x - y$ plane according to (2.10)) with probability $1/2$. Thus the *joint* probability that Alice obtains the outcome corresponding to Bloch vector \mathbf{a} and Bob obtains the outcome corresponding to Bloch vector \mathbf{b} is

$$\Pr(\mathbf{a}, \mathbf{b}) = \Pr(\mathbf{b} | \mathbf{a})\Pr(\mathbf{a}) = \Pr(\mathbf{a} | \mathbf{b})\Pr(\mathbf{b}) = \frac{1}{2} \cos^2\left(\frac{\xi_{\mathbf{ab}}}{2}\right). \quad (2.13)$$

As there is no information communicated between Alice and Bob by measurement the time ordering of their measurements in the above argument can be reversed with no observable consequences. There are two ways in which they can obtain the same result

$$\Pr(\text{same}) = \Pr(\mathbf{a}, \mathbf{b}) + \Pr(-\mathbf{a}, -\mathbf{b}) = \cos^2\left(\frac{\xi_{\mathbf{ab}}}{2}\right). \quad (2.14)$$

The case for opposite results consists of replacing either \mathbf{a} (or \mathbf{b}) by $-\mathbf{a}$ (or $-\mathbf{b}$) in (2.12). Note however that in that case the angle used on the right hand side is $\xi_{-\mathbf{ab}} = \xi_{\mathbf{a}-\mathbf{b}} = \pi - \xi_{\mathbf{ab}}$ (c.f. figure 2.1) giving the result $\sin^2(\xi_{\mathbf{ab}}/2)$ when re-expressed in terms of the same angle as is used in (2.12) so that the probabilities of the two orthogonal outcomes sum to unity. In order to win the game Alice and Bob need to give the same answer in three of the cases and the opposite answer in one of the cases

$$\begin{aligned} \Pr(\text{win}) = & \Pr(\text{same} | HH)\Pr(HH) + \Pr(\text{same} | HT)\Pr(HT) \\ & + \Pr(\text{same} | TH)\Pr(TH) + \Pr(\text{opposite} | TT)\Pr(TT). \end{aligned} \quad (2.15)$$

Each case occurs with an equal probability of $1/4$. All of the possible outcomes satisfying the victory conditions of the game are enumerated in figure 2.2. For each coin flip outcome they can give a winning answer $\cos^2(\pi/8)$ of the time. Thus by (2.15) they win the game with a probability of

$$\Pr(\text{win}) = \cos^2(\pi/8) \approx 85\% \quad (2.16)$$

outperforming the classically possible 75%.

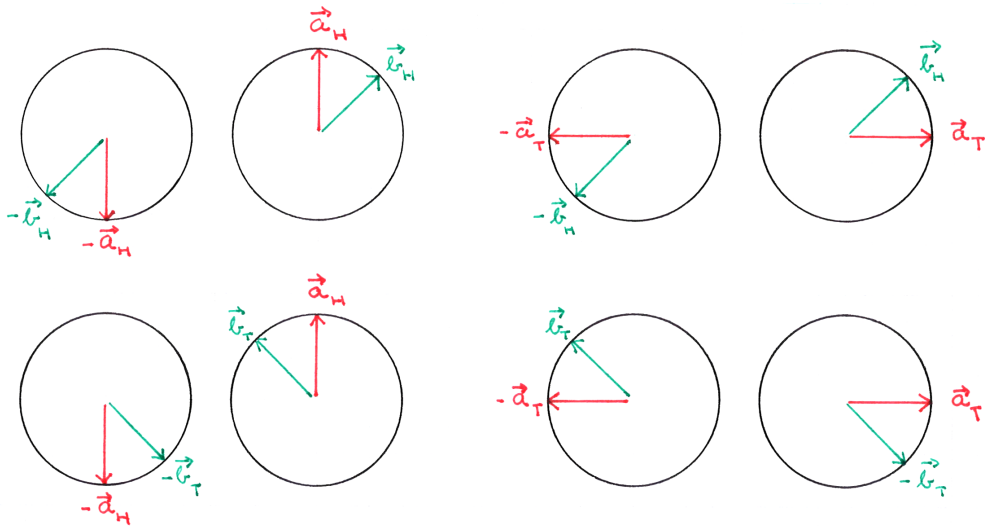


Figure 2.2: Alice's and Bob's Bloch vectors corresponding to the outcomes satisfying the rules of the game for each of the coin flip results. In each case their Bloch vectors subtend an angle of $\pi/8$.

2.2.2 Partial Bell state analysis

To illustrate the new possibilities afforded by the correlation properties of Bell states and their measurement consider quantum teleportation first proposed by Bennett et al. [55]. Suppose Alice and Bob share an entangled pair of qubits $|\Psi^-\rangle_{AB}$ and Alice wishes to send a qubit in some unknown state $|\psi\rangle_{A'}$ to Bob. She can do this by performing a Bell state measurement on the unknown qubit and her half of the entangled qubit pair and communicating the result of the measurement to Bob. The classical communication is required as only in one of the four cases does Bob's qubit become the unknown qubit $|\psi\rangle$ however in the other three cases Bob's qubit is only a local Pauli operation $\{\hat{\sigma}_x, \hat{\sigma}_y, \hat{\sigma}_z\}$ away from the original qubit $|\psi\rangle$. This can be most easily shown following [55] by re-expressing the state $|\psi\rangle_{A'}|\Psi^-\rangle_{AB}$ in terms of Bell states of the $A'A$ qubit pair rather than of the AB qubit pair

$$|\psi\rangle_{A'} \otimes |\Psi^-\rangle_{AB} = -\frac{1}{2} \{i|\Phi^+\rangle_{A'A} \otimes \hat{\sigma}_y|\psi\rangle_B - |\Phi^-\rangle_{A'A} \otimes \hat{\sigma}_x|\psi\rangle_B + |\Psi^+\rangle_{A'A} \otimes \hat{\sigma}_z|\psi\rangle_B + |\Psi^-\rangle_{A'A} \otimes |\psi\rangle_B\}. \quad (2.17)$$

where tensor products have been explicitly left in to aid the eye in separating the systems. The Pauli operators effect rather simple transformations on the computational basis states

$$\hat{\sigma}_z : \begin{cases} |0\rangle \mapsto |0\rangle \\ |1\rangle \mapsto -|1\rangle \end{cases} \quad \hat{\sigma}_x : \begin{cases} |0\rangle \mapsto |1\rangle \\ |1\rangle \mapsto |0\rangle \end{cases} \quad \hat{\sigma}_y : \begin{cases} |0\rangle \mapsto i|1\rangle \\ |1\rangle \mapsto -i|0\rangle \end{cases} \quad (2.18)$$

Then it is immediately obvious from the form of (2.17) that Alice obtains any four of the Bell states with probability $1/4$. In each of these cases Bob's qubit collapses to a Pauli operator times the original state to be teleported. As each of the Pauli operators squares to the identity, $\hat{\sigma}_{x,y,z}^2 = 1$, this mismatch with the original state can be undone by applying the appropriate Pauli operator.

In order to be able to do this Alice and Bob must share an entangled qubit to begin with. In general, as illustrated by this example, entanglement is a resource for quantum computational protocols. The need for Bell state analysis in this protocol is manifest. The first experimental realisation of this by Bouwmeester et al. [56] has been with photon polarisation states. Optical angular momentum provides a means of realising entanglement in a larger state space. This motivates its study.

2.3 Spontaneous parametric down conversion

Parametric downconversion is a nonlinear effect arising due to second order nonlinear susceptibility of noncentrosymmetric media [57, §1]. In parametric down conversion a pump photon of frequency ω_p is absorbed into a virtual energy level, whose lifetime is restricted by the Heisenberg uncertainty relation, which then emits two photons (signal and idler) of lower frequencies ω_s, ω_i [57, §1]. It is true for all three-wave mixing phenomena that energy and in the case of a crystal much wider than the laser beam transverse momentum are conserved within the electromagnetic field

$$\omega_p = \omega_s + \omega_i \quad (2.19)$$

$$p_p^\perp = p_s^\perp + p_i^\perp. \quad (2.20)$$

Spontaneous parametric down conversion comes in two types known simply as I and II [58, §21.2]. Type I down conversion creates a pair of photons of the same polarisation whereas type II downconversion creates photons of orthogonal polarisation. Due to momentum conservation in the transverse plane the photons emerge with opposite transverse momenta but there is no preferred direction along which the photon pair should emerge.

Hence there is a cone of possible locations where a photon may be detected. Due to the different refractive indices experienced by the two polarisation modes the cones along which the two photons are created separate in type II down conversion (c.f. figure 2.3). When photons are captured from the region where the two cones overlap there is no way to know which photon is horizontally polarised and which one is vertically polarised resulting in a polarisation entangled state [59]. However for the purposes of the following chapter we are interested in type I down conversion. This leads to photon pairs that differ in only their orbital angular momentum value and transverse position.

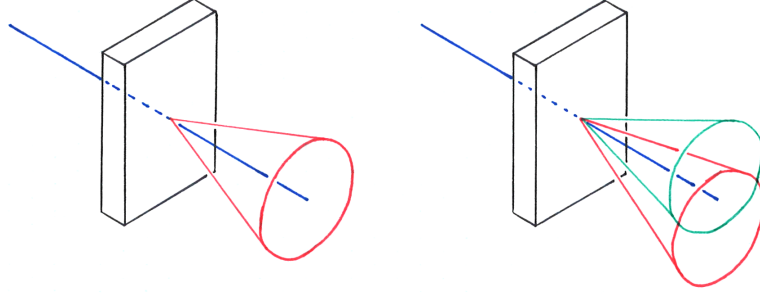


Figure 2.3: Type I (*left*) and type II (*right*) parametric downconversion geometries. In both cases the angle defining the cone is greatly exaggerated. The block represents the nonlinear crystal, the line perpendicular to the block represents the pump beam and the two cones represent the possible directions in which the signal and idler photons are produced.

2.3.1 Phase matching

The interaction Hamiltonian for spontaneous parametric down conversion must have a term $\hat{a}_s^\dagger \hat{a}_i^\dagger \hat{a}_p$ that correspond to the absorption of a pump photon and the emission of a signal and an idler photon. To maintain Hermiticity this must be complemented by its adjoint [17, §22.4]. Once the signal and idler fields have been generated difference frequency generation also takes place which leads to amplification of the fields. The amplification they undergo in the time interval while they traverse the crystal is assumed to be sufficiently small that no significant drain on the pump beam occurs. Thus the pump beam in the interaction can be treated classically and \hat{a}_p^\dagger can be replaced by a scalar amplitude α_p to give [17, §22.4]

$$\hat{H}_I \propto \frac{1}{V} \int_V \chi^{(2)} e^{i(\mathbf{k}^{(p)} - \mathbf{k}^{(s)} - \mathbf{k}^{(i)}) \cdot \mathbf{r}} \alpha_p(\mathbf{k}^{(p)}) \hat{a}^\dagger(\mathbf{k}^{(s)}) \hat{a}^\dagger(\mathbf{k}^{(i)}) d\mathbf{r} + \widehat{h.c.} \quad (2.21)$$

where V is the volume of the crystal of dimensions L_x, L_y, L_z centered at the origin, $\chi^{(2)}$ is a scalar second order susceptibility and $\widehat{h.c.}$ denotes the hermitean conjugate. To illustrate the phase matching criterion it is possible to consider only one signal and one idler mode and follow a similar reasoning to the perturbative multimode treatments of [17, 60, 61]. This proceeds by writing down the Hamiltonian and finding the state for a short interaction time by a first order expansion of the time evolution operator in the interaction picture. Thus the starting point is the interaction Hamiltonian

$$\hat{H}_I \propto \frac{1}{V} \chi^{(2)} \prod_{j=x,y,z} \text{sinc} \left(\frac{k_j^{(p)} - k_j^{(s)} - k_j^{(i)}}{2} L_j \right) \alpha_p(\mathbf{k}^{(p)}) \hat{a}^\dagger(\mathbf{k}^{(s)}) \hat{a}^\dagger(\mathbf{k}^{(i)}) d\mathbf{r} + \widehat{h.c.} \quad (2.22)$$

where $\text{sinc}(x) = \sin(x)/x$. The perturbative approach to finding the downconverted biphoton state following [17, §22.4] proceeds by

$$|\psi(t)\rangle = e^{-\frac{i}{\hbar} \int_0^t \hat{H}_I dt'} |\psi(0)\rangle \approx \left(\mathbb{1} - \frac{i}{\hbar} \int_0^t \hat{H}_I dt' \right) |\psi(0)\rangle. \quad (2.23)$$

Now for illustrating the phase matching condition a lot of the details can be neglected here as the main concern is how the state depends on the wave vectors of the signal and idler photons. From the above equations (2.21) and (2.23) it is clear the amplitude of detecting a photon pair in the $\hat{a}^\dagger(\mathbf{k}^{(s)})$ and $\hat{a}^\dagger(\mathbf{k}^{(i)})$ modes has its \mathbf{k} dependence governed by

$$\psi(\mathbf{k}^{(s)}, \mathbf{k}^{(i)}) \propto \prod_{j=x,y,z} \text{sinc} \left(\frac{k_j^{(p)} - k_j^{(s)} - k_j^{(i)}}{2} L_j \right). \quad (2.24)$$

The quantity $\Delta k_j = k_j^{(p)} - k_j^{(s)} - k_j^{(i)}$ is the phase mismatch in the $j = x, y, z$ direction.

Longitudinal Considering only the z -component of (2.24) one obtains information about the efficiency of the process related to how closely perfect phase matching was achieved [62, §2]. It shows that the probability of the emission process is maximised at $\Delta k_z = 0$ and drops off rapidly, periodically dropping to zero whenever the phase mismatch is an integer multiple of π . We are working under the assumption that the crystal is thin (typically 1-3mm [63, 64]).

Transverse Of the transverse components something different can be concluded due to the geometry of the process. Typically the width of the crystal in both transverse directions is much larger than the beam waists of the pump and downconverted beams. The system can be said to have translational symmetry in the transverse plane. This implies conservation of momentum in the transverse plane. This limit of the amplitude (2.24) can be studied by taking the limit

$$\lim_{L_{j'} \rightarrow \infty} \text{sinc} \left(\frac{L_{j'} \Delta k_{j'}}{2} \right) \rightarrow \delta(\Delta k_{j'}) \quad (2.25)$$

where the index j' only takes the values x, y corresponding to the transverse directions. Noting that the pump beam defines the optic axis and the transverse plane, $\mathbf{k}^{(p)}$ has no component in the transverse plane and the transverse phase mismatch reduces to $\Delta k_{j'} = k_{j'}^{(s)} + k_{j'}^{(i)}$. Hence the transverse amplitude of detection can be well approximated by

$$\psi^\perp(k_x^{(s)}, k_y^{(s)}, k_x^{(i)}, k_y^{(i)}) \propto \delta(k_x^{(s)} + k_x^{(i)}) \delta(k_y^{(s)} + k_y^{(i)}) \quad (2.26)$$

and using this state it can be shown that the transverse momentum conservation in SPDCspontaneous parametric downconversion implies entanglement in the orbital angular momentum of the biphotons [65].

2.3.2 Angular momentum conservation and entanglement

The entanglement of optical angular momentum modes arises quite naturally in spontaneous parametric down conversion as a result of transverse momentum conservation. To illustrate that (2.26) leads to angular momentum entanglement the simple argument of [66, §8], which we follow here is sufficient. Since the argument only involves applying a sequence of Fourier transformations it shows clearly that transverse phase matching implies immediately angular momentum entanglement. The first step is to convert (2.26) into position representation by the usual Fourier transform

$$\psi^\perp(x^{(s)}, y^{(s)}, x^{(i)}, y^{(i)}) \propto \delta(x^{(i)} - x^{(s)}) \delta(y^{(i)} - y^{(s)}). \quad (2.27)$$

When changed to polar coordinates this expression involves a periodic delta function, $\delta(\varphi^{(i)} - \varphi^{(s)})$ in the azimuthal argument as angular positions differing by 2π are indistinguishable. Analogously to the Fourier transform of the usual Dirac delta, the periodic Dirac delta has a Fourier series representation

$$\delta_{2\pi}(\varphi^{(i)} - \varphi^{(s)}) = \frac{1}{2\pi} \sum_{l=-\infty}^{\infty} e^{il(\varphi^{(i)} - \varphi^{(s)})} \quad (2.28)$$

which is readily recognised as carrying the characteristic phase dependence of angular momentum states

$$\frac{1}{2\pi} \sum_{l=-\infty}^{\infty} |l\rangle_i | -l\rangle_s. \quad (2.29)$$

The emitted photons can be emitted in any pair of complimentary directions [61]. By the rotational invariance we can expect we expect angular momentum to be conserved. Hence for a pump beam of zero angular momentum the signal and idler photons must have angular momenta opposite in value $l_s = -l_i$. This is verified in expression (2.29). This also appears to be the case observed in experiment by [67].

This result that angular momentum is conserved and that this leads to entangled states is generally true for a pump beam of any angular momentum leading to downconverted states of the form

$$\sum_l \psi_l |l\rangle_s |l_{\text{pump}} - l\rangle_i. \quad (2.30)$$

More generally it is true for arbitrary superposition of Laguerre-Gaussian modes (under colinear phase matching) in which case the downconverted biphoton does not have a well defined combined angular momentum but is generally entangled [63].

2.3.3 Experimental demonstration of optical angular momentum entanglement

Correlation of the orbital angular momentum of downconverted photons has been measured for pump beams of zero and non-zero angular momenta [67, 68]. In these experiment sensitivity to phases between terms in the entangled state (2.30) has been demonstrated to make sure that the correlations arise at the amplitude level rather than at the probability level. The correlations arising from entanglement have been measured in both the orbital angular momentum and the angle basis within the same experiment [69].

To fully demonstrate entanglement of the orbital angular momentum degree of freedom photon pairs with such entanglement have been used to violate Bell inequalities in both two [70] and three dimensional sub-spaces [71] of the angular momentum state space. Entanglement between four photons has recently also been realised [72] using the orbital angular momentum degree of freedom.

Chapter 3

Beam splitter and Mach-Zehnder interferometer

This chapter is devoted to the study of the beam splitter and the Mach-Zehnder interferometer as these will be key components of the problems studied in later chapters. Using these optical devices the basic properties of superposition and of interference are explored. The material in this chapter can be found in standard pedagogical texts such as [3] and [4].

3.1 Beam splitter

The beam splitter is a partially reflecting device. For an incoming wave of some amplitude A_0 an amount rA_0 is reflected and tA_0 is transmitted where r and t are the complex reflection and transmission coefficients respectively [3, §3.2]. Let us consider waves with quantised amplitudes \hat{b}_1^\dagger and \hat{b}_2^\dagger before the beam splitter and \hat{a}_1^\dagger and \hat{a}_2^\dagger after the beam splitter as shown in figure 3.1. We consider single particle input states impinging on the beam

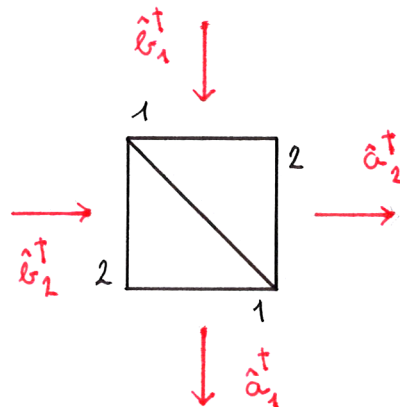


Figure 3.1: The beam splitter with its ports and input/output modes labelled. Quantised amplitudes \hat{b}^\dagger describe light before the beam splitter and amplitudes \hat{a}^\dagger describe light after the beam splitter.

splitter. These are described by $|\text{in}_j\rangle = \hat{b}_j^\dagger|\text{vac}\rangle$ and the output states leaving the beam splitter are correspondingly described in terms of output mode creation operators $|\text{out}_j\rangle = \hat{a}_j^\dagger|\text{vac}\rangle$. Let r_1 and t_1 be the reflection and transmission coefficients that lead to output 1 and likewise let r_2 and t_2 be the reflection and transmission coef-

ficients that lead to output 2 (i.e. the coefficients are labelled so that their subscript indicates which mode they reflect/transmit *into*). The input from both ports are both reflected and transmitted. The modes before and after the beam splitter are related by

$$\begin{pmatrix} \hat{b}_1^\dagger \\ \hat{b}_2^\dagger \end{pmatrix} = \begin{pmatrix} t_1 & r_2 \\ r_1 & t_2 \end{pmatrix} \begin{pmatrix} \hat{a}_1^\dagger \\ \hat{a}_2^\dagger \end{pmatrix} \quad (3.1)$$

The matrix in (3.1) represents the beam splitter operator denoted by $\widehat{\text{BS}}$. Its matrix elements $\text{BS}_{ij} = \langle \text{out}_j | \widehat{\text{BS}} | \text{in}_i \rangle$

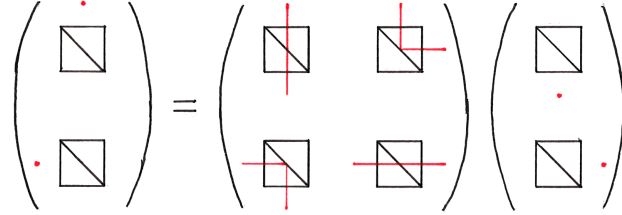


Figure 3.2: The four distinct possibilities of traversing the beam splitter. These correspond to the ways in which a particle in a particular input mode can be connected by a path to a particle in a particular output mode. The amplitudes with which these happen are those of the matrix elements in (3.1).

describe the amplitude with which a particle in given input mode (i) makes it to a given output mode (j). These possibilities of traversing the beam splitter are depicted in figure 3.2. There are some conditions on the transition amplitudes. The commutation relations satisfied by the modes after the beam splitter must be identical to those satisfied by the modes before the beam splitter. From this follows the unitarity of the beam splitter matrix of equation (3.1)

$$[\hat{a}_1, \hat{a}_1^\dagger] = [\hat{b}_1, \hat{b}_1^\dagger] = 1 \quad \Rightarrow \quad |t_1|^2 + |r_2|^2 = 1 \quad (3.2)$$

$$[\hat{a}_2, \hat{a}_2^\dagger] = [\hat{b}_2, \hat{b}_2^\dagger] = 1 \quad \Rightarrow \quad |t_2|^2 + |r_1|^2 = 1$$

$$[\hat{a}_1, \hat{a}_2^\dagger] = [\hat{b}_1, \hat{b}_2^\dagger] = 0 \quad \Rightarrow \quad t_1^* r_1 + r_2^* t_2 = 0. \quad (3.3)$$

The Hermitian conjugate of the relation on the left hand side (LHS) of (3.3) yields the complex conjugate of the right hand side (RHS). No new information is to be learnt from it. The relations (3.2) and (3.3) can be summarised in matrix form as

$$\widehat{\text{BS}}^\dagger \widehat{\text{BS}} = \widehat{\text{BS}} \widehat{\text{BS}}^\dagger = 1 \quad (3.4)$$

Let the transmission and reflection coefficients be written in terms of real variables as $t_j = |t_j| e^{i\tau_j}$ and $r_j = |r_j| e^{i\rho_j}$ where j can take values 1 or 2. From (3.3) one obtains the relation

$$\frac{|r_1| |t_1|}{|r_2| |t_2|} = e^{i(\pi + \tau_2 + \tau_1 - \rho_1 - \rho_2)} = 1 \quad (3.5)$$

where the second equality follows from the simultaneous conditions of the left hand side of the first equality being real and positive and the right hand side having unit magnitude. By eliminating either the reflection coefficients or the transmission coefficients from the left hand side of (3.5) using equations (3.2) one obtains that $|t_1| = |t_2|$ and that $|r_1| = |r_2|$. The two transmission coefficients can differ from each other only by a phase and the same goes for the two reflection coefficients. This freedom in phase is restricted by

$$\pi + \tau_2 + \tau_1 = \rho_1 + \rho_2 \quad (3.6)$$

obtained from (3.5). A symmetric beam splitter $t_1 = t_2 = t$, $r_1 = r_2 = r$ achieves this by $\rho = \tau + \pi/2$. The most general beam splitter can be created out of a symmetric beam splitter by appending the two output modes with phases α_1, α_2 and one of the input modes with a phase β_2 . A phase for the fourth port is not necessary as it can be absorbed into the global phase (therefore any other set of three out of the four ports will do). The beam splitter matrix so obtained

$$\begin{pmatrix} t_1 & r_2 \\ r_1 & t_2 \end{pmatrix} = \begin{pmatrix} te^{i\alpha_1} & re^{i(\alpha_1+\beta_2)} \\ re^{i\alpha_2} & te^{i(\alpha_2+\beta_2)} \end{pmatrix} \quad (3.7)$$

satisfies the phase restriction (3.5) on a beam splitter matrix. The sum of the phases of the new reflection coefficients contains the sum of all three appended phases and so does the sum of the transmission coefficients. Hence the reflection and transmission coefficients of the general beam splitter (3.7) satisfy (3.6) if those of the symmetric beam splitter do. An example used commonly in the balanced beam splitter case is obtained with $\alpha_1 = 0, \alpha_2 = \frac{3\pi}{2}, \beta_2 = \frac{3\pi}{2}$ is

$$\begin{pmatrix} t_1 & r_2 \\ r_1 & t_2 \end{pmatrix} = \frac{1}{\sqrt{2}} \begin{pmatrix} 1 & 1 \\ 1 & -1 \end{pmatrix} \quad (3.8)$$

Due to being able to discard a global phase we choose the convention $t = |t|, r = i|r|$ for symmetric beam splitters throughout this text. Within this convention the most general symmetric beam splitter that satisfies (3.2) is

$$t = \cos(\theta), \quad r = i\sin(\theta). \quad (3.9)$$

We will mostly be referring to balanced ($\theta = \pi/4$) beam splitters which we will denote without the subscripts when this is clear from the context

$$\begin{pmatrix} t_{1:1} & r_{1:1} \\ r_{1:1} & t_{1:1} \end{pmatrix} = \frac{1}{\sqrt{2}} \begin{pmatrix} 1 & i \\ i & 1 \end{pmatrix}. \quad (3.10)$$

In chapter 4 we will also be making use of beam splitters that split the power of an impinging beam in a 2:1 ratio

$$\begin{pmatrix} t_{2:1} & r_{2:1} \\ r_{2:1} & t_{2:1} \end{pmatrix} = \frac{1}{\sqrt{3}} \begin{pmatrix} \sqrt{2} & i \\ i & \sqrt{2} \end{pmatrix}. \quad (3.11)$$

Implicit in the above analysis, due to the use of commutation relations (3.2) and (3.3), is that the beam splitter acts on bosons (as the motivating example is light impinging on it). However we can also consider such a device acting on fermions [8] such as those used in neutron interferometry [9, 10]. In that case the *anti*-commutators of the modes before and after the beam splitter satisfy identical relations

$$\{\hat{a}_1, \hat{a}_1^\dagger\} = \{\hat{b}_1, \hat{b}_1^\dagger\} = 1 \quad \Rightarrow \quad |t_1|^2 + |r_2|^2 = 1 \quad (3.12)$$

$$\{\hat{a}_2, \hat{a}_2^\dagger\} = \{\hat{b}_2, \hat{b}_2^\dagger\} = 1 \quad \Rightarrow \quad |t_2|^2 + |r_1|^2 = 1$$

$$\{\hat{a}_1, \hat{a}_2^\dagger\} = \{\hat{b}_1, \hat{b}_2^\dagger\} = 0 \quad \Rightarrow \quad t_1^* r_1 + r_2^* t_2 = 0. \quad (3.13)$$

The transition from commutators to anti-commutators reflects the differing nature of bosons and fermions under particle exchange as elaborated upon in section 2.1.3. The same relations on the transmission and reflection coefficients are obtained as were obtained for a device acting on bosons in (3.2) and (3.3). Both the commutator and the anti-commutator are bilinear which is their main property from which these relations follow. We shall compare and contrast the action of a beam splitter on two-particle states in chapter 5.

3.1.1 Single particle inputs

Let us consider a single particle input to a beam splitter and ask where the particle ends up. The most general such input is

$$|\text{in}_\psi\rangle = (\psi_1 \hat{b}_1^\dagger + \psi_2 \hat{b}_2^\dagger) |\text{vac}\rangle \quad (3.14)$$

where the normalisation condition $|\psi_1|^2 + |\psi_2|^2 = 1$ is observed. The probabilities of finding this particle in input ports 1 and 2 (i.e. detecting the particle before letting it enter the beam splitter) are

$$\langle \text{in}_\psi | \hat{b}_1^\dagger \hat{b}_1 | \text{in}_\psi \rangle = |\psi_1|^2 \quad (3.15)$$

$$\langle \text{in}_\psi | \hat{b}_2^\dagger \hat{b}_2 | \text{in}_\psi \rangle = |\psi_2|^2 \quad (3.16)$$

There are of course two special cases

$$|\text{in}_1\rangle = \hat{b}_1^\dagger |\text{vac}\rangle \quad (3.17)$$

$$|\text{in}_2\rangle = \hat{b}_2^\dagger |\text{vac}\rangle. \quad (3.18)$$

These states represent particles that are with certainty in port 1 and 2 respectively. Therefore these will be referred to as states of definite port mode number. These are somewhat special for the reason that when one asks about the whereabouts of a particle one expects the answer in terms of states of well defined port number rather than in the $\frac{1}{\sqrt{2}} (\hat{b}_1^\dagger \pm e^{i\phi} \hat{b}_2^\dagger) |\text{vac}\rangle$ basis. Let us take the case with the particle being incident on input 1. The output state is

$$|\text{in}_1\rangle = (t \hat{a}_1^\dagger + r \hat{a}_2^\dagger) |\text{vac}\rangle \quad (3.19)$$

according to (3.1). Now one can ask what the probability is of finding the particle in output 1 and in output 2. These are given by the expectation values

$$\langle \text{in}_1 | \hat{a}_1^\dagger \hat{a}_1 | \text{in}_1 \rangle = |t|^2 \quad (3.20)$$

$$\langle \text{in}_1 | \hat{a}_2^\dagger \hat{a}_2 | \text{in}_1 \rangle = |r|^2. \quad (3.21)$$

The particle is found to have made its way output 1 with probability $|t|^2$ or to have made its way to output 2 with probability $|r|^2$. The relation (3.2) means that the particle emerges out of the beam splitter with unit probability however in general we do not know with certainty which port it will emerge from. The case for input $\hat{b}_2^\dagger |\text{vac}\rangle$ differs from the above analysis only in the labelling of the output ports. It is found in output 2 with probability $|t|^2$ or in output 1 with probability $|r|^2$. If the input is particle of a well defined port mode number then the particle ends up in either of the output modes with some probability determined by the amplitude of reflection and transmission.

Now consider the general case (3.14). If both amplitudes ψ_1 and ψ_2 are non zero then one cannot say which input port the particle represented by (3.14) is in. As the input is a superposition of being in each of the input ports both processes (evolution from $\hat{b}_1^\dagger |\text{vac}\rangle$ input and evolution from $\hat{b}_2^\dagger |\text{vac}\rangle$ input) happen in superposition

$$|\text{in}_\psi\rangle = (\psi_1 \hat{b}_1^\dagger + \psi_2 \hat{b}_2^\dagger) |\text{vac}\rangle = [(\psi_1 t + \psi_2 r) \hat{a}_1^\dagger + (\psi_1 r + \psi_2 t) \hat{a}_2^\dagger] |\text{vac}\rangle. \quad (3.22)$$

Again the particle ends up in either of the output modes with some probability but that probability is the sum of amplitudes of reaching that output from input mode 1 and of reaching it from input mode 2. Interference

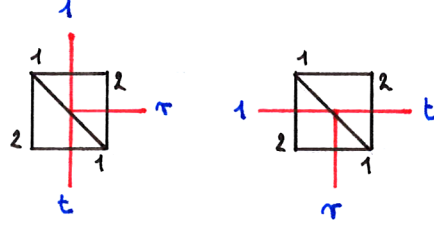


Figure 3.3: The contribution to each of the output port modes that a particle impinging with unit amplitude on input port 1 (left) and on input port 2 (right) makes. If the input is a superposition of input ports 1 and 2 with amplitude ψ_1 and ψ_2 then the contribution to each output port is the weighted linear combination of each of these c.f. figure 3.4

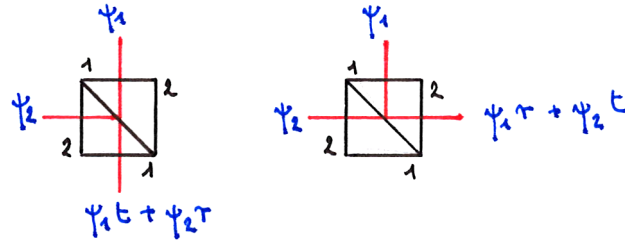


Figure 3.4: The contribution the input amplitude from each input port makes to output port 1 (left) and to output port 2 (right)

manifests in the probabilities for being found in output 1 or 2

$$\langle \text{in}_\psi | \hat{a}_1^\dagger \hat{a}_1 | \text{in}_\psi \rangle = |\psi_1 t + \psi_2 r|^2 \quad (3.23)$$

$$\langle \text{in}_\psi | \hat{a}_2^\dagger \hat{a}_2 | \text{in}_\psi \rangle = |\psi_1 r + \psi_2 t|^2. \quad (3.24)$$

Upon having detected the particle in one of the ports it is not possible to know (even in principle) which input port the particle originated in and hence how it got to the detector unless the input state (3.22) has a vanishing ψ_1 or ψ_2 . Let us consider a click in output port 1 for example. The particle either originated in port 1 and got transmitted (this happens with amplitude $\psi_1 t$) or it originated in port 2 and got reflected (this happens with amplitude $\psi_2 r$) in superposition. It is not possible to differentiate between these two alternatives as they both lead to the same physical output state $\hat{a}_1^\dagger |\text{vac}\rangle$. This interference can be controlled if one has control over the input amplitudes ψ_1, ψ_2 . The dependence of the amplitudes on the relative phase of the two alternatives is the hallmark of interference. It occurs every time several processes or paths lead to the same physical outcome [11, §1].

In particular it can happen (depending on how the input state is prepared) that the particle emerges from a given one of the output ports with unit probability. Consider the input amplitudes $\psi_1 = t^*, \psi_2 = r^*$. Then by the beam splitter properties (3.2) and (3.3) the output probabilities (3.23) and (3.24) say that the particle emerges in output port 1 with certainty. Conversely if $\psi_1 = r^*, \psi_2 = t^*$ then it emerges in output port 2 with certainty. While one cannot say with certainty which input port the particle represented by states

$$|\text{out}_1\rangle = (t^* \hat{b}_1^\dagger + r^* \hat{b}_2^\dagger) |\text{vac}\rangle, \quad (3.25)$$

$$|\text{out}_2\rangle = (r^* \hat{b}_1^\dagger + t^* \hat{b}_2^\dagger) |\text{vac}\rangle \quad (3.26)$$

occupies one can say with certainty in which port it will end up. This is quite different from a classical particle being input to port 1 or 2 with probability $|\psi_1|^2$ or $|\psi_2|^2$ respectively. The probability of ending up in output ports 1 and 2 for such a classical particle are

$$\begin{aligned} |\psi_1|^2 |t|^2 + |\psi_2|^2 |r|^2 &> 0 \\ |\psi_1|^2 |r|^2 + |\psi_2|^2 |t|^2 &> 0 \end{aligned} \quad (3.27)$$

respectively. These probabilities can never reach zero if neither $|r|^2$ nor $|t|^2$ are zero unlike the probabilities (3.23) and (3.24). That is the only cases for which an output probability can vanish in the classical scenario is if the device is purely transmitting or purely reflecting and there is no lack of knowledge regarding which of the input ports the particle impinges on. It is worth noting that the statement that ‘one does not know in which input the particle is’ is true for both a classical particle impinging on one of the input ports with some probability P_j each and for a quantum particle impinging on one of the input ports with some amplitude ψ_j each.

Note the reverse nature (with respect to each other) of the two scenarios of starting with the particle in a given port with certainty and of ending up with the particle in a given port with certainty. However there is a subtle difference between preparing a particle in a given port mode and detecting a particle in a given port mode. In the former case the starting amplitude is unity (up to a phase) however in the latter case the output amplitude need not have unit magnitude as it is possible to detect a particle for which the probability of detection in that given mode is less than one. Hence they are not exactly each others reverse in general but only if either $\psi_1 t + \psi_2 r = 1$ or $\psi_1 r + \psi_2 t = 1$. These similarities can be seen by comparing figures 3.3 and 3.4.

For the special case of the symmetric balanced beam splitter the states of definite output port (3.25) and (3.26) in terms of the input ports become

$$|\text{out}_1\rangle = \frac{1}{\sqrt{2}} (\hat{b}_1^\dagger - i\hat{b}_2^\dagger) |\text{vac}\rangle = \hat{b}_r^\dagger |\text{vac}\rangle = |\text{in}_r\rangle, \quad (3.28)$$

$$|\text{out}_2\rangle = \frac{-i}{\sqrt{2}} (\hat{b}_1^\dagger + i\hat{b}_2^\dagger) |\text{vac}\rangle = -i\hat{b}_l^\dagger |\text{vac}\rangle = -i|\text{in}_l\rangle \quad (3.29)$$

which are significant enough examples to warrant naming them. They are named in analogy with the circular polarisation modes L, R expressed in terms of horizontal H and vertical V polarisations.

Consider again the general input state (3.14) now with the amplitude values $\psi_1 = \frac{1}{\sqrt{2}}, \psi_2 = \pm \frac{1}{\sqrt{2}}$. The input states take the form

$$|\text{in}_\pm\rangle = \frac{1}{\sqrt{2}} (\hat{b}_1^\dagger \pm \hat{b}_2^\dagger) |\text{vac}\rangle. \quad (3.30)$$

For the output states one finds that

$$\frac{t \pm r}{\sqrt{2}} (\hat{a}_1^\dagger \pm \hat{a}_2^\dagger) |\text{vac}\rangle = (t \pm r) |\text{out}_\pm\rangle. \quad (3.31)$$

The state has the same structure in terms of the output modes as it does in terms of the input modes. The only change is a global phase $t \pm r = e^{\pm i\theta}$ for the most general symmetric beam splitter. It is not possible to say with certainty in which input port the particle represented by $|\text{in}_\pm\rangle$ is and neither is it possible to say with certainty in which output port it will be detected. What is possible to say about this particle though is that its state is unaltered (up to a global phase) by the beam splitter.

3.1.2 Mode swap

The symmetric beam splitter is subject to symmetry under the swapping of the two modes

$$\hat{M} : \begin{pmatrix} t_1 & r_2 \\ r_1 & t_2 \end{pmatrix} \mapsto \begin{pmatrix} t_2 & r_1 \\ r_2 & t_1 \end{pmatrix}. \quad (3.32)$$

This symmetry underpins the aforesaid property of $|\text{in}_\pm\rangle$ under the beam splitter transform [12]. It will also prove useful for studying biparticle interference especially in the case of several degrees of freedom. The symmetric beam splitter transform commutes with this operation

$$[\widehat{\text{BS}}, \hat{M}] = 0 \quad (3.33)$$

so eigenvalues with respect to \hat{M} are conserved by it. The reason for this is that the symmetric beam splitter can be written as

$$\widehat{\text{BS}} = \frac{1}{\sqrt{2}} (\mathbb{1} + i\hat{M}) \quad (3.34)$$

Beam splitter evolution in the \hat{M} eigenstate decomposition simply consists of picking up a phase depending on the \hat{M} eigenvalue. Let us review how the 3 families of basis states that were considered so far behave under mode swapping

$$\hat{M} : \begin{cases} \hat{a}_1^\dagger \mapsto \hat{a}_2^\dagger, & \hat{a}_l^\dagger \mapsto i\hat{a}_r^\dagger, & \hat{a}_+^\dagger \mapsto \hat{a}_+^\dagger \\ \hat{a}_2^\dagger \mapsto \hat{a}_1^\dagger, & \hat{a}_r^\dagger \mapsto -i\hat{a}_l^\dagger, & \hat{a}_-^\dagger \mapsto -\hat{a}_-^\dagger \end{cases} \quad (3.35)$$

Given that the modes $\hat{a}_1^\dagger, \hat{a}_2^\dagger$ and $\hat{a}_l^\dagger, \hat{a}_r^\dagger$ are related to each other by a beam splitter transform (up to a phase) and that the ordering of the mode swapping and the beam splitter transform does not matter it is expected that the latter two are mapped onto each other by \hat{M} given that the former two are. However \hat{a}_\pm^\dagger are eigenmodes of this symmetry operation.

3.1.3 Biparticle input states

In treating biparticle states a distinctly quantum issue arises. When writing down a two-particle state of a second quantised system we may consider either $\hat{a}_i^\dagger \hat{a}_j^\dagger |\text{vac}\rangle$ or $\hat{a}_j^\dagger \hat{a}_i^\dagger |\text{vac}\rangle$, where $|\text{vac}\rangle$ denotes the vacuum state and \hat{a}_i^\dagger and \hat{a}_j^\dagger denote creation operators of two modes i and j of a certain degree of freedom that may or may not be distinct. The ordering in itself does not matter but if both orderings appear in a formula they represent particle exchanged alternatives of each other. The two physically equivalent alternatives are related by a phase of 0 or π depending on whether the two particles are bosons or fermions respectively. This is due to the fact that a pair of identical particles when exchanged is physically equivalent to the unexchanged alternative so the two states may differ by a phase only [11, §4]. However exchanging the pair twice gets the particle pair back to its original state hence

$$\hat{X}^{(\hat{a}^\dagger)} \hat{X}^{(\hat{a}^\dagger)} = \mathbb{1} \quad (3.36)$$

where $\hat{X}^{(\hat{a}^\dagger)}$ is the particle exchange operator. Using the connection between spin and statistics [13] this symmetry requirement on an otherwise arbitrary biparticle state characterised by ψ can be expressed as

$$\hat{X}^{(\hat{a}^\dagger)} |\psi, s\rangle = (-1)^{2s} |\psi, s\rangle \quad (3.37)$$

where s is the spin of the particles constituting the particle pair. The choice of the biparticle being bosons or fermions can be achieved by setting the commutator or the anticommutator of the creation operators to zero.

A product of operators can always be written as half the sum of their commutator and anticommutator

$$\hat{a}_i^\dagger \hat{a}_j^\dagger = \frac{1}{2}(\hat{a}_i^\dagger, \hat{a}_j^\dagger) + \frac{1}{2}[\hat{a}_i^\dagger, \hat{a}_j^\dagger]. \quad (3.38)$$

The significance of this is that even without requiring either of the terms in it to vanish, the states produced by their action on $|\text{vac}\rangle$ are endowed with the defining property of bosons and fermions (3.37) under particle exchange. In the interest of notational convenience when dealing with particle pairs let us introduce some new notation in which (3.38) takes the form

$$\hat{A}_{ij}^\dagger = \hat{B}_{ij}^\dagger + \hat{F}_{ij}^\dagger. \quad (3.39)$$

In addition let us introduce symmetrising $\{\}$ and antisymmetrising $[\]$ braces around index pairs so that the commutator and anticommutator in (3.38) take the form

$$\hat{B}_{ij}^\dagger = \hat{A}_{\{ij\}}^\dagger \quad (3.40)$$

$$\hat{F}_{ij}^\dagger = \hat{A}_{[ij]}^\dagger. \quad (3.41)$$

Note that this is not an alternate notation for the commutator and anticommutator but for exchange symmetric and antisymmetric components (under the exchange of indices) of an object with two indices. The difference will be apparent and of significance in chapter 5 where particle pairs with two degrees of freedom are dealt with. Particle exchange is performed by the exchange of the properties of the particles thus in this formalism by the exchange of the indices

$$\hat{X}^{(\hat{a}^\dagger)} : \hat{A}_{ij}^\dagger |\text{vac}\rangle \mapsto \hat{A}_{ji}^\dagger |\text{vac}\rangle. \quad (3.42)$$

The two terms in (3.39) satisfy

$$\hat{B}_{ji}^\dagger |\text{vac}\rangle = \hat{B}_{ij}^\dagger |\text{vac}\rangle, \quad (3.43)$$

$$\hat{F}_{ji}^\dagger |\text{vac}\rangle = -\hat{F}_{ij}^\dagger |\text{vac}\rangle, \quad (3.44)$$

hence we may identify them as boson and fermion pair creation operators respectively. Under any transformation of a particle pair creation operator \hat{A}^\dagger the symmetric part $\hat{B}^\dagger = (\hat{A}^\dagger + \hat{X}^{(\hat{a}^\dagger)} \hat{A}^\dagger)/2$ keeps track of bosonic behaviour and the antisymmetric part $\hat{F}^\dagger = (\hat{A}^\dagger - \hat{X}^{(\hat{a}^\dagger)} \hat{A}^\dagger)/2$ keeps track of fermionic behaviour. The restriction to bosons or fermions corresponds to dropping the appropriate half of the expression.

A pair of bosons each of which have the same two-mode degree of freedom can occupy three distinct states

$$\frac{1}{\sqrt{2}} \hat{A}_{11}^\dagger |\text{vac}\rangle, \quad \frac{1}{\sqrt{2}} \hat{A}_{22}^\dagger |\text{vac}\rangle \quad \text{and} \quad \hat{A}_{\{12\}}^\dagger |\text{vac}\rangle. \quad (3.45)$$

Only one state is realisable by such a fermion pair, namely

$$\hat{A}_{[12]}^\dagger |\text{vac}\rangle. \quad (3.46)$$

Building on the significance of mode swapping with respect to the states $|\text{in}_\pm\rangle$ (c.f. (3.30)) the first two of the biboson states (3.45) are instead combined as $\frac{1}{2}(\hat{A}_{11}^\dagger \pm \hat{A}_{22}^\dagger) |\text{vac}\rangle$. It is perhaps easiest to understand the beam

splitter's effect on these states by rewriting them in terms of the single particle \hat{M} eigenmodes (3.30) [12] as

$$\frac{1}{2}(\hat{A}_{11}^\dagger + \hat{A}_{22}^\dagger) = \frac{1}{2}(\hat{A}_{++}^\dagger + \hat{A}_{--}^\dagger) \quad (3.47)$$

$$\frac{1}{2}(\hat{A}_{12}^\dagger + \hat{A}_{21}^\dagger) = \frac{1}{2}(\hat{A}_{++}^\dagger - \hat{A}_{--}^\dagger) \quad (3.48)$$

$$\frac{1}{2}(\hat{A}_{11}^\dagger - \hat{A}_{22}^\dagger) = \frac{1}{2}(\hat{A}_{+-}^\dagger + \hat{A}_{-+}^\dagger) \quad (3.49)$$

$$\frac{1}{2}(\hat{A}_{12}^\dagger - \hat{A}_{21}^\dagger) = -\frac{1}{2}(\hat{A}_{+-}^\dagger - \hat{A}_{-+}^\dagger). \quad (3.50)$$

Both terms in the right hand side of (3.49) and (3.50) pick up zero phase as \hat{a}_+^\dagger and \hat{a}_-^\dagger pick up opposite phases when passing through the beam splitter. Hence the states $\frac{1}{2}(\hat{A}_{11}^\dagger - \hat{A}_{22}^\dagger)|\text{vac}\rangle$ and $\hat{A}_{[12]}^\dagger|\text{vac}\rangle$ are eigenstates of the beam splitter. This statement about the latter is the fermion equivalent of the Hong-Ou-Mandel effect [14]. \hat{A}_{++}^\dagger and \hat{A}_{--}^\dagger pick up phases i and $-i$ respectively due to (3.31) meaning that (3.47) and (3.48) are mapped onto each other by the balanced beam splitter. In the case of a general symmetric beam splitter parametrised according to (3.9) they pick up phases $e^{\pm i\theta}$ and the two states (3.47) and (3.48) are mixed by the beam splitter rather than mapped onto each other.

$$\widehat{\text{BS}}: \begin{cases} \frac{1}{2}(\hat{A}_{++}^\dagger + \hat{A}_{--}^\dagger) \mapsto \cos(2\theta)\frac{1}{2}(\hat{A}_{++}^\dagger + \hat{A}_{--}^\dagger) + i\sin(2\theta)\frac{1}{2}(\hat{A}_{++}^\dagger - \hat{A}_{--}^\dagger) \\ \frac{1}{2}(\hat{A}_{++}^\dagger - \hat{A}_{--}^\dagger) \mapsto i\sin(2\theta)\frac{1}{2}(\hat{A}_{++}^\dagger + \hat{A}_{--}^\dagger) - \cos(2\theta)\frac{1}{2}(\hat{A}_{++}^\dagger - \hat{A}_{--}^\dagger) \end{cases} \quad (3.51)$$

This is the Hong-Ou-Mandel effect [15] and its reverse [12]. Hence (using the notation introduced in (3.39)) the transition matrix for the beam splitter when extended to biparticles is

$$\begin{pmatrix} \frac{1}{2}(\hat{B}_{11}^\dagger + \hat{B}_{22}^\dagger) \\ \hat{B}_{12}^\dagger \\ \frac{1}{2}(\hat{B}_{11}^\dagger - \hat{B}_{22}^\dagger) \\ \hat{F}_{12}^\dagger \end{pmatrix} \mapsto \begin{pmatrix} r^2 + t^2 & 2rt & 0 & 0 \\ 2rt & r^2 + t^2 & 0 & 0 \\ 0 & 0 & 1 & 0 \\ 0 & 0 & 0 & 1 \end{pmatrix} \begin{pmatrix} \frac{1}{2}(\hat{B}_{11}^\dagger + \hat{B}_{22}^\dagger) \\ \hat{B}_{12}^\dagger \\ \frac{1}{2}(\hat{B}_{11}^\dagger - \hat{B}_{22}^\dagger) \\ \hat{F}_{12}^\dagger \end{pmatrix}. \quad (3.52)$$

Alternatively the structure of the transition matrix in (3.52) may be understood through the simultaneous restrictions placed on it by its commutation with \hat{M} and $\hat{X}^{(a^\dagger)}$. Any physical Hamiltonian must respect the indistinguishability of identical particles [16, §54]. If it does so then it (and the finite transformation generated by it) must commute with the particle exchange operator.

$$[\widehat{\text{BS}}, \hat{X}^{(a^\dagger)}] = 0. \quad (3.53)$$

It has already been established in (3.33) that the beam splitter also commutes with the port mode swap operator. Hence only those states may mix under evolution due to a beam splitter that share an eigenvalue with respect to each \hat{M} and $\hat{X}^{(a^\dagger)}$. The operator $\hat{X}^{(a^\dagger)}$ allows the three \hat{B}^\dagger 's to mix only amongst themselves but \hat{M} allows $\frac{1}{2}(\hat{B}_{11}^\dagger - \hat{B}_{22}^\dagger)$ to mix only with \hat{F}_{12}^\dagger .

3.1.4 Hong-Ou-Mandel dip

As it is an important tool in quantum optics [3] (its use in the timing of photons in chapter 6 serves as an example of this) let us look at the Hong-Ou-Mandel effect

$$\hat{B}_{12}^\dagger|\text{vac}\rangle \mapsto rt(\hat{B}_{11}^\dagger + \hat{B}_{22}^\dagger)|\text{vac}\rangle + (r^2 + t^2)\hat{B}_{12}^\dagger|\text{vac}\rangle \quad (3.54)$$

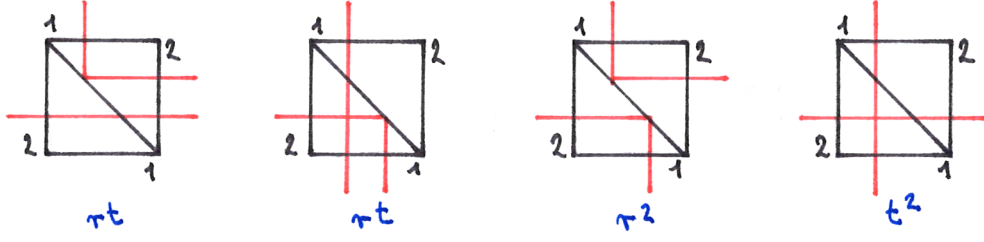


Figure 3.5: All the possible outcomes of a Hong-Ou-Mandel experiment. Note that only three of these lead to outcomes that are physically distinct. Hence the rightmost two always occur in superposition and interfere destructively for photons but constructively for fermions. The leftmost two paths are not an option for fermions as they lead to two particles ending up in the exact same state. The lateral displacement of the beams with respect to the face of the beam splitters is fictional and is for illustrative purposes only. If the experiment was implemented with these displacements then it would serve as a property by which the particles port of origin can be distinguished.

in greater detail. The above is what happens when the two photons impinging on the beam splitter are identical in every way. This includes amongst other things the time at which they arrive at the beam splitter. Suppose that a photon pair described by

$$|\psi\rangle = \iint \psi(\omega_1, \omega_2) e^{i\omega_2 \delta t} \hat{a}_1^\dagger(\omega_1) \hat{a}_2^\dagger(\omega_2) d\omega_1 d\omega_2 |\text{vac}\rangle \quad (3.55)$$

is incident on a beam splitter. The $e^{i\omega_2 \delta t}$ factor means that the photon in input port 2 has been delayed by some time δt . Taking the expectation value

$$\iint \langle \psi | \hat{E}_1^{(-)}(t_1) \hat{E}_2^{(-)}(t_2) \hat{E}_2^{(+)}(t_2) \hat{E}_1^{(+)}(t_1) | \psi \rangle dt_1 dt_2 \quad (3.56)$$

gives the coincidence count rate as

$$\propto |t|^4 + |r|^4 + ((r^*t)^2 + (rt^*)^2) \frac{\iint \psi^*(\omega_2, \omega_1) \psi(\omega_1, \omega_2) e^{-i(\omega_2 - \omega_1) \delta t} d\omega_1 d\omega_2}{\iint |\psi(\omega_1, \omega_2)|^2 d\omega_1 d\omega_2}. \quad (3.57)$$

$\hat{E}_1(t_1)$ and $\hat{E}_2(t_2)$ are electric fields after the beam splitter at times t_1 and t_2 respectively. The integration over detection times is required as the resolving time of photodetectors is much larger than the coherence time of the photons typically involved in such experiments [17, §22.4.7]. For a photon pair anticorrelated in frequency about a central frequency of $\omega_0/2$

$$\psi(\omega_1, \omega_2) = \delta(\omega_0 - \omega_1 - \omega_2) \exp\left(-\frac{(\omega_1 - \omega_2)^2}{2\sigma^2}\right) \quad (3.58)$$

such as that obtained from parametric downconversion the coincidence count rate takes the form

$$|t|^4 + |r|^4 + ((r^*t)^2 + (rt^*)^2) \exp\left(-\left(\frac{\sigma \delta t}{2}\right)^2\right). \quad (3.59)$$

This is the famous Hong-Ou-Mandel dip as reported in [15]. Strictly speaking the state

$$|\psi\rangle = \iint \psi(\omega_1, \omega_2) \hat{a}_1^\dagger(\omega_1) \hat{a}_2^\dagger(\omega_2) |\text{vac}\rangle d\omega_1 d\omega_2 = \int \exp\left(-\frac{2\omega^2}{\sigma^2}\right) \hat{a}_1^\dagger\left(\frac{\omega_0}{2} + \omega\right) \hat{a}_2^\dagger\left(\frac{\omega_0}{2} - \omega\right) |\text{vac}\rangle d\omega \quad (3.60)$$

created from (3.58) with the substitution $\omega_1 = \omega_0/2 + \omega$ is not normalisable without including a spectrum for ω_0 . However in arriving at the coincidence count rate (3.59) one can make use of the appearance of an ill-behaved term $\delta(0)$ in both the numerator and denominator of (3.57).

Let us now consider (3.59) in the case of a balanced beam splitter. For photons separated by a large time interval δt only the first two terms contribute and the resulting coincidence count rate of $1/2$ is the same as that for independent particles. However if the photons arrive at the same time then the second two terms cancel the first two terms exactly leading to a vanishing coincidence count rate. This transition from large separation time to a vanishing separation time between the photons corresponds to a distinguishable to indistinguishable transition. The transition matrix in (3.52) accounts only this indistinguishable case.

3.2 Mach-Zehnder interferometer

A Mach-Zehnder interferometer is constructed by bringing the two outputs of a beam splitter together on another beam splitter [3, §3.3] as shown in figure 3.6. For notational convenience the first beam splitter is always oriented and labelled according to figure 3.1 and the second beam splitter is labelled such that output 1 and 2 leads to input 1 and 2 respectively thereby allowing for the two paths to inherit the labels 1 and 2. There is a phase e^{ikL_j}

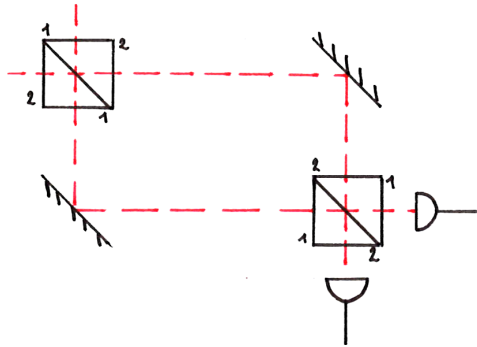


Figure 3.6: A schematic of a Mach-Zehnder interferometer. The dotted lines indicate the available spatial paths.

associated with traversing the path j where $k = 2\pi/\lambda$ is the wave number and L_j is the optical path length. In a vacuum this coincides with the path length L'_j as measured by a ruler. In general they are related by $L_j = nL'_j$ where n is the refractive index of the medium. However only the relative phase between the two paths is relevant. One can always absorb the phase associated with one of the paths into the unobservable global phase. A relative phase between the two paths can be introduced by changing the path lengths by an amount shorter than the typical length of the pulses involved in the experiment.

3.2.1 Interference of paths in the interferometer

Like the beam splitter the Mach-Zehnder interferometer has two input modes and two output modes. However now there are two paths between any given input and output modes. One can think of the Mach-Zehnder interferometer as the first beam splitter creating a superposition state (from a state of definite port number) which then acts as the input to the second beam splitter. The output probabilities then vary depending on the relationship between the input amplitudes to the *second* beam splitter. When looking at the entire setup this variation in output probabilities is achieved by manipulating two equivalent paths internal to the interferometer.

Consider an input $\hat{b}_1^\dagger|\text{vac}\rangle$ and let the output mode of concern be port 1. The particle can reach output 1 via path 1 (with amplitude $t^2e^{i\phi_1}$) or via path 2 (with amplitude $r^2e^{i\phi_2}$) in superposition. The transition amplitude between input mode 1 and output port mode 1 is therefore given by

$$MZ_{11} = t^2e^{i\phi_1} + r^2e^{i\phi_2}. \quad (3.61)$$

Similar calculations hold for the other three input-output combinations. These are depicted in figure 3.7 and are

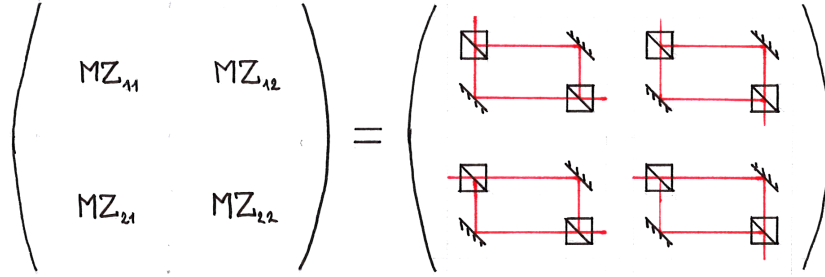


Figure 3.7: Matrix elements for a Mach-Zehnder interferometer.

computed as

$$\begin{pmatrix} \hat{b}_1^\dagger \\ \hat{b}_2^\dagger \end{pmatrix} = \begin{pmatrix} t & r \\ r & t \end{pmatrix} \begin{pmatrix} e^{i\phi_1} & 0 \\ 0 & e^{i\phi_2} \end{pmatrix} \begin{pmatrix} t & r \\ r & t \end{pmatrix} \begin{pmatrix} \hat{a}_1^\dagger \\ \hat{a}_2^\dagger \end{pmatrix} = \begin{pmatrix} t^2 e^{i\phi_1} + r^2 e^{i\phi_2} & rt(e^{i\phi_1} + e^{i\phi_2}) \\ rt(e^{i\phi_1} + e^{i\phi_2}) & r^2 e^{i\phi_1} + t^2 e^{i\phi_2} \end{pmatrix} \begin{pmatrix} \hat{a}_1^\dagger \\ \hat{a}_2^\dagger \end{pmatrix}. \quad (3.62)$$

This gives the transition amplitudes of a single two input mode by two output mode device that is distinct from the beam splitter but a black box just the same. One can also consider superposition inputs to the Mach-Zehnder interferometer and the output amplitudes are computed the same way as they were for the beam splitter

$$(\psi_1 \hat{b}_1^\dagger + \psi_2 \hat{b}_2^\dagger) = [(\psi_1 MZ_{11} + \psi_2 MZ_{21}) \hat{a}_1^\dagger + (\psi_1 MZ_{12} + \psi_2 MZ_{22}) \hat{a}_2^\dagger] |\text{vac}\rangle. \quad (3.63)$$

where the matrix elements have not been written out in full in the interest of brevity. Such inputs ($\psi_1, \psi_2 \neq 0$)

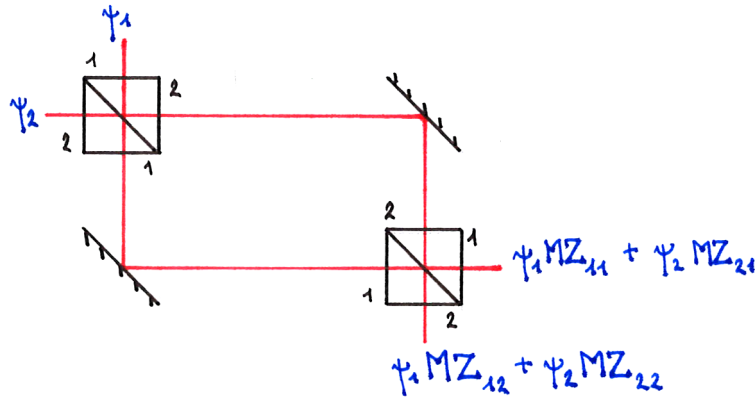


Figure 3.8: How the Mach-Zehnder interferometer mixes the input amplitudes for a general superposition input state.

provide additional opportunities for interference in the output probabilities due to control over the input amplitudes which can (and will in chapter 4) be considered as due to internal paths of a yet larger interferometer.

It is instructive to compute the explicit values of the transition amplitudes in the balanced beam splitter case to gain a qualitative understanding of how the output amplitudes depend on path length differences when perfect

interference is possible. The amplitudes of reaching port 1 and 2 from port 1 are

$$MZ_{11} = e^{i\phi_1} t^2 + e^{i\phi_2} r^2 = -ie^{i\frac{\phi_2+\phi_1}{2}} \sin\left(\frac{\phi_2 - \phi_1}{2}\right) \quad (3.64)$$

$$MZ_{12} = e^{i\phi_1} r t + e^{i\phi_2} r t = ie^{i\frac{\phi_2+\phi_1}{2}} \cos\left(\frac{\phi_2 - \phi_1}{2}\right) \quad (3.65)$$

respectively where $\phi_2 - \phi_1 = k(z_2 - z_1)$ is the phase difference due to path length difference. One may use 2:1 beam splitters in which case it is manifest that (3.64) will never reach zero due to $|t_{2,1}^2|^2 \neq |r_{2,1}^2|^2$ whereas (3.65) may do so. There is a bias in the interferometer that favours sending the particle (for this specific input state) via path 1. (For an input in port 2 the interferometer favours path 2.)

3.2.2 Mach-Zehnder interferometer with marked paths

If one of the paths is marked in some way so that it is possible to tell which path the particle traversed then the amplitude for emerging at a given output port no longer depends on the relative phase of the two spatial paths. The distinguishing of paths means that a property of a particle is changed in some detectable way depending on which path it takes. There exists in principle a measurement that can tell them apart. We use the polarisa-

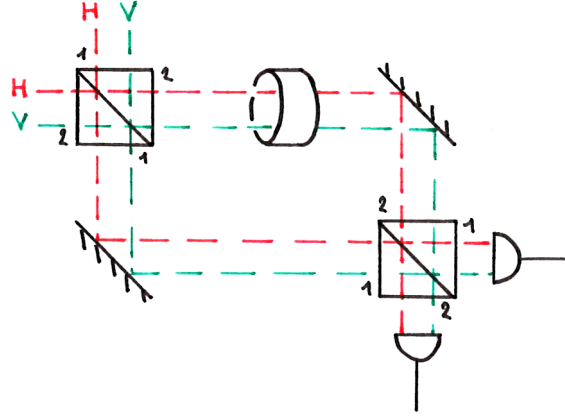


Figure 3.9: A schematic of a Mach-Zehnder interferometer with a polarisation rotator in arm 2. The dotted lines indicate the available paths in the extended sense i.e. they depict both polarisation modes in both spatial modes.

tion degree of freedom for marking paths and consider all production and detection of photons to happen in the horizontal-vertical basis. Hence states of definite polarisation refer to $\hat{a}_H^\dagger|\text{vac}\rangle, \hat{a}_V^\dagger|\text{vac}\rangle$. Suppose that path 2 is appended with a half-wave plate, depicted as a cylinder in figure 3.9. Let the fast and slow axes of the crystal line up with the orientations

$$\hat{a}_{\nearrow}^\dagger|\text{vac}\rangle = \frac{1}{\sqrt{2}}(\hat{a}_H^\dagger + \hat{a}_V^\dagger)|\text{vac}\rangle \quad \hat{a}_{\searrow}^\dagger|\text{vac}\rangle = \frac{1}{\sqrt{2}}(\hat{a}_H^\dagger - \hat{a}_V^\dagger)|\text{vac}\rangle \quad (3.66)$$

so that the net effect of the half-wave plate, upon introducing a relative phase of $e^{i\pi}$ between the $\hat{a}_{\nearrow}^\dagger|\text{vac}\rangle$ and $\hat{a}_{\searrow}^\dagger|\text{vac}\rangle$ polarisations [18], is to rotate the horizontal and vertical polarisations into each other

$$\widehat{\text{HWP}} : \begin{cases} \hat{a}_{2H}^\dagger|\text{vac}\rangle \mapsto \hat{a}_{2V}^\dagger|\text{vac}\rangle \\ \hat{a}_{2V}^\dagger|\text{vac}\rangle \mapsto \hat{a}_{2H}^\dagger|\text{vac}\rangle. \end{cases} \quad (3.67)$$

Any additional phase due to the half-wave plate may be absorbed into the phase $e^{i\phi_2}$ due to path 2. One way to



Figure 3.10: A half-wave plate with its axes bisecting the angle subtended by the horizontal and vertical directions rotates the two polarisations into each other. Modes not containing any light are illustrated with a broken line as in figure 3.2.2. For the rest of the figures the two polarisation modes are shown as the same spatial path and the polarisation of the light at any given point is indicated by colour (vertical mode is red horizontal mode is green)

view the marked Mach-Zehnder interferometer of figure 3.9 is as a four input and four output device with two polarisation modes in each port providing the extra modes as shown in figure 3.9. If the input is a particle in one of the ports and in one of the two polarisation modes each with certainty i.e. $\hat{b}_{1H}^\dagger|\text{vac}\rangle, \hat{b}_{1V}^\dagger|\text{vac}\rangle, \hat{b}_{2H}^\dagger|\text{vac}\rangle$ or $\hat{b}_{2V}^\dagger|\text{vac}\rangle$ then there are no two ‘paths’ (in the extended sense so as to include polarisation) that lead to the same output state (note that this includes port number *and* polarisation). There are two spatial paths that lead to output port 2 but they result in physically distinct outcomes, as distinguished by polarisation, at the output.

Consider the input state $\hat{b}_{2H}^\dagger|\text{vac}\rangle$. It is in port 2 with certainty and in addition to this condition it is horizontally polarised with certainty (when measured in the horizontal-vertical basis). We are interested in the probability that the particle emerges in output port 1. In this case the probability of emerging in output port 1 is the sum of the probabilities of a horizontally polarised photon emerging in port 1 and of a vertically polarised photon emerging in port 1 as shown in figure 3.11. Hence the absence of interference between the two paths of the interferometer.

Interference in this system has not been removed however. The state space has been increased and the input

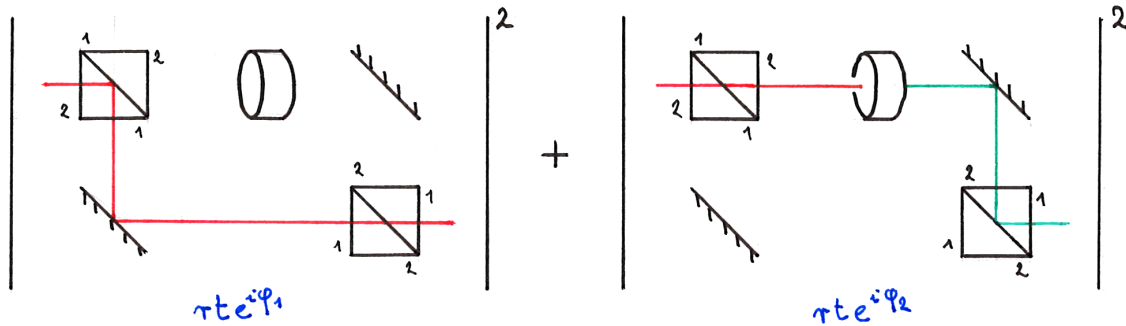


Figure 3.11: The possible paths leading to a photon in output port 1 if the input is horizontally polarised in input port 2.

states have been restricted to be ones that do not allow for two or more paths in state space leading to physically identical outcomes. Similarly to the beam splitter interference in the output probabilities is possible but only if the input is a superposition of the states of well defined port number and polarisation.

Suppose the input is a superposition of the horizontal and vertical polarisation states in input 2

$$(\psi_H \hat{b}_{2,H}^\dagger + \psi_V \hat{b}_{2,V}^\dagger)|\text{vac}\rangle. \tag{3.68}$$

Now there are two ways of ending up in output 1 with horizontal polarisation. (We specify both port mode and polarisation modes as it is qualitatively akin to having four output port modes and one being interested in the probability of the particle emerging from just one of these.) Having originated horizontally polarised

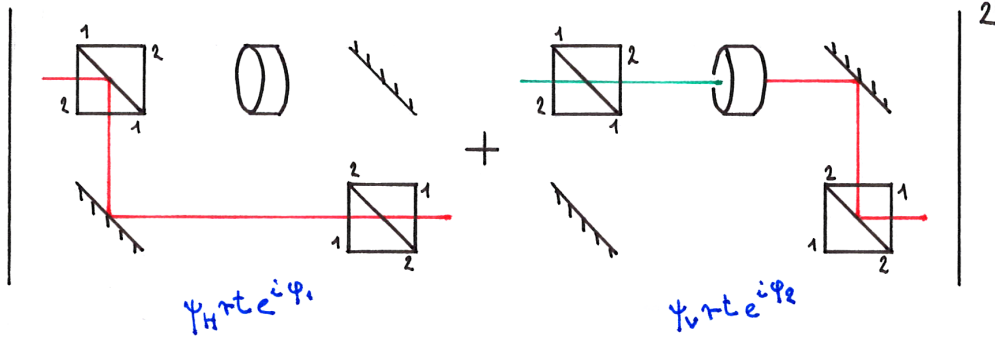


Figure 3.12: The possible paths leading to a horizontally polarised photon in output port 1 if the input is a superposition of polarisation modes in one of the input ports. Similar calculations hold for for the remaining 3 physically distinct outcomes.

and taken path 1 (with amplitude $\psi_H r t e^{i\phi_1}$) or having originated vertically polarised and having taken path 2 (with amplitude $\psi_V r t e^{i\phi_2}$) both lead to the same output state as shown in figure 3.12. Interference is again exhibited but it is due to the input being a superposition (in the polarisation degree of freedom this time) rather than due to equivalent paths inside the interferometer. The amplitude $r t (\psi_V e^{i\phi_2} + \psi_H e^{i\phi_1})$ for this process is reminiscent of the amplitudes in (3.22) and (3.63). The interference occurs between amplitudes that describe the input superposition.

One could also chose input states of a fixed polarisation and with a superposition describing the port mode degree of freedom

$$(\psi_1 \hat{\delta}_{1H}^\dagger + \psi_2 \hat{\delta}_{2H}^\dagger |vac\rangle) \tag{3.69}$$

to illustrate that the polarisation degree of freedom is not the thing responsible for salvaging interference but that an output amplitude is the sum of two amplitudes (each of them a product of a transmission and an input amplitudes). The probability of ending up in output port 1 with horizontal polarisation when the input state is (3.69) is illustrated in figure 3.13. Input states entangled in port and polarisation modes (just to enumerate all

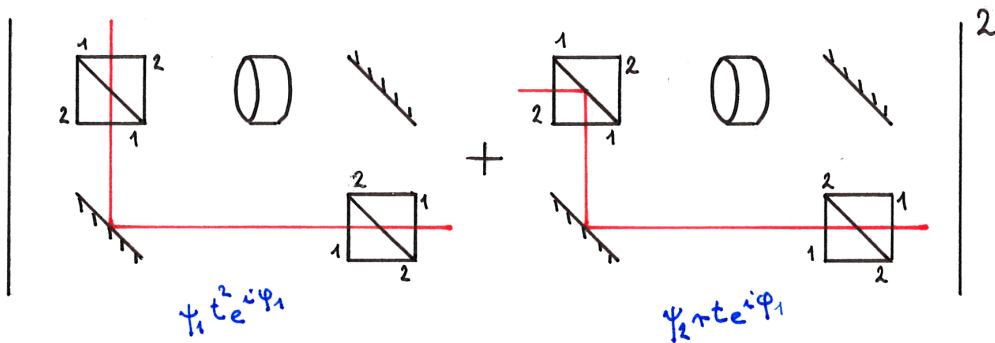


Figure 3.13: The possible paths leading to a horizontally polarised photon in output port 1 if the input particle is horizontally polarised in a superposition of port modes 1 and 2. Similar calculations hold for for the remaining 3 physically distinct outcomes.

the distinct possibilities) are also possible

$$(\psi_{1H} \hat{\delta}_{1H}^\dagger + \psi_{2V} \hat{\delta}_{2V}^\dagger) |vac\rangle \tag{3.70}$$

and result in interference. The probability of ending up in output port 1 with horizontal polarisation with this input is illustrated in figure 3.14.

However if one is interested in simply the probability of ending up in output port 1 whatever the polarisation

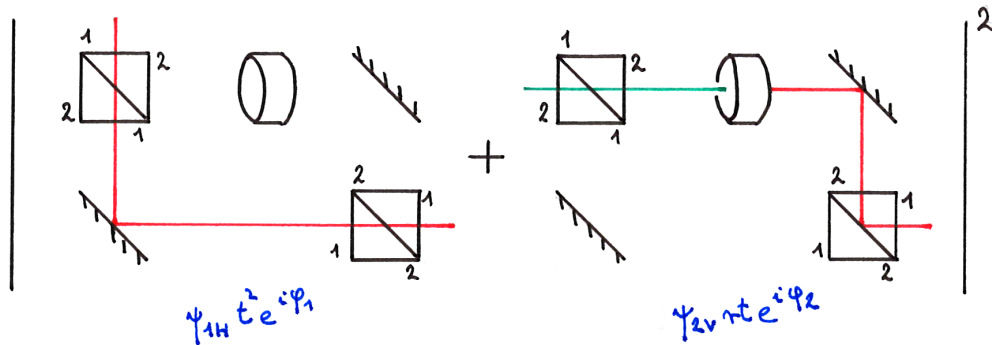


Figure 3.14: The possible paths leading to a horizontally polarised photon in output port 1 if the input particle is a superposition of being horizontally polarised in port 1 and of being vertically polarised in port 2. Similar calculations hold for the remaining 3 physically distinct outcomes.

then the result is still a sum of two probabilities each of which is sensitive to variations in the relative phase between the paths. If one insists on the input states being one of $\hat{b}_{1H}^\dagger|\text{vac}\rangle, \hat{b}_{1V}^\dagger|\text{vac}\rangle, \hat{b}_{2H}^\dagger|\text{vac}\rangle, \hat{b}_{2V}^\dagger|\text{vac}\rangle$ rather than allowing for a superposition of these then one can consider the system under investigation to be part of a larger interferometer that starts with one of these states and creates the superposition state that is the input to the Mach-Zehnder interferometer. In this way interference due to the input state being a superposition and interference due to equivalent internal paths in an interferometer are not conceptually distinct.

Chapter 4

Nested Mach-Zehnder interferometer with weakly marked paths

It is well known that in a single-particle interferometer, we can obtain interference or which-path information. If we know which path the particle took then we lose the interference pattern. It has been suggested, however, that it is possible to *weakly* mark the paths and yet retain interference. Here we present a critical analysis of this proposal.

This work was motivated by the experiment of Danan et al. [1] where the paths were distinguished by the time dependent transverse displacement of the beam. The problem is reduced to two spatial modes as only two are necessary to describe the time dependent transverse spatial profile to within the accuracy of the experiment (i.e. to within first order of a parameter in which a Taylor expansion is made). These correspond to the unperturbed and perturbed part of the light. Within the latter information about which of the paths perturbed the light is obtained from the time dependence of the amplitudes.

The content of this chapter is original work done in collaboration with Václav Potoček based on the publication [19]. Though the formalism used is that of quantum optics the phenomena described here are interference effects of waves of either Maxwell or de Broglie type. In fact the experiment reported in [1] that is being analysed was carried out using a bright light laser.

4.1 Introduction

Recently there has been a proposal by Vaidman [20] to obtain which-way information from a photon in a nested Mach-Zehnder interferometer by weak measurement. This has been implemented by Danan et al. [1] where the measurement was performed by weakly marking each path by reflecting the light off of a vibrating mirror (see Fig. 4.1) and measuring the time varying intensity difference across two halves of a quadrant detector placed at one of the outputs. This has generated much interest in both theoretical [21,22] and experimental [23–29] contexts due mainly to the controversial conclusion that the photons follow disconnected paths in the interferometer.

The point of issue arises when maximum possible destructive interference towards mirror F is arranged. The assumption that this is *complete* destructive interference, i.e., that light reaching the detector D could have gone only via the lower path in Fig. 4.1, led to the curious observation of the vibrational frequencies of mirrors A and B along with that of C in the spectrum of the signal and yet the absence of frequencies of E and F . A further surprise—that at first seems to support the assumption of complete destructive interference in the inner interferometer—was the disappearance of all three frequencies A , B and C upon blocking the lower path

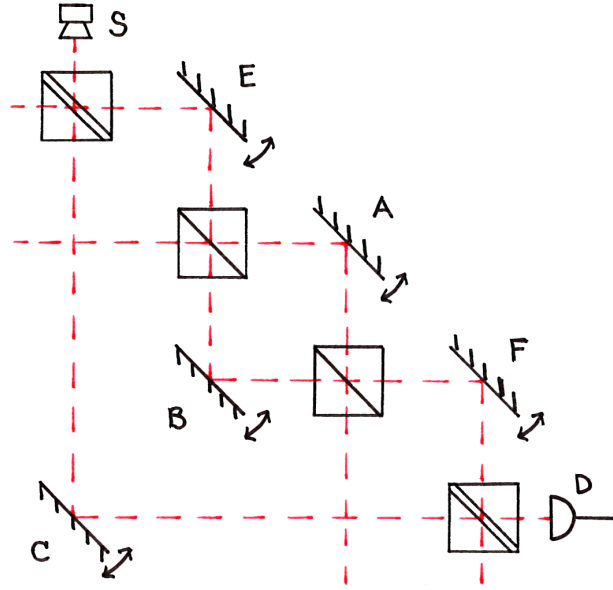


Figure 4.1: A schematic of the nested Mach-Zehnder interferometer. The beam splitters with double lines denote 2:1 beam splitters with $t_{2:1} = 1/\sqrt{3}$, $r_{2:1} = i\sqrt{2/3}$. The mirrors vibrate with unique frequencies thereby marking the paths. S is the source of light and D is a quadrant detector. All spatial paths supported by the interferometer are indicated.

containing only mirror *C*, suggesting an interpretation that the photons did not reach the mirrors *A* and *B* via *E* and *F* but rather as a disconnected part of their path via *C*. The explanation put forward by Danan et al. is based on the two-state vector formalism pioneered by Aharonov et al. [30], linking the presence (or absence) of the peaks at *A, B* (*E, F*) to the simultaneous presence (or the lack of) both forward- and backward-propagating states from the source and the detector.

Once one acknowledges that there is a non-negligible leakage from the inner Mach-Zehnder interferometer due to the fact that the two paths are partially distinguished, i.e., that light from paths containing mirrors *A* and *B* does have a means of reaching the detector, the mystery vanishes. Salih [23] and Saldanha [24] both recognised the significance of the leakage. Salih argued that in the case that true complete destructive interference towards mirror *F* is arranged by setting mirrors *A* and *B* to vibrate at the same frequency but with opposite phase no ground is given for the claims of Danan et al. Saldanha has provided a phenomenological description of the interference by showing numerically that the leakage acts as a first-order correction to the beam profile and that this leakage, when mixing with the light from arm *C*, acts to displace the light beam in the transverse plane, thereby imprinting it with the signatures of mirrors *A* and *B*. Moreover, Danan et al., in the supplementary material appended to their paper¹, have themselves shown that there is a non-negligible leakage by blocking light from mirror *F* and observing the peaks corresponding to mirrors *A* and *B* disappear, although this was interpreted by them as evidence for the lack of electronic noise in the set-up. Bartkiewicz et al. [29] have attempted to provide a minimal fully quantum treatment working in the frequency domain only. However they have assumed that the effect of the vibrating mirrors is to imprint the which-way information using mutually orthogonal (i.e. perfectly distinguishable) states, hence their assumptions as well as results disagree with those of the experiment they are describing.

We put Saldanha's description on a simple analytical footing by modelling the effect of the mirrors as a first-order Hermite-Gaussian perturbation to the light in the interferometer. We derive an effective observable that

¹Supplement I to [1]

shows explicitly that the perturbed portion of the light (carrying the which-way information) must mix with the unperturbed part to give a non-vanishing signal. Within this context we discuss the experimental results presented in [1]. Once the formalism is properly set up simple arguments based on the trade-off between path distinguishability and visibility of interference can be employed to understand the results in all cases, in particular in the counter intuitive case of arm *C* being blocked for which a simple analysis in the two-state vector formalism fails due to weak values becoming singular [25]. Further we show that by appropriate tuning of the path lengths the signatures of certain mirrors may be hidden. We work throughout in the standard quantum optical formalism. The treatment may be transposed to the classical domain by using a coherent state as an input or by replacing annihilation and creation operators by complex field amplitudes. The validity of our quantum treatment extends to fermion interferometry such as that based on neutrons, as all the relevant states and observables can also be constructed for fermions. This chapter is structured as follows: In Section 4.2 we begin by establishing the formalism to be used to describe the interferometer. In Section 4.3, we use the formalism in a quantum path sum approach to obtain an analytical description of the detector output and discuss the immediate observations made possible by our method. In Section 4.4, we match our results to those measured in [1]. In Section 4.5, we propose a small amendment of the system in which novel phenomena can be observed. Finally, we conclude our results.

4.2 Production and detection of slightly tilted Gaussian beams

Let us consider a monochromatic paraxial beam going along the z axis incident at a mirror inclined at an angle $\pi/4 + \vartheta$ to its axis in the xz plane, as illustrated in Fig. 4.2. Inspired by the experiment [1], we will only consider minuscule tilt angles ϑ for which no point of the mirror's surface is displaced more than a fraction of a wavelength over the principal cross section of the beam, as modelled by its beam waist w_0 . Mathematically, we will assume the condition

$$w_0\vartheta \ll \lambda, \quad (4.1)$$

or equivalently

$$kw_0\vartheta \ll 2\pi, \quad (4.2)$$

where λ is the wavelength and $k = 2\pi/\lambda$ the wave number. For the typical values in the experiment [1], $\lambda \approx 700$ nm, $w_0 \approx 1$ mm, and $\vartheta_{\max} \approx 300$ nrad, the peak value of the left hand side of (4.2) is three orders of magnitude smaller than π . For such small angles ϑ , the polarization axes in the reflected beam can be treated as independent of the deviation and a scalar wave description is fully sufficient. Moreover, the reflected beam is simply an analytic continuation of the incident beam in the reflected coordinate system (x_r, y_r, z_r) as per Fig. 4.2.

4.2.1 Mode structure

It will be more practical to work in the untilted coordinate system (x', y', z') where the reflected beam is rotated by the angle 2ϑ . If the incident beam is paraxial with respect to z and described by a scalar complex field $u(x, y, z, t) = \psi(x, y, z)e^{i(kz - \omega t)}$, the reflected beam is paraxial with respect to z' and similarly described by

$$\psi'(x', y', z') = e^{2ik\vartheta x' - 2ik\vartheta^2(z' - z'_M)} \psi(x' - 2\vartheta(z' - z'_M), y', z'), \quad (4.3)$$

where z'_M denotes the z coordinate of the point of intersection of the mirror with the beam axis. This transformation represents a symmetry of the paraxial wave equation (1.22) with respect to shear transforms [31]. At $z' = z'_M$,

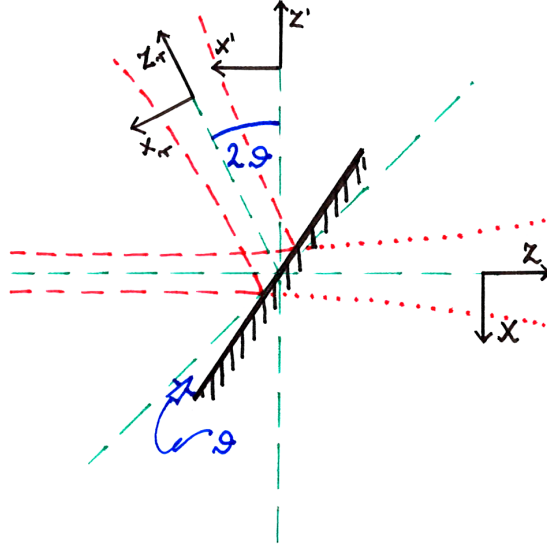


Figure 4.2: Geometry of a tilted mirror and the original and reflected coordinate systems. The system (x_r, y_r, z_r) corresponds to (x, y, z) reflected with respect to the actual location of the mirror while (x', y', z') is reflected with respect to 45° . The y axis is not affected by the reflection ($y = y' = y_r$) and is not depicted. Both the tilt angle ϑ and the beam divergence are vastly exaggerated.

and with the condition (4.2) in mind, (4.3) can be written as

$$\psi'(x', y', z'_M) = \psi(x', y', z'_M) + 2ik\vartheta x' \psi(x', y', z'_M) + O((kw_0\vartheta)^2). \quad (4.4)$$

Specifically, if the incident wave is Gaussian of the form

$$\psi(x, y, z) = \text{HG}_{00}(x, y, z) = \sqrt{\frac{2}{\pi w_0^2}} \frac{z_R}{z_R + iz} e^{-\frac{k(x^2 + y^2)}{2(z_R + iz)}}, \quad (4.5)$$

where w_0 is the beam waist $z_R = \frac{1}{2}kw_0^2$ is the Rayleigh range, the second term of the right hand side of (4.4) represents a first-order Hermite-Gaussian wavefront

$$\text{HG}_{10}(x, y, z) = \sqrt{\frac{2}{\pi w_0^2}} \left(\frac{z_R}{z_R + iz} \right)^2 \frac{2x}{w_0} e^{-\frac{k(x^2 + y^2)}{2(z_R + iz)}} = \frac{2x}{w_0} \frac{z_R}{z_R + iz} \text{HG}_{00}(x, y, z) \quad (4.6)$$

superimposed on the former profile. After the reflection (4.4), the beam profile is described by

$$\psi'(x', y', z') = \text{HG}_{00}(x', y', z') + ikw_0\vartheta \frac{z_R + iz_M}{z_R} \text{HG}_{10}(x', y', z') + O((kw_0\vartheta)^2). \quad (4.7)$$

Thus a slightly displaced Gaussian beam is the superposition of an undisplaced Gaussian beam and a Hermite-Gaussian beam as shown in figure 4.3. This result generalises rather straight forwardly to reflections off of several tilted mirrors, whose angles ϑ allow for slow time variation. We will consider the tilts of all the mirrors, denoted $\vartheta_A(t)$ through $\vartheta_F(t)$, to be bounded by a common ϑ at all times satisfying (4.2). The Gaussian term remains after each reflection with the same amplitude (up to a correction of the order $O[(kw_0\vartheta)^2]$) and represents a ‘‘carrier wave’’ common to the whole optical path. Each of the mirrors adds a first-order Hermite-Gaussian component

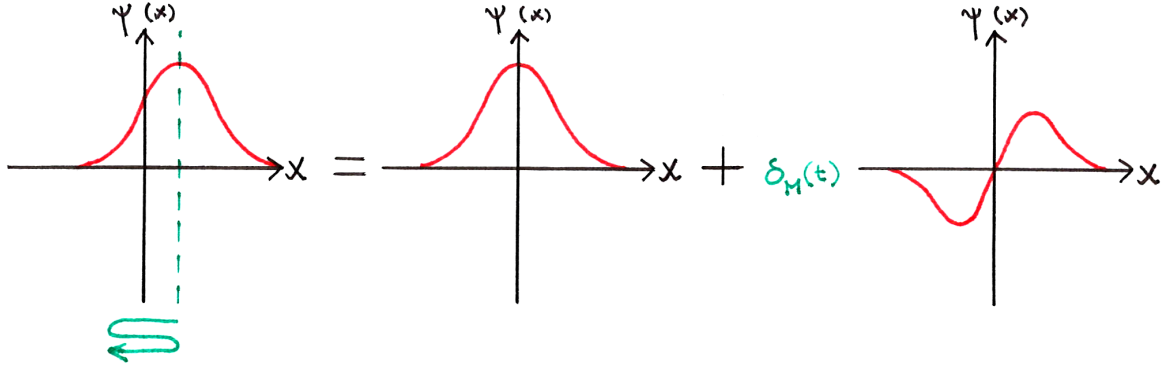


Figure 4.3: A slightly displaced Gaussian beam can be decomposed into an undisplaced Gaussian beam and a Hermite-Gaussian correction with a small amplitude (again undisplaced). Consider the extremal cases. When $\delta_M(t)$ is positive the Hermite-Gaussian correction increases the amplitude on the right ($x > 0$) and decreases it on the left ($x < 0$) thus having shifted the beam to the right. When $\delta_M(t)$ is negative then by identical reasoning the beam is shifted to the left. The time variation between these two extremes, denoted by the green wiggly line, is encoded in the time dependence of $\delta_M(t)$.

with an amplitude

$$\delta_M(t) = ikw_0\vartheta_M(t)\frac{z_R + iz_M}{z_R} \quad (4.8)$$

relative to the carrier wave, where $\vartheta_M(t)$ is the tilt of the mirror $M \in \{A, B, C, E, F\}$ and z_M represents the optical distance from the source, where the beam is collimated. (It is important to add that the rectangular configuration of the interferometer defines the 'x' direction, and thus the orientation of Hermite-Gaussian modes, in every path segment unambiguously.) In fact, summing these contributions is sufficient to describe the effect of several consecutive mirrors. Of course, each of the successive mirrors will also apply a transformation to the side terms added by the previous reflections but these will be second order in $kw_0\vartheta$ and can be neglected.

The mirrors A, B, C, E, F oscillate at frequencies ω_A to ω_F , which are assumed to be all mutually different but each of them many orders of magnitude smaller than ω_0 . (In [1] the former are of the order of hundreds of Hz, as compared to the optical frequency of $\omega_0 = 2.4 \times 10^{15}$ rad/s.) In this case there is no need to take into account any time-frequency uncertainty or finite propagation time effects and the time dependence of the angles $\vartheta_M(t)$ can be simply reflected in an explicit time dependence of the optical state incident at the detector.

The above results are valid for a monochromatic case with an error of $O((\omega_0/\lambda)^{-4})$ due to the paraxial wave approximation used. Under a narrow bandwidth assumption, their validity can be extended to quasi monochromatic waves, affecting only the propagation factor $e^{i(kz - \omega t)}$. The resulting error terms are of the order $O((\Delta\omega/\omega_0)(\omega_0/\lambda)^{-2})$ and for a typical optical laser source of coherence length ~ 1 m are strongly dominated by the former. In other words, we can assume that for a sufficiently narrow vicinity of ω_0 the spatial mode structure does not change significantly.

The mode structure (4.7) from classical optics transfers rather straight forwardly to the quantum treatment of the problem. A single particle with a temporal profile $f(t)$ that satisfies the narrow bandwidth approximation that has reflected off of mirror M is described by

$$|\psi\rangle = \int_{\mathbb{R}} f(t) \left(\hat{a}_{00}^\dagger(t) + ikw_0\vartheta_M(t)\frac{z_R + iz_M}{z_R}\hat{a}_{10}^\dagger(t) \right) dt |\text{vac}\rangle \quad (4.9)$$

where the temporal profile of course satisfies the normalisation condition $\int_{-\infty}^{\infty} |f(t)|^2 dt$. Thus two things happen in superposition at a vibrating mirror when light in the Gaussian mode impinges on it. Light simply gets reflected

with unit amplitude as for a stationary mirror and light reflects off of the mirrors and in addition gets excited into the first order Hermite-Gaussian mode with amplitude $\delta_M(t)$. The sum of the modulus squared of these amplitudes sums to more than unity but that is because the lowest order corrections to the amplitude of reflecting off of a mirror unexcited are second order in δ_M .

4.2.2 Detection

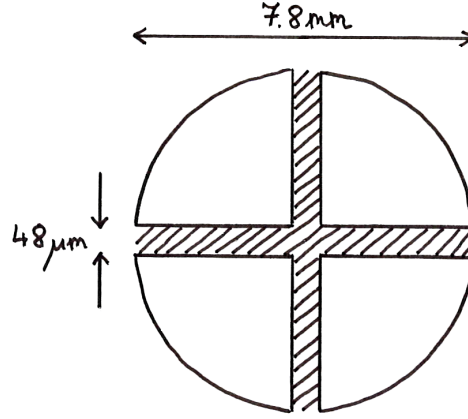


Figure 4.4: A schematic of a quadrant detector. The shaded area is the gap between detectors. The values of detector area radius and gap size are shown for the First Sensor QP50-6-SD2 used in [1].

The measurement of the beam position at the output of the interferometer is done with a quadrant detector. This is an arrangement of four photodetectors in a two by two array as shown in figure 4.4. The active detector area for the quadrant detector used in [1] has a diameter of 7.8mm and the gap between the detectors is $48\mu\text{m}$ [32]. The differences in intensity between the four detectors allow one to measure the position of a laser beam [33] with respect to the centre of the detector. With the 300 nrad tilt of the mirrors the displacement of the beam is at most on the order of microns for an optical setup a few meters long. The diameter of the beam used in the experiment [1] is 1.2 mm. This is exceeded sufficiently by the active detector area for its finite size to not be a factor when integrating over intensity in the transverse plane as detected by the detector. Considering that the beam waist defines a region in which the intensity of the beam drops to $1/e$ of its maximum, losses due to this gap can be neglected as it covers only $\sim 1/20$ of the beam. In effect when considering the intensity measured by half of the detector it can be assumed that the intensity of the entire half-plane is being recorded. Let us now consider a quadrant detector placed further along the beam at $z = z_D$. The idealised model of the detector measures the total intensity difference between two half-planes in the direction of the displacement:

$$\widehat{\Delta I}(t) = \int_{x=0}^{+\infty} \int_{y \in \mathbb{R}} \hat{S}(x, y, z_D, t) dy dx - \int_{x=-\infty}^0 \int_{y \in \mathbb{R}} \hat{S}(x, y, z_D, t) dy dx. \quad (4.10)$$

If, according to (4.7), the modes HG_{00} and HG_{10} are sufficient to describe the state of the beam at any instant, we can restrict the operator to the relevant subspace to get an effective observable. Doing so and carrying out the explicit integration gives

$$\widehat{\Delta I}_e(t) = I_0 \left(e^{-i\zeta(z_D)} \hat{a}_{00}^\dagger(t') \hat{a}_{10}(t') + h.c. \right) \quad (4.11)$$

where

$$I_0 = \hbar\omega_0 \sqrt{\frac{2}{\pi}}, \quad t' = t - \frac{z}{c}, \quad \text{and} \quad \zeta(z_D) = \arctan \frac{z_D}{z_R} \quad (4.12)$$

is the Gouy phase. (We note that if the detector is not geometrically ideal, as assumed above, only the prefactor I_0 changes to reflect the geometry as long as it is symmetric with respect to the axis of the undisplaced beam.) From this formula, we see that it is of great importance that both the carrier Gaussian wave and the Hermite-Gaussian correction are incident at the detector plane simultaneously for a nonzero signal to be obtained. Moreover, the response is linear in both the amplitudes, which will be crucial for allowing sensitivity to first order in the perturbations caused by the mirrors.

Let us examine the expectation value of the observable (4.11) with the state (4.9)

$$\langle \psi | \hat{a}_{00}^\dagger(t') \hat{a}_{10}(t') | \psi \rangle = ikw_0 \vartheta_M(t) \frac{z_R + iz_M}{z_R} |f(t')|^2 \quad (4.13)$$

and hence

$$\langle \psi | \widehat{\Delta I}(t) | \psi \rangle = \langle \psi | \widehat{\Delta I}_e(t) | \psi \rangle = 2kw_0 \vartheta_M(t) I_0 \frac{z_D - z_M}{\sqrt{z_R^2 + z_D^2}} |f(t')|^2. \quad (4.14)$$

where again $t' = t - z/c$ is retarded time. This result illustrates the fact that right after the mirror ($z_D \approx z_M$), the Hermite-Gaussian component only modifies the local phase of the wave profile but the intensity remains parity-symmetric, resulting in zero $\langle \widehat{\Delta I} \rangle$. The further the detector is placed from the mirror, the longer optical length both the waves propagate freely, resulting in their superposition forming a displaced Gaussian profile as argued by Saldanha [24] and producing a nonzero differential signal. With constant I_0 , z_M , and z_D , the differential signal is proportional to $\vartheta_M(t)$ (within the small angle approximation). At large distances the differential intensity saturates at the limit value of $2I_0kw_0\vartheta$. In [1] the mirrors are located at similar positions $z_M \ll z_R$ whereas for the detector it holds that $z_D \lesssim z_R$. In order to illustrate the core of our argument without the burden of unnecessary detail, we will reflect this in the following by leaving out terms of the form z_M/z_R , $M \in \{A, B, C, E, F\}$, so that the term $(z_R + iz_M)/z_R$ in equation (4.8) reduces to 1. That is we work with the limiting value of the observable (4.14) corresponding to the detector being far away from the mirrors. The analysis is equally tractable but less transparent without this simplification.

One more important observation is that (4.14) does not significantly depend on small variations in path length (of the order of λ). This allows us to denote in the following the position of the detector by a single z_D coordinate even in the case of interference of several distinct paths including small differences in optical path length to obtain relative phases.

In the rest of this chapter, we will take the liberty of leaving out the time argument and the second spatial index (which is always zero) of \hat{a} and \hat{a}^\dagger for the sake of brevity, as well as the time argument of $\widehat{\Delta I}$, e.g.,

$$\widehat{\Delta I} = I_0 \left(e^{-i\zeta(z_D)} \hat{a}_0^\dagger \hat{a}_1 + h.c. \right). \quad (4.15)$$

The result (4.14) indicates that any time dependence of the input state will only serve as a prefactor (in retarded time) in the output state within the global assumptions.

4.3 Contribution of the distinct paths

In Fig. 4.1, we can identify three possible spatial paths from the input to the detector, determined by a reflection off the mirrors E, A, F , or E, B, F , or C only. These paths will be denoted by A, B , and C after the mirrors unique to them. Each of these paths enters the path sum with an equal weight of $|t_{2,1}^2| = |r_{2,1}^2 t_{1,1}^2| = |r_{2,1}^2 r_{1,1}^2| = 1/3$ and

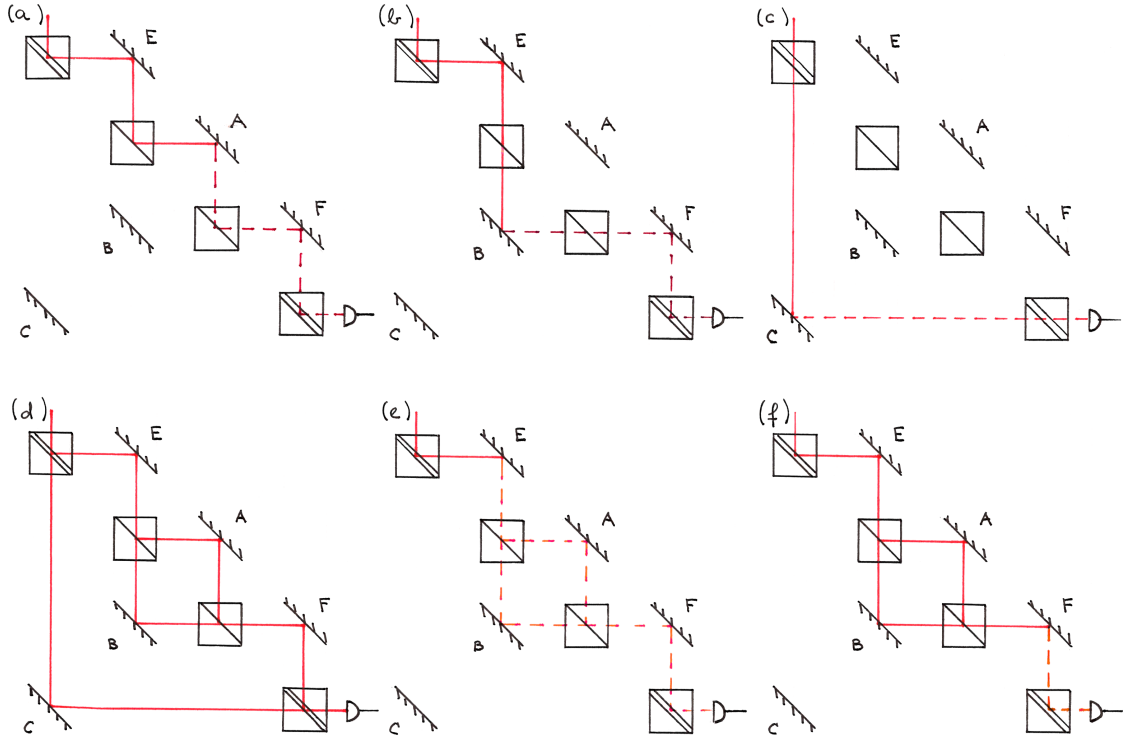


Figure 4.5: All the ways light can traverse the nested Mach-Zehnder interferometer such that it is perturbed by at most one mirror. Interfering paths are shown on the same diagram. Contributions (a)-(c) provide fully decisive which-way information while contributions (e) and (f) provide only partial which-way information in ruling out path C and contribution (d) provides no which-way information.

with a phase $e^{i\phi_{A,B,C}}$ that includes the phase acquired during reflection and transmission. The 2:1 beam splitters are realised by means of polarisers and polarising beam splitters in [1] but in a way that is indistinguishable from polarisation-independent beam splitters with a fixed input polarisation at the measurement stage. As was shown in the previous section each path contributes a Gaussian component $\hat{a}_0^\dagger|\text{vac}\rangle$ with unit amplitude (up to corrections of order δ^2) and a Hermite-Gaussian component $\hat{a}_1^\dagger|\text{vac}\rangle$ with amplitude $\sum_M i\delta_M(t)$ where the summation is over the mirrors along that path. The net contribution of these three paths then to the output state at the detector is

$$|\psi_{\text{out}}(t)\rangle = \frac{1}{3} \left(\alpha_0 \hat{a}_0^\dagger + \sum_{M \in \{A,B,C,E,F\}} \alpha_M(t) \hat{a}_1^\dagger \right) |0\rangle + O(\delta^2), \quad (4.16)$$

where

$$\begin{aligned} \alpha_0 &= e^{i\phi_A} + e^{i\phi_B} + e^{i\phi_C}, \\ \alpha_M(t) &= e^{i\phi_M} i\delta_M(t), \quad M \in \{A,B,C\}, \\ \alpha_M(t) &= \left(e^{i\phi_A} + e^{i\phi_B} \right) i\delta_M(t), \quad M \in \{E,F\}. \end{aligned} \quad (4.17)$$

From this general form of the output state we can make several observations. The Gaussian term, $\hat{a}_0^\dagger|0\rangle$, has the same coefficient (to the first order) as if all the mirrors were stationary with zero tilt angles ϑ_M , therefore it represents the part of the state with full visibility of interference but no distinction between the paths. All of the which-way information (i.e., values dependent on $\vartheta_M(t)$) is contained in the coefficient of the Hermite-Gaussian component $\hat{a}_1^\dagger|0\rangle$ and prevented from further influencing the carrier wave by the orthogonality of the two modes. The amplitude of $\hat{a}_1^\dagger|0\rangle$ is linear in all angles $\vartheta_M(t)$. The constant of proportionality will always be nonzero

for $\alpha_A(t)$, $\alpha_B(t)$, and $\alpha_C(t)$, unless the corresponding path is blocked. However, $\alpha_E(t)$ and $\alpha_F(t)$ in the $\hat{a}_1^\dagger|\text{vac}\rangle$ component are undergoing interference of the same quality as paths A and B do in the $\hat{a}_0^\dagger|\text{vac}\rangle$ component. The last point is a direct consequence of the fact that the terms containing $\delta_A(t)$, $\delta_B(t)$, and $\delta_C(t)$ come from exactly one of the three paths each, while the terms containing $\delta_E(t)$ or $\delta_F(t)$ appear in both paths A and B and therefore interfere the in same way as the carrier Gaussian wave in these two paths. Thus the output state can be split into three components with different characters with respect to path distinguishability. The Gaussian component carries no which-way information. This is shown in figure 4.5 (d) in which all three paths interfere. The Hermite-Gaussian component then breaks further down into two components. The part that corresponds to being marked by mirrors E or F carries partial which-way information in that they exclude path C but these still undergo interference as shown in figures 4.5 (e) and (f) respectively as these mirrors do not distinguish between paths A and B . Finally the component corresponding to being marked by mirror A , B or C shown in figure 4.5 (a), (b) and (c) respectively carries full which-way information.

We propose this simple explanation as a fully traditional alternative to the explanation given in the conclusions section of [1], and moreover, one to be readily foreseen from the fact that which-way marking at mirrors E and F does not distinguish between two interfering paths.

4.4 Analysis of the relevant cases

Due to copyright reasons these figures are removed from the electronic copy.

Please see print version or figure 2 (a) of ref. [1].

Please see print version or figure 2 (b) of ref. [1].

(a) When the inner interferometer is tuned to constructive interference towards mirror F peaks corresponding to all the mirrors are observed.

(b) When the inner interferometer is tuned to destructive interference towards mirror F peaks corresponding to mirrors E and F are not observed.

Please see print version or figure 2 (c) of ref. [1].

Please see print version or figure 5 of Supplement I to ref. [1].

(c) When mirror F is blocked while the inner interferometer is tuned destructive interference towards mirror F only one peak corresponding to mirror C is observed.

(d) When mirror C is blocked while the inner interferometer is tuned destructive interference towards mirror F no peaks are observed.

Figure 4.6: The power spectra presented in [1] (a,b,c) and Supplement I (d) appended to it for the various configurations of the nested Mach-Zehnder interferometer.

For ease of comparison the results of [1] are reproduced in figure 4.6. Quantifying our results, direct applica-

tion of the output state (4.16) to the effective observable (4.15) yields the differential signal as

$$\langle \psi_{\text{out}}(t) | \widehat{\Delta I} | \psi_{\text{out}}(t) \rangle = \frac{2I_0}{9} \sum_M \Re \left(e^{-i\zeta(z_D)} \alpha_0^* \alpha_M(t) \right). \quad (4.18)$$

Inserting for the values of α_M results in meaningful simplification only in the case where the phases ϕ_A , ϕ_B , ϕ_C are equal or differ by integer multiples of π . By setting $e^{i\phi_A} = e^{i\phi_C} = e^{i\Phi}$ and $e^{i\phi_B} = \pm e^{i\Phi}$ in (4.17) one can see that $\alpha_0^* \alpha_M$ is purely imaginary under this restriction and $|\alpha_0|$ takes the value 2 ± 1 for the constructive (+) and destructive (−) interferences arranged in the inner Mach-Zehnder interferometer. The expectation value of the differential intensity is then

$$\langle \psi_{\text{out}}(t) | \widehat{\Delta I} | \psi_{\text{out}}(t) \rangle = \frac{2I_0}{9} \sin \zeta(z_D) |\alpha_0| \left(\delta_A(t) \pm \delta_B(t) + \delta_C(t) + (|\alpha_0| - 1)(\delta_E(t) + \delta_F(t)) \right) + O(\delta^2). \quad (4.19)$$

This result agrees perfectly with the experimental results in [1] in the studied cases with path C opened shown in figures 4.6 (a) and (b). In particular, if all the three paths are aligned for constructive interference, then $e^{i\phi_A} = e^{i\phi_B} = e^{i\phi_C}$ and $|\alpha_0| = 3$. This results in equal sensitivities to displacements from mirrors A, B and C and double sensitivities to displacements from mirrors E and F , which in turn agrees with the 1 : 4 ratios of the peaks in the power spectrum of the intensity. If path B is brought completely out of phase with path A and consequently with C , then $|\alpha_0| = 1$, which explains the same factors in front of the three peaks A, B and C as in the above case as well as the disappearance of any peaks at E and F in the spectral analysis of the signal.

To complete our comparison with [1], we show the correspondence of (4.19) to the experimental results in which paths F and C are individually blocked shown in figures 4.6 (c) and (d) respectively. In the case of path F or C being blocked $e^{i\phi_{A,B}}$ or $e^{i\phi_C}$ must be replaced by zero, respectively, in (4.17). By examining (4.17) and (4.18) the consequences of these conditions may readily be seen. Blocking path F results in a single peak at C as the only non-vanishing coefficients in the output state are $\alpha_C(t)$ and crucially α_0 showing that any light carrying information about the inner Mach-Zehnder interferometer has been prevented from reaching the detector. Blocking path C results in the vanishing of $\alpha_C(t)$ and in $|\alpha_0|$ taking the value $|\exp(i\phi_A) + \exp(i\phi_B)|$. In the case when constructive interference is arranged in the inner Mach-Zehnder interferometer all peaks along the A and B paths show up as the carrier wave reaches the detector via these paths and so do all the perturbations caused by the mirrors along these paths. When destructive interference is arranged, however, α_0 vanishes and—with the carrier wave absent—so does the entire signal.

4.5 Tunability of the peak heights

The analysis presented above shows that it is possible to reproduce the features described in [1] using conventional quantum optical theory without recourse to spatially disconnected paths. We can make some predictions for further effects based on this theory. From (4.9) we can see that if the relative phase of the Gaussian and Hermite-Gaussian components could in principle be modified independently, the differential signal could be artificially strengthened or damped. For example, if the phase of the $\hat{a}_0^\dagger | \text{vac} \rangle$ component was modified by an amount of $\zeta(z_M) - \zeta(z_D) + \frac{\pi}{2}$, the expectation value of $\widehat{\Delta I}$ would become the limit value, as if the detector was placed at infinity. Similarly, if the phase of the Gaussian component was modified by $\zeta(z_M) - \zeta(z_D)$, the differential signal would vanish. Although unexplored in [1], the experiment readily provides means of achieving this. All one needs to do is break the condition of the paths being aligned in phase (or completely out of phase). This can be best illustrated with path C unblocked, paths A and B with opposite phases, and allowing an extra phase shift by statically displacing the mirror C . (In [1] only the mirror B was displaced to control relative phases of the paths.)

In this setting, the values of the coefficients in (4.16) can be written as

$$\begin{aligned}\alpha_0 &= e^{i\phi_C}, \\ \alpha_M(t) &= e^{i\phi_M} i \delta_M(t), \quad M \in \{A, B, C\}, \\ \alpha_E(t) &= \alpha_F(t) = 0\end{aligned}\tag{4.20}$$

and the detector signal as

$$\langle \psi_{\text{out}}(t) | \widehat{\Delta I} | \psi_{\text{out}}(t) \rangle = \frac{2I_0}{9} \left(\sin(\phi_C - \phi_A + \zeta(z_D)) (\delta_A(t) - \delta_B(t)) + \sin \zeta(z_D) \delta_C(t) \right).\tag{4.21}$$

Thus the relative strengths of the peaks at A and B to that of the peak at C can be tuned by simply moving the mirror C . In particular, by matching the phase difference of $\phi_A - \phi_C$ to the Gouy phase $\zeta(z_D)$ (more precisely, to the Gouy phase difference $\zeta(z_D) - \zeta(z_{A,B})$ had the approximation $z_{A,B} \ll z_R$ been not taken) and keeping $\phi_B - \phi_A = \pi$ fixed, the peaks at A and B (or either of them individually for $z_A \neq z_B$) may disappear completely.

4.6 Conclusions

We have modelled the experiment presented in [1] using only waves propagating forward in time and the interference of the possible paths. This allowed us to attribute the disappearance of peaks E and F in transitioning from maximum to minimum possible interference towards mirror F to simple interference of paths in the inner Mach-Zehnder interferometer as mirrors E and F do not distinguish between paths A and B . We have also shown that the simultaneous disappearance of all three remaining peaks when blocking path C while maintaining destructive interference between the other two paths follows from the need for the perturbed wave $\hat{a}_1^\dagger |\text{vac}\rangle$ to mix with the unperturbed carrier wave $\hat{a}_0^\dagger |\text{vac}\rangle$. The necessary presence of $\hat{a}_0^\dagger |\text{vac}\rangle$ for a non-vanishing signal means that interference between all the unblocked paths is a crucial part of the weak which-way measurement.

As a novel contribution to the discussion of this experimental setup we found the crucial dependence of the relative heights of the peaks in [1] on the three phases $\phi_{A,B,C}$ associated with the three path lengths. In particular we have shown that some of these may be made to vanish by tuning the three path lengths. This shows by explicit construction that interpreting the lack of trace of a given mirror in the signal to mean that the photon has not interacted with that mirror is erroneous. Furthermore we have also found a hitherto unexplored tuning of the interferometer in which, without blocking any of the paths, the trace of only mirror C is present in the output signal.

Chapter 5

Two-particle interference

This chapter is concerned with Hong-Ou-Mandel interference in the case of particles possessing several degrees of freedom (DoF). The basic principles are the same as that of chapter 4. The new feature one must take into account here is that some of the alternative paths leading to a particular physical outcome are related by the exchange of particles. Hence the phase relationship of the amplitudes of these alternative paths are defined by the symmetry of the biparticle under particle exchange. Of the three exchanges possible on a biparticle with two degrees of freedom (DoF₁, DoF₂, Particle) only two are independent. We study the interaction of a biparticle with a beam splitter. The beam splitter cares about only one (the spatial) degree of freedom.

The content of this chapter is an original contribution done in collaboration with Václav Potoček and Stephen Barnett published in the Journal of Optics [73].

5.1 Introduction

In a quantum mechanical description identical particles must be treated as indistinguishable. These come in two different families, bosons and fermions, distinguished by their spin or helicity. States describing bosons are symmetric under the exchange of particles and states describing fermions are antisymmetric under the exchange of particles [74, §14].

In the quantum mechanical description of any process different alternatives by which the process might happen add at the amplitude level rather than at the probability level if the two alternatives lead to physically indistinguishable outcomes [11, §1]. It is this that gives rise to interference phenomena. In particular whether identical particles are exchanged or not during a physical process constitute such indistinguishable alternatives. As a result of this bosons and fermions exhibit behaviour quite distinct from one another [75].

This interference due to exchanged alternatives has been demonstrated for photons in the classic experiment of Hong, Ou and Mandel [15] in which one photon is incident on each face of a balanced beam splitter. If the modes occupied by the two particles interfere then the two photons always exit the beam splitter together [3, §6]. This is in contrast to the behaviour for distinguishable particles that exit together with probability 1/2. As the two photons are made indistinguishable by adjusting their arrival times this results in the characteristic Hong-Ou-Mandel dip. This provides a useful tool to demonstrate the interference of two modes [76] also in the case when the distinguishable to indistinguishable transition is achieved by a degree of freedom other than time of arrival [77]. The fermion counterpart to Hong-Ou-Mandel interference has also been demonstrated, by showing that two electrons in the same spin state impinge on a beam splitter and the result is that they never leave in the same arm [14]. This is consistent with the Pauli exclusion principle as both phenomena stem from the same underlying principle that quantum states describing fermions are antisymmetric under exchange of the two par-

ticles.

It is possible for the photons to exhibit fermion-like statistics at a beam splitter by leaving through different ports if the transverse spatial profile [78] or polarisation state [79] is chosen suitably. In both cases these are antisymmetric states forcing the state describing the spatial path degree of freedom to be antisymmetric.

The key feature resulting in the different behaviour of bosons and fermions at a beam splitter is the different symmetry that states describing them satisfy in the path degree of freedom [8]. In this chapter we consider particles with multiple quantum numbers and show that control can be exerted over how the overall exchange symmetry is distributed between the exchange symmetries of the two different quantum numbers. We use path and orbital angular momentum as physical examples of these quantum numbers, allowing us to probe the symmetry in the path quantum numbers using only a beam splitter. We show that for both bosons and fermions it is possible to obtain the full range of allowed output statistics exhibited by bosons, fermions or mixtures of them. This includes the extremal cases of purely bosonic and purely fermionic statistics. It is implicit in the construction of our chosen states that the orbital angular momentum state can have arbitrarily large dimensionality.

5.2 Indistinguishable particles with two degrees of freedom

In the case of two degrees of freedom, the indices i and j in (3.42) are replaced by pairs of numbers (i, u) and (j, v) . To describe a state of a particle with two degrees of freedom two numbers need to be specified in place of just one. Here i, j are two modes of the first degree of freedom (later to be the port modes) and u, v are two modes of the second degree of freedom (these will be angular momenta). In the particle pair creation operators we group the indices of the same degree of freedom together according to

$$\hat{a}_{iu}^\dagger \hat{a}_{jv}^\dagger = \hat{A}_{ijuv}^\dagger \quad (5.1)$$

so that the second degree of freedom is seen as an extension to the first in (3.39). We distinguish the degrees of freedom only by numbers as there is no restriction on what these may be other than that they must be independent degrees of freedom. For example position and spin coordinates are a suitable choice of degrees of freedom for this analysis however position and momentum coordinates are not as these two degrees of freedom act non-trivially on the same state space. A position state can be expressed as a superposition of momentum modes so exchanging the momentum properties of two particles is necessarily accompanied by exchanging the position properties. This is the case for all conjugate degrees of freedom, e.g. angular position and angular momentum, but also more generally for any two noncommutative observables, for example x and y components of spin.

5.2.1 Exchange operators

Either of the exchanges of the numbers corresponding to *only one* of the degrees of freedom

$$\hat{X}^{(1)} : \hat{A}_{ijuv}^\dagger |\text{vac}\rangle \mapsto \hat{A}_{jiuv}^\dagger |\text{vac}\rangle, \quad (5.2)$$

$$\hat{X}^{(2)} : \hat{A}_{ijuv}^\dagger |\text{vac}\rangle \mapsto \hat{A}_{ijvu}^\dagger |\text{vac}\rangle \quad (5.3)$$

on its own is no longer sufficient to implement particle exchange. Particle exchange now means the simultaneous exchange of *both properties* [16, 74]. The equivalence between the exchange of particles and of occupied modes remains valid only by thinking of modes in a slightly more general way. We consider modes to be composite if they are specified by several constituent modes from distinct degrees of freedom. The exchange of the two occupied composite modes as outlined above is then equivalent to particle exchange. If the two particles are degenerate

with respect to one of the constituent degrees of freedom we need not consider that degree of freedom as part of the composite mode for the analysis of exchange symmetries as long as this degeneracy remains. In this way degeneracy with respect to a degree of freedom corresponds to the removal of that degree of freedom. Degeneracy with respect to a composite degree of freedom means degeneracy with respect to all its constituent degrees of freedom.

In the case of multiple degrees of freedom, one can always partition a composite degree of freedom into two constituent degrees of freedom which themselves may or may not be further decomposable. For this reason it is sufficient to consider only two degrees of freedom to illustrate the principal difference between one and multiple degrees of freedom.

For two degrees of freedom the equivalence between particle exchange and the exchange of modes takes the form [16, §58]

$$\hat{X}^{(1)}\hat{X}^{(2)} = \hat{X}^{(2)}\hat{X}^{(1)} = \hat{X}^{(\hat{a}^\dagger)}. \quad (5.4)$$

Symmetry under exchange of particles is distributed between the two constituent degrees of freedom in the sense of the above relation. The exchange operators are Hermitian and square to the identity so they each have possible eigenvalues of 1 or -1 . The combination of (5.4) and of (3.37) gives the constraint on the eigenvalues of exchange operators

$$X^{(1)}X^{(2)} = (-1)^{2s}. \quad (5.5)$$

If the symmetries in the two degrees of freedom are each well-defined, bosons must have the same exchange symmetry in both whereas fermions must have opposite symmetries [79]. Mathematically one can express this as

$$\hat{S}^{(1)}\hat{S}^{(2)} + \hat{A}^{(1)}\hat{A}^{(2)} = \hat{S}^{(\hat{a}^\dagger)} \quad (5.6)$$

$$\hat{S}^{(1)}\hat{A}^{(2)} + \hat{A}^{(1)}\hat{S}^{(2)} = \hat{A}^{(\hat{a}^\dagger)} \quad (5.7)$$

where the symmetriser and antisymmetriser (for $k = 1, 2, \hat{a}^\dagger$) are constructed out of the exchange operators as

$$\hat{S}^{(k)} = \frac{\mathbb{1} + \hat{X}^{(k)}}{2} \quad \hat{A}^{(k)} = \frac{\mathbb{1} - \hat{X}^{(k)}}{2}. \quad (5.8)$$

When looking at only one of the degrees of freedom it is possible to have a state that does not have a well defined symmetry under the exchange of mode numbers and yet does not violate the requirement (3.37) that the particle pair are either bosons or fermions and not a superposition of the two

$$|\psi, s\rangle = \psi_S |X^{(1)} = 1, s\rangle + \psi_A |X^{(1)} = -1, s\rangle. \quad (5.9)$$

This is not possible if there is only one degree of freedom available or equivalently when degeneracy in all but one degree of freedom is imposed on the particle pair. Unless ψ_S or ψ_A vanish applying either $\hat{X}^{(1)}$ or $\hat{X}^{(2)}$ to this state will produce a state linearly independent of $|\psi, s\rangle$. This is what is meant by the state of the first or second degree of freedom not having a well defined symmetry. However it will always be the case that after applying both exchange operators one obtains $(-1)^{2s}|\psi, s\rangle$. Each of the exchange operators need not correspond to symmetries of the state but their product must.

5.2.2 Biparticle excitations of modes

Let us consider explicitly the particle symmetrised (\hat{B}^\dagger) and particle antisymmetrised (\hat{F}^\dagger) biparticle modes. Port modes and orbital angular momentum modes are used for the first and second degree of freedom respectively from here on. This choice is due to a feasible experimental implementation for photons discussed towards the end of the

chapter. It is not necessary to make a particular choice for the degrees of freedom until the next section but it is linguistically convenient. The port modes available to the particles are 1 and 2 of which they may occupy the same one (an unavoidable consequence of considering biparticle evolution under the beam splitter even if the starting point is particles occupying different ports). However it shall be ensured that the angular momentum modes l and j available to the biparticle are distinct ($l \neq j$). If the angular momentum numbers were to be identical then the physics would reduce to that of Hong-Ou-Mandel interference for a biparticle with a single degree of freedom as discussed in chapter 2. All the possible such biparticle states are obtained by

$$\hat{B}_{11lj}^\dagger = \frac{1}{2}\{\hat{a}_{1l}^\dagger, \hat{a}_{1j}^\dagger\}, \quad \hat{F}_{11lj}^\dagger = \frac{1}{2}[\hat{a}_{1l}^\dagger, \hat{a}_{1j}^\dagger], \quad (5.10)$$

$$\hat{B}_{22lj}^\dagger = \frac{1}{2}\{\hat{a}_{2l}^\dagger, \hat{a}_{2j}^\dagger\}, \quad \hat{F}_{22lj}^\dagger = \frac{1}{2}[\hat{a}_{2l}^\dagger, \hat{a}_{2j}^\dagger], \quad (5.11)$$

$$\hat{B}_{12lj}^\dagger = \frac{1}{2}\{\hat{a}_{1l}^\dagger, \hat{a}_{2j}^\dagger\}, \quad \hat{F}_{12lj}^\dagger = \frac{1}{2}[\hat{a}_{1l}^\dagger, \hat{a}_{2j}^\dagger], \quad (5.12)$$

$$\hat{B}_{21lj}^\dagger = \frac{1}{2}\{\hat{a}_{2l}^\dagger, \hat{a}_{1j}^\dagger\} \quad \text{and} \quad \hat{F}_{21lj}^\dagger = \frac{1}{2}[\hat{a}_{2l}^\dagger, \hat{a}_{1j}^\dagger] \quad (5.13)$$

acting on the vacuum. In (5.10) and (5.11) (i.e. when both particles are in the same port mode) one may as well put the symmetrising brace $\{\}$ around lj for the \hat{B}^\dagger 's and the antisymmetrising braces $[\]$ around lj for the \hat{F}^\dagger 's. As the port mode is necessarily exchange symmetric ($X^{(1)} = 1$), due to the two numbers being identical, the particle exchange symmetry defines the angular momentum exchange symmetry ($\hat{X}^{(2)} = \hat{X}^{(a^\dagger)}$).

In (5.12) and (5.13) (i.e. when modes of both the port degree of freedom and the angular momentum degree of freedom are distinct) this is however not the case. Each of these is composed in equal parts of angular momentum exchange symmetric and antisymmetric pieces

$$\hat{B}_{12lj}^\dagger = \hat{A}_{\{12\}\{lj\}}^\dagger + \hat{A}_{[12][lj]}^\dagger \quad \hat{B}_{21lj}^\dagger = \hat{A}_{\{12\}\{lj\}}^\dagger - \hat{A}_{[12][lj]}^\dagger \quad (5.14)$$

$$\hat{F}_{12lj}^\dagger = \hat{A}_{\{12\}\{lj\}}^\dagger + \hat{A}_{[12][lj]}^\dagger \quad \hat{F}_{21lj}^\dagger = \hat{A}_{\{12\}\{lj\}}^\dagger - \hat{A}_{[12][lj]}^\dagger. \quad (5.15)$$

The relations (5.14) and (5.15) are re-statements of (5.6) and (5.7) respectively in terms of creation operators. However the defining property (for the present purposes) of the biparticle modes (5.12) and (5.13) is a one-to-one correspondence between port mode numbers and angular momentum numbers (1 goes with l and 2 goes with j in (5.12) and the converse is true in (5.13)). The sense in which this correspondence is to be understood is that when the biparticle creation operators are written out in terms of single particle creation operators 1 and l are in the subscript of the same creation operator and so are 2 and j in (5.12) and of course the converse pairing is true for (5.13). \hat{A}_{12lj}^\dagger can be interpreted as the particle with angular momentum l being in port 1 and the particle with angular momentum j being in port 2 (where \hat{A}^\dagger may be either \hat{B}^\dagger or \hat{F}^\dagger). The converse relation between port mode numbers and angular momentum numbers is true for \hat{A}_{21lj}^\dagger .

5.3 Beam splitter

In a Hong-Ou-Mandel experiment with such bipoarticles the outcome in which angular momentum l ends up in output port 1 is physically distinct from the outcome in which angular momentum l ends up in output port 2. The particle represented by (5.12) and (5.13) are in this sense distinguishable. It is worth noting that the particles are only distinguishable in this sense as long as there is no process that can transfer angular momentum between the two particles.

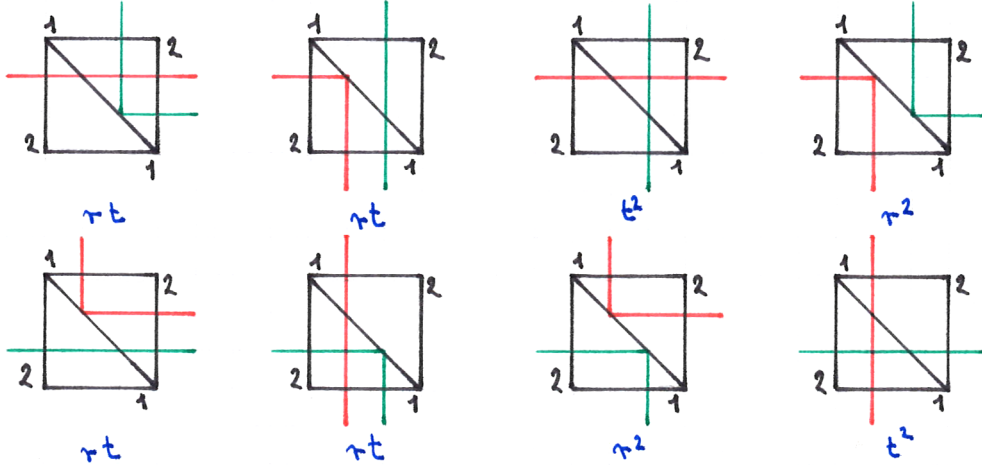


Figure 5.1: All the possible distinct outcomes derived from two possible inputs in a Hong-Ou-Mandel experiment with a particle carrying angular momentum l (green) and a particle carrying angular momentum j (red). The two rows represent inputs that are angular momentum exchanged alternatives of each other. Each column contains a single physical outcome, hence processes in the same column interfere with each other. These diagrams correspond to the bottom two rows of matrix elements in (5.16).

$$\begin{pmatrix} \hat{A}_{11l,j}^\dagger \\ \hat{A}_{22l,j}^\dagger \\ \hat{A}_{12l,j}^\dagger \\ \hat{A}_{21l,j}^\dagger \end{pmatrix} \rightarrow \begin{pmatrix} t^2 & r^2 & rt & rt \\ r^2 & t^2 & rt & rt \\ rt & rt & t^2 & r^2 \\ rt & rt & r^2 & t^2 \end{pmatrix} \begin{pmatrix} \hat{A}_{11l,j}^\dagger \\ \hat{A}_{22l,j}^\dagger \\ \hat{A}_{12l,j}^\dagger \\ \hat{A}_{21l,j}^\dagger \end{pmatrix} \quad (5.16)$$

Where \hat{A}^\dagger may be substituted by either \hat{B}^\dagger or \hat{F}^\dagger . This mimicks the statistics for distinguishable particles. To make the particle pair indistinguishable one needs to remove the association between the values of the two degrees of freedom. This can be done by (anti)symmetrising either the first or the second degree of freedom numbers with respect to exchange. Doing this to either degrees of freedom are equivalent due to the link between the two via particle exchange (5.4). To understand how the beam splitter acts on two particle multimode states it is more convenient to consider (anti)symmetrising in the port mode degree of freedom as that is the degree of freedom that the beam splitter manipulates. In the basis in which the biparticles are symmetrised and antisymmetrised in the port modes the matrix representation of \widehat{BS} takes the form

$$\begin{pmatrix} \frac{1}{\sqrt{2}}(\hat{A}_{11l,j}^\dagger + \hat{A}_{22l,j}^\dagger) \\ \frac{1}{\sqrt{2}}(\hat{A}_{12l,j}^\dagger + \hat{A}_{21l,j}^\dagger) \\ \frac{1}{\sqrt{2}}(\hat{A}_{11l,j}^\dagger - \hat{A}_{22l,j}^\dagger) \\ \frac{1}{\sqrt{2}}(\hat{A}_{12l,j}^\dagger - \hat{A}_{21l,j}^\dagger) \end{pmatrix} \rightarrow \begin{pmatrix} r^2 + t^2 & 2rt & 0 & 0 \\ 2rt & r^2 + t^2 & 0 & 0 \\ 0 & 0 & 1 & 0 \\ 0 & 0 & 0 & 1 \end{pmatrix} \begin{pmatrix} \frac{1}{\sqrt{2}}(\hat{A}_{11l,j}^\dagger + \hat{A}_{22l,j}^\dagger) \\ \frac{1}{\sqrt{2}}(\hat{A}_{12l,j}^\dagger + \hat{A}_{21l,j}^\dagger) \\ \frac{1}{\sqrt{2}}(\hat{A}_{11l,j}^\dagger - \hat{A}_{22l,j}^\dagger) \\ \frac{1}{\sqrt{2}}(\hat{A}_{12l,j}^\dagger - \hat{A}_{21l,j}^\dagger) \end{pmatrix} \quad (5.17)$$

where again \hat{A}^\dagger may be substituted by either \hat{B}^\dagger or \hat{F}^\dagger as the remaining choice in exchange symmetry of the angular momentum degree of freedom accommodates either. This now looks like the behaviour for indistinguishable particles (3.52) with the difference that all four transformations are now possible for both bosons and fermions. This means in particular that for states neither symmetric nor antisymmetric in the port mode degree of freedom $\hat{A}_{12l,j}^\dagger$, which is now a possibility, only the antisymmetric component gives rise to coincidence counts after the beam splitter.

In (5.17) the port modes have been (anti)symmetrised with respect to \hat{M} . However that means that they are also (anti)symmetrised with respect to the port mode exchange operator $\hat{X}^{(P)}$. The relationship between the eigenstates

of the port mode swap \hat{M} and port mode exchange $\hat{X}^{(P)}$ operators is shown in table 5.1.

	$\chi^{(P)} = 1$	$\chi^{(P)} = -1$
$M = 1$	$\hat{A}_{11lj}^\dagger + \hat{A}_{22lj}^\dagger$ $\hat{A}_{12lj}^\dagger + \hat{A}_{21lj}^\dagger$	Not possible
$M = -1$	$\hat{A}_{11lj}^\dagger - \hat{A}_{22lj}^\dagger$	$\hat{A}_{12lj}^\dagger - \hat{A}_{21lj}^\dagger$

Table 5.1: Port symmetry basis for two particle states classified according to both port mode swap and port mode exchange operator eigenvalues.

5.4 General one particle per port input state

Let us assume for notational purposes that the input state is such that the two particles occupy distinct port modes. Recall that in addition to this it is assumed that the particles occupy distinct angular momentum modes. Given this let ψ_{lj} and ψ_{jl} denote the amplitudes of the two physically distinct ways in which the two distinct angular momenta can be assigned to the two distinct port modes. The first index denotes the angular momentum in port 1 and the second index denotes the angular momentum in port 2. The angular momentum exchange symmetric and antisymmetric states can be thought of as superpositions of the two distinct ways in which the angular momenta can be distributed among the two port modes.

A general input state that contains one particle in each input port with an angular momentum distribution can in general be split into symmetric and antisymmetric components with respect to angular momentum exchange. For a state under the assumptions of the previous paragraph this looks like

$$|\text{in}\rangle = \sum_{l \neq j} \psi_{lj} \hat{A}_{12lj}^\dagger |\text{vac}\rangle = \sum_{j < l} \left(\psi_{lj} \hat{A}_{12lj}^\dagger + \psi_{jl} \hat{A}_{12jl}^\dagger \right) |\text{vac}\rangle = 2 \sum_{j < l} \left(\psi_{(lj)} \hat{A}_{12(lj)}^\dagger + \psi_{[lj]} \hat{A}_{12[lj]}^\dagger \right) |\text{vac}\rangle, \quad (5.18)$$

where \hat{A}^\dagger may be either \hat{B}^\dagger or \hat{F}^\dagger if the port mode exchange symmetry is the same or the opposite of the angular momentum exchange symmetry respectively. The factor of two in the last expression arises from the use of the symmetrisation and antisymmetrisation notation around the index pairs. The angular momentum exchange symmetry properties of a state parametrised in this way may readily be classified by the symmetry properties of the matrix Ψ composed of matrix elements ψ_{lj} . The most convenient feature of representing the state by the matrix Ψ is that states related by the exchange of angular momentum numbers correspond to elements of the matrix Ψ that are related by transposition. The diagonal terms correspond to components of the state that are degenerate in angular momentum (not included in (5.18) but shall be dealt with briefly towards the end of the next section) and the off-diagonal symmetric and antisymmetric components under transposition correspond to angular momentum exchange symmetric and antisymmetric states respectively. Two special classes of states will be used in the following. These are states for which the sum of angular momenta is well defined (i.e. $l + j$ is the same for each term in (5.18)) and states for which the difference in the two angular momenta is well defined. (For one particle per port states let the difference in angular momenta be defined as the angular momentum in port 2 minus the angular momentum in port 1 for consistency in the use of minus signs.) In matrix form these are states

that have non-zero elements along a single diagonal and along a single anti-diagonal respectively, for example

$$\Psi_{\Sigma l=1} = \begin{pmatrix} & & & & \\ & 0 & 0 & 0 & \ddots \\ & 0 & 0 & \psi_{01} & \\ & 0 & \psi_{10} & 0 & \\ & \ddots & & & \end{pmatrix} \quad \Psi_{\Delta l=1} = \begin{pmatrix} & & & & \\ & \ddots & & & \\ & 0 & \psi_{-10} & 0 & \\ & 0 & 0 & \psi_{01} & \\ & 0 & 0 & 0 & \ddots \end{pmatrix}. \quad (5.19)$$

Note that as the angular momentum numbers parametrising the entries extend to infinity in both directions the element ψ_{00} is in the middle of the matrix. The ability to introduce a phase between the lower left and upper right triangles of Ψ allows one to tune the exchange symmetry of the angular momentum state. Consider the case in which these exchanged alternatives occur with amplitudes equal in magnitude but differing in phase

$$\psi_{jl} = e^{i\phi(l,j)}\psi_{lj}. \quad (5.20)$$

From rearranging the above expression so that the relative phase is expressed on the left hand side one finds that the phase must satisfy

$$\phi(l,j) = -\phi(j,l). \quad (5.21)$$

If the amplitudes of the one particle per port input state satisfy the restriction (5.20) then the angular momentum exchange symmetric and antisymmetric components are modulated by $\phi(l,j)$ according to

$$\psi_{(lj)} = \frac{1}{2} \left(1 + e^{i\phi(l,j)} \right) \psi_{lj} = e^{-i\frac{\phi(l,j)}{2}} \cos\left(\frac{\phi(l,j)}{2}\right) \psi_{lj} \quad (5.22)$$

$$\psi_{[lj]} = \frac{1}{2} \left(1 - e^{i\phi(l,j)} \right) \psi_{lj} = -ie^{-i\frac{\phi(l,j)}{2}} \sin\left(\frac{\phi(l,j)}{2}\right) \psi_{lj}. \quad (5.23)$$

Note that while control is exerted over the angular momentum exchange symmetry of the state explicitly by the relative phase between the angular momentum exchanged alternatives the port exchange symmetry is necessarily also controlled by virtue of the restriction (5.4).

Only the port exchange antisymmetric part of the state will lead to coincidence counts after a 50:50 symmetric beam splitter according to (5.17). Thus this control over phase between the distinguishable alternatives $\hat{a}_{1l}^\dagger \hat{a}_{2j}^\dagger$ and $\hat{a}_{1j}^\dagger \hat{a}_{2l}^\dagger$ translates directly into variation in coincidence counts. In general the amount of variation introduced into the coincidence counts is dependent on the values of l and j .

Consider the special case when the exchanged alternatives of all angular momentum pairs are related by the same relative phase

$$\psi_{jl} = e^{i\text{sgn}(l-j)\vartheta} \psi_{lj}. \quad (5.24)$$

For a state of this type the phase between interfering terms is the same for all interfering pairs of biparticle modes. The input state (5.18) separates cleanly into symmetric and antisymmetric parts

$$|\text{in}\rangle = 2e^{-i\frac{\vartheta}{2}} \left(\cos\left(\frac{\vartheta}{2}\right) \sum_{j<l} \psi_{lj} \hat{A}_{12[lj]}^\dagger - i \sin\left(\frac{\vartheta}{2}\right) \sum_{j<l} \psi_{lj} \hat{A}_{12[lj]}^\dagger \right) |\text{vac}\rangle. \quad (5.25)$$

This is not a requirement but makes the demonstration of the effect clear as the coincidence counts of all angular momentum components are suppressed by the same amount for a given value of the parameter ϑ hence angular momentum dependent detection is not required to observe the functional dependence of coincidence counts on the relative phase.

(after a reflection of the transverse spatial profile in port 2) produces a state of exactly the required form (5.26) for the demonstration of multimode Hong-Ou-Mandel interference. For $\lambda = 1$ this looks like

$$\Psi_{\lambda=1} = \frac{1}{\sqrt{2}} \begin{pmatrix} & & & & & & \\ & \ddots & & & & & \\ \ddots & 0 & c_{-21} & 0 & 0 & 0 & \\ & c_{-12} & 0 & c_{-10} & 0 & 0 & \\ & 0 & c_{01} & 0 & c_{0-1} & 0 & \\ & 0 & 0 & c_{10} & 0 & c_{1-2} & \\ & 0 & 0 & 0 & c_{2-1} & 0 & \ddots \\ & & & & & \ddots & \end{pmatrix} \quad (5.28)$$

where the coefficients c_{lj} are the amplitudes of a biphoton being produced by downconversion with angular momentum l and j in ports 1 and 2 respectively. The sum of the indices in each of the antidiagonals indicates which component of (5.27) that antidiagonal originated from. For an arbitrary λ the indices of the antidiagonals sum to $\pm|\lambda|$ and the two antidiagonals are separated by $2|\lambda| - 1$ antidiagonals composed of only 0's. The property that the interfering terms are present with equal amplitudes is ensured by the fact that the amplitudes do not depend on which photon has which angular momentum ($c_{lj} = c_{jl}$) and that only the magnitudes of the angular momenta determine the amplitude associated with downconversion ($c_{lj} = c_{|l||j|}$) [63]. Due to these symmetries of c_{lj} a state so produced contains only angular momentum exchange symmetric terms to begin with

$$\frac{1}{\sqrt{2}} \sum_{l=-L}^{L-\lambda} (c_{l,-l-\lambda}|l, l+\lambda\rangle + c_{l+\lambda,-l}|l+\lambda, l\rangle) = \sum_{l=-L}^{L-\lambda} c_{|l|,|l+\lambda|} \frac{|l, l+\lambda\rangle + |l+\lambda, l\rangle}{\sqrt{2}}. \quad (5.29)$$

Upon introducing a phase by rotation of port 2 before the beam splitter, as illustrated in Figure 5.2, the exchange antisymmetric part is introduced

$$\sum_{l=-L}^{L-\lambda} c_{|l|,|l+\lambda|} e^{i(l+\frac{\lambda}{2})} \left[\cos\left(\frac{\lambda\theta}{2}\right) \frac{|l, l+\lambda\rangle + |l+\lambda, l\rangle}{\sqrt{2}} + i \sin\left(\frac{\lambda\theta}{2}\right) \frac{|l, l+\lambda\rangle - |l+\lambda, l\rangle}{\sqrt{2}} \right]. \quad (5.30)$$

Due to typographic reasons (a lot of information being contained in the indices) from (5.29) onward we switch to Dirac notation $\hat{B}_{12l,j}^\dagger|\text{vac}\rangle = |l, j\rangle$ where the first number in the ket represents the angular momentum in port 1 and the second number in the ket represents the angular momentum in port 2. In this notation only the angular momentum exchange symmetry is given explicitly, the port exchange symmetries are left implicit.

If the pump beam were to be in the superposition ($|\text{OAM}_{\text{pump}} = \lambda\rangle - |\text{OAM}_{\text{pump}} = -\lambda\rangle$)/ $\sqrt{2}$ then the downconverted state would have only angular momentum exchange antisymmetric terms to begin with. These two possible pump beams for $\lambda = 1$ correspond to first order Hermite-Gaussian modes oriented at right angles to each other. These were used to demonstrate the existence of both peaks and dips in multimode Hong-Ou-Mandel interference [78]. As photons are bosons the angular momentum and the port exchange symmetries must be the same. Further we know that only the port antisymmetric states give rise to coincidence counts after passing through a symmetric 50:50 beam splitter. Thus the variation in coincidence counts is expected to vary as

$$\sin^2\left(\frac{\lambda\theta}{2}\right). \quad (5.31)$$

If the same experiment is run with a Gaussian pump (zero angular momentum) then after a reflection in one of the arms we have the state

$$\sum_{l=-L}^L c_{ll}|l, l\rangle. \quad (5.32)$$

While the rotation of one of the arms introduces a phase that is not global it does not lead to a variation of coincidence counts as there are no two two-particle terms in this sum that are interfering. The only effect to be observed is Hong-Ou-Mandel interference irrespective of the introduced phase. The root cause of this is that the two angular momentum numbers in each of the ports is the same in each term in (5.32) so no antisymmetric angular momentum state can be constructed and the problem reduces to Hong-Ou-Mandel interference with only one degree of freedom. This could in principle be used for calibration or as a control run to make sure that no variation in coincidence counts is attributable to some other feature of the experiment.

Yingwen Zhang *et al.* [81] have performed this experiment with the state obtained directly from downconversion run with a pump beam of zero angular momentum

$$\sum_{l \neq 0} c_{l,-l} |l, -l\rangle = \sum_{l=1}^L c_{l,l} (|l, -l\rangle + |-l, l\rangle). \quad (5.33)$$

which does not have the property that the angular momentum difference is the same between the two ports for all terms. Nevertheless the same method of introducing a relative phase still has the effect of rotating between the exchange symmetric and exchange antisymmetric subspaces

$$\sum_{l=1}^L \sqrt{2} c_{l,l} \left[\cos(l\theta) \frac{|l, -l\rangle + |-l, l\rangle}{\sqrt{2}} - i \sin(l\theta) \frac{|l, -l\rangle - |-l, l\rangle}{\sqrt{2}} \right]. \quad (5.34)$$

From the above expression it is clear that the angular momentum symmetric subspace vanishes for $l\theta = (2n + 1)\frac{\pi}{2}$ where n is an integer hence for the choice of $\theta = \pi/2$ only the odd valued angular momenta give rise to coincidence counts. In their version of the experiment the angular momentum dependence of the coincidence count suppression is exploited to act as an angular momentum parity filter.

5.6 Conclusions

We have shown that the statistics of particles incident on a beam splitter can be tuned if they possess an additional degree of freedom. The range of statistics attainable includes that of identical bosons, identical fermions and those of distinguishable particles. The entire range of behaviour is attainable in implementations whether the underlying particles are bosons or fermions. This sheds new light on the role of the particle type in interference experiments and means of overriding the natural statistics induced by spin, or as a convenient way of studying bosonic and fermionic as well as intermediate statistics in a single experiment. Alternatively, one could use the theory presented in the main text to inquire on the symmetry properties of a given two-particle state.

We proposed an experimental set-up by which the above concepts can be tested using angular momentum-entangled photons generated by spontaneous parametric down conversion. In this scheme the change attained in the output statistics depends on the angular momentum of the pump beam and a rotation angle.

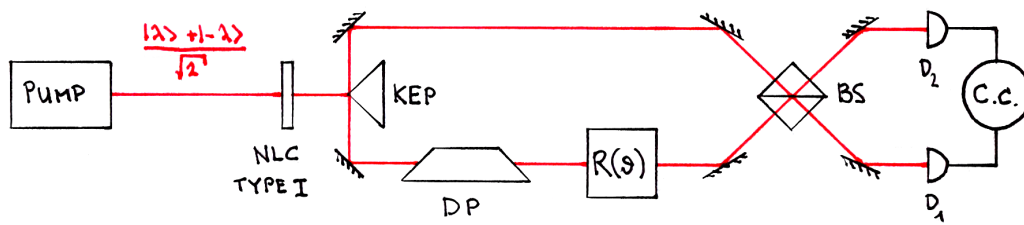


Figure 5.2: The $\frac{1}{\sqrt{2}}(|\lambda\rangle + |-\lambda\rangle)$ pump beam illuminates a non-linear crystal (NLC) that performs type I downconversion. The resulting state is split into two arms by a knife edge prism (KEP). In the bottom arm the angular momentum is flipped using a Dove prism (DP) and a rotation is performed using a system of 2 more Dove prisms (note that a single Dove prism rotated appropriately about the beam axis can perform the composite reflection and rotation). This setup is also suitable for use with an $|\lambda = 0\rangle$ pump to illustrate that an angular momentum degenerate state cannot be affected by a rotation in arm 1.

Chapter 6

Slow light in free space

This chapter deals with how the group velocity of a pulse of light is affected by the transverse spatial structure of the mode that the pulse is excited in. It is important to note that by “transverse” we mean the plane transverse to the propagation direction. Any spatial structure in this plane is achieved by a distribution of k -vectors not all aligned with the propagation direction. As one would expect from an intuitive geometrical picture the resulting delay is given by ‘how much’ the k -vectors are off by in pointing in the propagation direction.

This chapter is based on work done in collaboration with Václav Potoček, Fiona Speirits and Stephen Barnett in the Quantum Theory group, with Jaqui Romero, Daniel Giovannini and Miles Padgett in the Optics group who performed the experiment and with Daniele Faccio from Heriott Watt University [2].

6.1 Introduction

The speed of light is trivially given as $\frac{c}{n}$, where c is the speed of light in free space and n is the refractive index of the medium. In free space, where $n = 1$, the speed of light is simply c . We show that the introduction of transverse structure to the light beam reduces the group velocity by an amount depending upon the aperture of the optical system. The delay corresponding to this reduction in the group velocity can be greater than the optical wavelength and consequently should not be confused with the $\approx \pi$ Gouy phase shift [82, 83]. We measure the delay as a function of the transverse spatial structure of single photons.

The slowing down of light that we observe in free space should also not be confused with slow, or indeed fast, light associated with propagation in highly nonlinear or structured materials [84, 85]. Even in the *absence* of a medium, the modification of the speed of light has previously been known. For example, within a hollow waveguide, the wave vector along the guide is reduced below the free-space value, leading to a phase velocity $v^{(\phi)}$ greater than c . Within the hollow waveguide, the product of the phase and group velocities is given as $v^{(\phi)}v_z^{(g)} = c^2$, thereby resulting in a group velocity $v_z^{(g)}$ along the waveguide less than c [86]. Although this relation for group and phase velocities is derived for the case of a hollow waveguide, the waveguide material properties are irrelevant. It is the transverse spatial confinement of the field that leads to a modification of the axial component of the wave vector, k_z . In general, for light of wavelength λ , the magnitude of the wave vector, $k_0 = \frac{2\pi}{\lambda}$, and its Cartesian components $\{k_x, k_y, k_z\}$ are related through

$$k_z^2 + k_x^2 + k_y^2 = k_0^2. \quad (6.1)$$

All optical modes of finite x, y spatial extent require non-zero k_x and k_y , which implies $k_z < k_0$, giving a corresponding modification of both the phase and group velocities of the light. In this sense, light beams with nonzero

Due to copyright reasons this figure is removed from the electronic copy.
Please see print version or figure 1 of ref [2].

Figure 6.1: Adding spatial structure to a light beam. (A) A Bessel beam can be created with an axicon, producing conical phase fronts of angle α . (B) A ray entering a confocal telescope at radius r will travel an additional distance proportional to $\cos^{-1}(\beta)$.

k_x and k_y are naturally dispersive, even in free space.

6.2 Group velocity and wave vectors

Here we derive an analytical relationship between the group velocity of a narrow bandwidth pulse in the z direction and the x and y components of the \mathbf{k} -vector \mathbf{k}_\perp . Recall from (1.48) and (1.49) that for a narrow bandwidth pulse the spread in frequencies is far smaller than the central optical frequency of the pulse so that the ratio of the two can be used as an expansion parameter. The result turns out to correspond to a geometric model. Let us first consider the more heuristic eikonal approach as it provides the gist of the more rigorous argument based on the wave model.

6.2.1 Eikonal model

Consider a plane wave at some angle α with respect to the direction in which propagation is of interest as in figure 6.1A. By the simple frequency-wavenumber relationship $ck_0 = \omega$ and (6.1)

$$\omega = c\sqrt{k_\perp^2 + k_z^2}. \quad (6.2)$$

This gives the phase and group velocities in the z -direction as

$$v_z^{(\phi)} = \frac{\omega}{k_z} = c \sqrt{1 + \frac{k_\perp^2}{k_z^2}} \quad (6.3)$$

$$\text{and } v_z^{(g)} = \frac{d\omega}{dk_z} = \frac{c}{\sqrt{1 + \frac{k_\perp^2}{k_z^2}}}. \quad (6.4)$$

When α is small (this is satisfied throughout the experiment) then $|k_\perp| \ll k_z \approx k_0$ in which case a binomial expansion of the group velocity (6.4) gives

$$v_z^{(g)} \approx c \left(1 - \frac{k_\perp^2}{2k_0^2} \right). \quad (6.5)$$

This foreshadows the result that when not a single plane wave but a multitude of them subtly non-colinear are considered the expectation of the transverse wave vector takes the place of the transverse wave vector in (6.5).

6.2.2 Wave model

The reciprocal of the group velocity along the propagation of direction, z , of a beam with phase profile $\phi(x, y, z; \omega)$ at a central frequency ω_0 is given by,

$$\frac{1}{v_z^{(g)}} = \left(\frac{\partial k_z}{\partial \omega} \right)_{\omega_0} = \frac{\partial^2 \phi(x, y, z; \omega_0)}{\partial z \partial \omega}. \quad (6.6)$$

To take an effective group velocity of an electromagnetic disturbance over a volume in which the velocity is changing, one needs to take a harmonic mean of the group velocity which consists of taking the reciprocal of the averaged reciprocal group velocity (6.6)

$$\bar{v}_z^{(g)} = \left(\frac{1}{z_2 - z_1} \int_{z_1}^{z_2} \frac{1}{v_z^{(g)}} dz \right)^{-1}. \quad (6.7)$$

However in averaging the reciprocal group velocity one must also weight it by the local intensity of the field $|\psi(x, y, z; \omega_0)|^2$. The reciprocal group velocity averaged over a volume bounded by the planes perpendicular to the direction of propagation at z_1 and z_2 consists of the expression

$$\frac{1}{z_2 - z_1} \int_{z_1}^{z_2} \iint_{x,y} |\psi(x, y, z; \omega_0)|^2 \frac{\partial^2 \phi(x, y, z; \omega_0)}{\partial z \partial \omega} dx dy dz \quad (6.8)$$

divided by the total weight

$$\iint_{x,y} |\psi(x, y, z; \omega_0)|^2 dx dy. \quad (6.9)$$

Let us first deal with the total weight. As the experiment takes place entirely in the paraxial regime the formal analogy between the paraxial wave equation (1.22) and the two dimensional Schrödinger equation (1.23) is exploited. Due to the formal correspondence we can borrow the ket representation in which the scalar beam profile $\psi(x, y, z; \omega)$ is represented by $|z, \omega\rangle$. Using this notationally compact way to deal with integrals over the transverse plane equation (6.9) becomes simply

$$\langle z, \omega_0 | z, \omega_0 \rangle. \quad (6.10)$$

For dealing with (6.8) one must bear in mind the relationship $\psi(x, y, z; \omega) = |\psi(x, y, z; \omega)| e^{i\phi(x, y, z; \omega)}$ so that the phase profile can be represented as $\text{Im} \{ \ln [\psi(x, y, z; \omega)] \}$. With this and extensive algebraic manipulation the expression

for the group velocity in the region bounded by planes (transverse to the propagation direction) at z_1 and z_2 boils down to

$$\bar{v}_z^{(g)} = (z_2 - z_1) / \text{Im} \left[\left(\frac{\partial}{\partial \omega} \langle z, \omega_0 | z, \omega \rangle \right)_{\omega_0} \right]_{z_1}^{z_2}. \quad (6.11)$$

This only gives positive phase speed (in other words, describes a wave travelling in the direction of the $+z$ axis) if the notation is chosen so that the kz term comes with a $+i$ coefficient in the exponent.

If we use this group velocity to calculate the time it takes a wave packet to cover the distance $z_2 - z_1$, we obtain

$$t = \text{Im} \left[\left(\frac{\partial}{\partial \omega} \langle z, \omega_0 | z, \omega \rangle \right)_{\omega_0} \right]_{z_1}^{z_2} = \left[\left(\frac{\partial \arg(\langle z, \omega_0 | z, \omega \rangle)}{\partial \omega} \right)_{\omega_0} \right]_{z_1}^{z_2}. \quad (6.12)$$

Thus the analytic expression for the delay of a non-planar wavefront, compared to a plane wave that travels at speed c (which we approximate with a collimated beam in the experiment) is,

$$\delta z = ct - (z_2 - z_1) = \left[\left(\frac{\partial \arg(\langle z, ck_0 | z, ck \rangle)}{\partial k} \right)_{k_0} - z \right]_{z_1}^{z_2} \quad (6.13)$$

where we have gone from dealing with frequencies to wave numbers using the relation $ck = \omega$ as applied to derivatives with respect to these variables. Our experiment is well within the paraxial approximation. Equation (6.13) can then be simplified even further in this case. The wave function $\psi(x, y, z; ck)$ evolves from z_1 to z_2 by the paraxial wave equation,

$$\frac{\partial \psi}{\partial z} = \frac{i}{2k} \nabla_{\perp}^2 \psi + ik\psi, \quad (6.14)$$

where $\nabla_{\perp}^2 = (\partial/\partial x)^2 + (\partial/\partial y)^2$. The paraxial wave equation takes this slightly unusual form as it is expressed in terms of the full function $\psi = ue^{ik_z z}$ whereas the paraxial wave equation in its usual form (1.22) governs u . Then

$$|z_2, ck\rangle = \exp\left(\frac{id}{2k} \nabla_{\perp}^2 + ikd\right) |z_1, ck\rangle, \quad (6.15)$$

where $d = z_2 - z_1$ is the distance across which propagation is being considered. With the above substitution

$$\left(\frac{\partial \langle z_2, ck_0 | z_2, ck \rangle}{\partial k} \right)_{k_0} = \langle z_1, ck_0 | \left(-\frac{id}{2k_0^2} \nabla_{\perp}^2 + id \right) |z_1, ck_0\rangle + \langle z_1, ck_0 | \frac{\partial}{\partial k} |z_1, ck_0\rangle \quad (6.16)$$

so that the delay (6.13) is given by

$$\begin{aligned} \left[\left(\frac{\partial \arg(\langle z_2, ck_0 | z_2, ck \rangle)}{\partial k} \right)_{k_0} - z \right]_{z_1}^{z_2} &= \text{Im} \frac{\langle z_1, ck_0 | \left(-\frac{id}{2k_0^2} \nabla_{\perp}^2 + id \right) |z_1, ck_0\rangle}{\langle z_1, ck_0 | z_1, ck_0 \rangle} - d \\ &= -\frac{d}{2k_0^2} \Re \frac{\langle z_1, ck_0 | \nabla_{\perp}^2 |z_1, ck_0\rangle}{\langle z_1, ck_0 | z_1, ck_0 \rangle} \end{aligned} \quad (6.17)$$

Note that ∇_{\perp}^2 can be written as $-\hat{\mathbf{k}}_{\perp}^2$, to denote a transverse wave vector, where

$$\hat{\mathbf{k}}_{\perp} = -i\nabla_{\perp}. \quad (6.18)$$

This implies that ∇_{\perp}^2 is a Hermitian operator and thus its expectation value is real. The final expression for δz is then

$$\delta z = \frac{d}{2k_0^2} \langle \hat{\mathbf{k}}_{\perp}^2 \rangle_{|z_1, ck_0\rangle}. \quad (6.19)$$

We can see that the effective group velocity

$$v_z^{(g)} = \frac{c}{1 + \frac{\langle \mathbf{k}_\perp^2 \rangle}{2k_0^2}} \approx c \left(1 - \frac{\langle \mathbf{k}_\perp^2 \rangle}{2k_0^2} \right) \quad (6.20)$$

is invariant under the free propagation and always smaller than c in agreement with the geometric ray optical model based on figure 6.1

6.3 Bessel beams

Extending upon the case of a mode within a hollow waveguide, an example of a structured beam is a Bessel beam 6.1, which is itself the description of a mode within a circular waveguide [82, 87]. In free space, Bessel beams can be created using an axicon (figure 6.1A), or its diffractive optical equivalent [88], that converts a plane wave into conical phase fronts characterised by a single radial component of the wave vector, $k_\perp = \sqrt{k_x^2 + k_y^2}$ [89–91]. This single value of the radial component gives a unique value of $k_z < k_0$ and hence uniquely defined phase and group velocities [92].

To avoid complications arising from the finite thickness of refractive optical elements, we use diffractive optics, idealised as having zero thickness. For a Bessel beam created with diffractive optics [88], characterised by k_\perp (with $k_\perp \ll k_0$), the axial component of the wave vector is given by $k_z = k_0 \sqrt{1 - \frac{k_\perp^2}{k_0^2}}$. The resulting phase velocity and group velocity along z are

$$v_z^{(\phi)} = c \left(1 - \frac{k_\perp^2}{2k_0^2} \right)^{-1} \quad (6.21)$$

$$\text{and } v_z^{(g)} = c \left(1 - \frac{k_\perp^2}{2k_0^2} \right) \quad (6.22)$$

This modification of the phase and group velocities of Bessel beams has been examined in the classical, many-photon regime. Subtle changes in velocity have been previously studied using Bessel beams in the microwave [93] and optical regimes [94–96].

We demonstrate the intrinsic and linear nature of this reduction in group velocity, by measuring the delay in the arrival time of single photons. Over a propagation distance of L , the reduction in the group velocity compared to the plane-wave case gives a delay of

$$\delta z_{Bessel} \approx L \frac{k_\perp^2}{2k_0^2} = \frac{L}{2} \alpha^2. \quad (6.23)$$

As an example, for an axicon designed to produce $\alpha = \frac{k_\perp}{k_0} = 4.5 \times 10^{-3}$ over a propagation distance of $1m$, we predict a delay of $\sim 30fs$, corresponding to a spatial delay of $10\mu m$.

To measure the arrival time of single photons with femtosecond precision we adopt a method relying upon a quantum effect, namely, the Hong-Ou-Mandel interference [15]. A parametric down-conversion source is used to produce photon pairs that are strongly correlated in their wavelengths and their generation time. One photon can then act as a reference, against which the arrival of the other photon can be compared figure 6.2. This second photon goes through a free-space propagation section, in which a first spatial light modulator can be programmed to act as a diffractive optical element implementing axicons or lenses. A second spatial light modulator then reverses the structuring introduced by the first. When the arrival times of the two photons incident on a beam splitter are matched to a precision better than their coherence time, both photons emerge from the same output port. Under this matched condition, the coincidence rate for detection at the two output ports of the beam splitter

Due to copyright reasons this figure is removed from the electronic copy.
Please see print version or figure 2 of ref [2].

Figure 6.2: Experimental apparatus. (A to D) A beta-barium borate (BBO) crystal is pumped by an ultraviolet (UV) laser to produce photon pairs via spontaneous parametric down conversion. Photon pairs are separated by a knife edge prism (KEP); a band-pass filter (BPF) sets the spectral profile of the down-converted light. Half-wave plates (HWP) are used to maximise the efficiency of the spatial light modulators (SLM) and match the polarisation of the polarisation-maintaining fibers (PMF). Signal and idler photons enter a fiber-coupled beam splitter (BS) [97], whose outputs are single mode fibers (SMF) connected to avalanche photodiodes (SPAD). The SPADs feed a coincidence counter.

falls to zero, which results in what is known as a Hong-Ou-Mandel dip. The position of the dip is recorded as a function of the spatial shaping of the photon propagating in free space.

6.3.1 Experimental results

Taking the Bessel beam as our first example, the transverse structuring can be turned on and off for each value of path delay. The corresponding position of the Hong-Ou-Mandel dip can then be directly compared between the two cases. Figure 6.3A shows the baseline-normalised coincidences for two different values of $\alpha = \frac{k_{\perp}}{k_0}$ (where we define the baseline as the coincidence count at path delay far from the dip position). In all cases the width of the Hong-Ou-Mandel dips is the same, set by the $10nm$ spectral bandwidth of the down-converted photons. The key result is that the Hong-Ou-Mandel dip associated with the Bessel beam is delayed with respect to the dip obtained for a collimated beam. We measure a delay of $2.7 \pm 0.8\mu m$ for the case of $\alpha_1 = 0.00225rad$ and $7.7 \pm 0.8\mu m$ for $\alpha_2 = 0.00450rad$. These measured values agree with theoretical predictions of $2.0\mu m$ and $8.1\mu m$ for α_1 and α_2 , respectively. The analytical form of this predicted delay (equation (6.23)) suggests a simple geometrical model, where the delay arises from the additional length of the diagonal ray, propagating at an angle α with respect to the optical axis. In figure 6.3B we compare the measured and predicted values for the delay, showing that equation (6.23) is valid over the range of angles that we tested for the Bessel beam.

6.4 Gaussian beam

Perhaps the most common form of spatial structuring of a light beam is focusing, which also leads to a modification of the axial component of the wave vector. We consider the propagation of light through a telescope comprising

Due to copyright reasons this figure is removed from the electronic copy.
Please see print version or figure 3 of ref [2].

Figure 6.3: Experimental results for a Bessel beam. (A) Measured Hong-Ou-Mandel dips for two values of α ($\alpha_1 = 0.00225$, red; $\alpha_2 = 0.00450$, blue) and the $\alpha = 0$ case (black), with corresponding best fits [15]. (B) Measured delays (open circles) and theoretical prediction from equation 1 (solid line), for different values of α . The delays are expressed with respect to the $\alpha = 0$ case, corresponding to an unstructured collimated beam.

Due to copyright reasons this figure is removed from the electronic copy.
Please see print version or figure 4 of ref [2].

Figure 6.4: Measured Hong-Ou-Mandel dips for collimated and focused Gaussian beams. (Left) Hong-Ou-Mandel dip comparison for collimated (black) and focused (red) Gaussian beam. Minima are marked by A and B. (Right) Hong-Ou-Mandel dip comparison for cases with an $r = 1.4mm$ centre stop (blue, corresponding to inset C), and an edge stop of the same radius (grey, corresponding to inset D). Minima are marked by C and D. The red dashed curve is shown as a reference.

two identical lenses separated by twice their focal length, f (i.e., a confocal telescope). Assuming a ray-optical model, a co-axial ray incident upon the first lens at radius r emerges from the second lens co-axially at the same radius but inverted about the optical axis (figure 6.1B). Comparing the on-axis separation of the lenses to this diagonal distance gives an additional distance travelled of $\delta z = L/\cos(\beta) - L \approx r^2/f$ where β is the angle between ray and optical axis. For a beam of Gaussian intensity distribution with $1/e^2$ radius w , the expectation value of r^2 is $\langle r^2 \rangle = w^2/2$. Therefore, the expected delay δz_{Gauss} for a Gaussian beam on transmission through a confocal telescope is

$$\delta z_{Gauss} = \frac{w^2}{2f} = \left(\frac{w}{f}\right)^2 \times \frac{f}{2} \quad (6.24)$$

where w is the waist of the input beam. The delay is a quadratic function of the quantity $\frac{w}{f}$, which can be considered as a measure of the beam divergence, defined by the numerical aperture of the system. The delay increases with increasing numerical aperture.

In the full theoretical model the quantity $\langle \hat{\mathbf{k}}_{\perp}^2 \rangle$, can be calculated as,

$$\langle \hat{\mathbf{k}}_{\perp}^2 \rangle = \frac{k_0}{z_R} \quad (6.25)$$

where $z_R = 2f^2/k_0w^2$ is the Rayleigh range. When inserted into the general expression for the delay (6.19) this leads to result (6.24) exactly as in our geometric calculation (figure 6.1B). As the delay increases with the square of the numerical aperture, the delay becomes progressively harder to detect at longer distances.

6.4.1 Experimental results

The delay arising from focusing is shown in figure 6.4. Trace A shows the position of the Hong-Ou-Mandel dip for the case of a collimated beam, and trace B shows its position for the case of $f = 0.40m$. We measure a delay of $7.7 \pm 0.4\mu m$ for the focused case. This is comparable to the predicted delay based on equation (6.24) which, for our beam of $w = 2.32 \pm 0.09mm$, is $6.7 \pm 0.6\mu m$.

6.4.2 Truncated beam

We further investigate the dependence of the delay upon the beam structure by introducing aperture restrictions to the beam, in the form of centre and edge stops (insets of figure 6.4). For the cases where we put sharp aperture restrictions (the centre and edge stops), a direct application of equation 6.19 leads to an infinite slowing down because of the diffraction on the boundaries which result to infinitely many orders. However, we can still give an estimate of the delays by recognising that

$$\delta z_{Gaussian} = \frac{w^2}{2f} = \left(\frac{w^2}{2}\right) \frac{1}{f} = \frac{\langle r^2 \rangle}{f}, \quad (6.26)$$

where $\langle r^2 \rangle$ is the expectation value of the square of the radius of the beam weighted by the Gaussian intensity distribution. For the cases where we insert centre and edge stops of radius 1.4 mm, we can normalise the resulting obstructed and truncated Gaussian distributions and calculate $\langle r^2 \rangle$. Doing so leads to delay estimate of $11.6\mu m$ and $2.1\mu m$ for the centre and edge stops, respectively, compared to the collimated case.

Results are shown in traces C and D in figure 6.4, together with the full-aperture focused beam case (red line, trace B). Trace C shows the dip with a centre stop of radius 1.4mm, as shown in inset C. A centre stop increases the expectation value of r^2 , thereby increasing the delay compared to the full-aperture case. We measure a dip position additionally delayed by $7.3 \pm 0.4\mu m$ compared to the full-aperture focused beam, giving a total delay of $15.0 \pm 0.6\mu m$. Next, we introduce an edge stop of the same radius, as shown in inset D. By restricting the aperture, the expectation value of r^2 is decreased, decreasing the delay with respect to the collimated case. Trace D shows the position of the Hong-Ou-Mandel dip, which is now reduced by $6.4 \pm 0.4\mu m$ with respect to the full-aperture case, resulting in a total delay compared to the collimated case of $1.3 \pm 0.6\mu m$.

6.5 Error analysis

It is important to consider three possible sources of systematic errors. First, the phase values of all the pixels of the spatial light modulator lie between 0 and 2π with an average value of $\approx \pi$. Regardless of what optical component is encoded on the spatial light modulators, the effective thickness of the liquid crystal, as averaged over the full aperture, remains the same. Consequently, the observed delay is not a result of the spatial light modulators themselves. Secondly, the width of the Hong-Ou-Mandel dip remains compatible with the interference filter used. Therefore the coherence time of the light is unchanged by the setting of the spatial light modulators and therefore the magnitude of the delays cannot be a result of spectral post-selection. Thirdly, one must ensure that the delays are not due to misalignment in the optical paths. In aligning the experiment, we used back-projection [98]. More importantly, the alignment for the cases where we have aperture restrictions remains the same (the coaxial apertures do not change the path of the beam). Hence, the delays we measure can only result from the transverse structure of the beam and indeed are consistent with our theoretical predictions.

Our measurement of group velocity is strictly a measurement of the difference in propagation speed between a reference photon and a spatially structured photon. No direct measurement of the speed of light is made. Within this manuscript, the velocity we measure is strictly the group velocity of the photons [99].

6.6 Conclusions

The speed of light in free space propagation is a fundamental quantity. It holds a pivotal role in the foundations of relativity and field theory, as well as in technological applications such as time-of-flight measurements. It has previously been experimentally established that single photons travel at the group velocity [99]. We have now shown that transverse structuring of the photon results in a decrease in the group velocity along the axis of propagation. We emphasise that in our full-aperture experiments, no pre- or post-selection is applied to the spatially structured photons, and that the group velocities are always compared over the same propagation distance, much as if they were in a race. The effect can be derived from a simple geometric argument, which is also supported by a rigorous calculation of the harmonic average of the group velocity. Beyond light, the effect observed will have applications to any wave theory, including sound waves. ‘

Chapter 7

Summary

Here we recapitulate only the chapters based on original contributions. In chapter 4 we examined the nested Mach-Zehnder interferometer in which each path is weakly marked by vibrating mirrors as reported in [1]. We found that the time dependent change introduced by the mirrors to the transverse spatial structure of the Gaussian mode propagating through the interferometer can be modelled as a perturbation. This means that two orthogonal modes of transverse spatial structure are required to describe light along each path of the interferometer corresponding to the unperturbed and perturbed parts of the light. Which-way information is contained only in the perturbed part of the light in the interferometer. The detection method used in the experiment that was analysed measured the side to side vibration of the beam by measuring the time dependent intensity imbalance across two halves of a quad-cell detector. In our two-mode model the unperturbed part of the light beam is ‘pushed’ from side to side by the perturbed part of the light beam. Hence the unperturbed part of the light beam, whilst carrying no which-way information, is essential for extracting which-way information from the perturbed part of the light beam. It is the understanding of this interplay between the two components of light in the interferometer that allowed us to interpret the experimental results reported in [1] without recourse to describing the light as having “been in the parts of the interferometer through which they could not pass”. We have also managed to find further interesting features exhibited by this interferometer by showing that for particular choices of distances at which the detector is placed not all of the which-way information is extractable from this particular measurement method.

In chapter 5 we examined Hong-Ou-Mandel interference for particle pairs possessing two degrees of freedom. We analysed the problem for boson pairs as well as fermion pairs. A notable feature of the Hong-Ou-Mandel effect is that for particle pairs possessing a single degree of freedom different behaviour is exhibited by bosons and fermions. Fermions never exit through the same port and bosons always exit through the same port. This is the result of the fundamentally different symmetry requirement that the two different types of particles satisfy under particle exchange being inherited by the state describing the spatial modes of the particle pair. We found that if the particle pairs have two degrees of freedom then the fundamental symmetry associated with the type of the particle pair can be distributed between the states describing the two different degrees of freedom so as to allow each type of particle pair to exhibit both behaviours. In fact the output statistics can be tuned to anything inbetween these two extremes. We presented a proposed scheme for achieving an experimental demonstration of this using photons obtained from spontaneous parametric downconversion with the additional degree of freedom being orbital angular momentum. This is a natural choice as photon pairs entangled in orbital angular momentum arise naturally in spontaneous parametric downconversion as discussed in chapter 2.

In chapter 6 we looked at how the transverse spatial structure of the mode that a pulse of light is propagating in effects the group velocity of that pulse of light. Transverse spatial structure in a light beam is created by having a

superposition of wave vectors pointing slightly off-axis with respect to the propagation direction. We found that the group velocity of a pulse excited in a particular mode of transverse spatial profile is a little slower than c and results from the off-axis component of the wave vectors hence linking the reduction of the group velocity to the spreading of the beam. The group velocity is given by the simple geometric relationship

$$v_z^{(g)} \approx c \left(1 - \frac{\langle \hat{\mathbf{k}}_{\perp}^2 \rangle}{2k_0^2} \right) \quad (7.1)$$

where k_0 is the magnitude of the wave vector of the quasi-monochromatic pulse of light and $\langle \hat{\mathbf{k}}_{\perp}^2 \rangle$ is the expectation value of the square of the transverse wave vector. In a sense light with transverse spatial structure does not take the shortest possible path as it travels sideways a little with respect to its direction of propagation but it does so in all transverse directions in superposition resulting in a spreading beam rather than a beam tilted with respect to the face of the transverse planes it is travelling between. In the experiment [2] this was measured using Hong-Ou-Mandel interference in which one of the photons received spatial structuring in addition to its Gaussian profile. This included focussing, a Bessel profile and truncation of the beam in the transverse plane. The extra path length needed for the unaltered photon to match the delay of the spatially structured photon was on the order of a several microns across a distance on the order of a meter.

Thanks for reading!

Bibliography

- [1] A. Danan, D. Farfurnik, S. Bar-Ad, and L. Vaidman. Asking photons where they have been. *Physical Review Letters*, 111:240402, Dec 2013.
- [2] Daniel Giovannini, Jacqueline Romero, Václav Potoček, Gergely Ferenczi, Fiona Speirits, Stephen M. Barnett, Daniele Faccio, and Miles J. Padgett. Spatially structured photons that travel in free space slower than the speed of light. *Science*, 347(6224):857–860, 2015.
- [3] Rodney Loudon. *The Quantum Theory of Light 3rd ed.* Oxford University Press, Oxford, third edition, 2000.
- [4] Gilbert Gynsberg, Alain Aspect, and Claude Fabre. *Introduction to Quantum Optics.* Cambridge University Press, 2010.
- [5] Anthony E. Siegman. *Lasers.* University Science Books, Sausalito, CA, 1986.
- [6] J. B. Götte and Barnett S. M. Light beams carrying orbital angular momentum. In David L. Andrews and Mohamed Babiker, editors, *The Angular Momentum of Light.* Cambridge University Press, 2013.
- [7] K.J. Blow, R. Loudon, S. J. D. Phoenix, and T. J. Shepherd. Continuum fields in quantum optics. *Physical Review A*, 42(7):4102, 1990.
- [8] Rodney Loudon. Fermion and boson beam-splitter statistics. *Physical Review A*, 58, 1998.
- [9] A. G. Klein and S. A. Werner. Neutron optics. *Reports on Progress in Physics*, 46:259–335, 1983.
- [10] Daniel M. Greenberger. The neutron interferometer as a device for illustrating the strange behavior of quantum systems. *Reviews of Modern Physics*, 55(4):875–892, 1983.
- [11] Richard P. Feynman, Robert B. Leighton, and Matthew Sands. *The Feynman Lectures On Physics*, volume 3. Addison-Wesley Publishing Company, Reading, Massachusetts, 1965.
- [12] John Jeffers. Interference and the lossless lossy beam splitter. *Journal of Modern Optics*, 47, 2000.
- [13] W. Pauli. On the connection between spin and statistics. *Progress of Theoretical Physics*, 5(4), 1950.
- [14] R. C. Liu, B. Odom, Y. Yamamoto, and S. Tarucha. Quantum interference in electron collision. *Nature*, 391, 1998.
- [15] C.K. Hong, Zhe-Yu Ou, and Leonard Mandel. Measurement of subpicosecond time intervals between two photons by interference. *Physical Review Letters*, 59, 1987.
- [16] P. A. M. Dirac. *The Principles of Quantum Mechanics.* Oxford University Press, Oxford, fourth edition, 1958.
- [17] Leonard Mandel and Emil Wolf. *Optical coherence and quantum optics.* Cambridge University Press, 1995.

- [18] Eugene Hecht and Alfred Zajac. *Optics*. Addison-Wesley, 1974.
- [19] Václav Potoček and Gergely Ferenczi. Which-way information in a nested Mach-Zehnder interferometer. *Physical Review A*, 92:023829, Aug 2015.
- [20] L. Vaidman. Past of a quantum particle. *Physical Review A*, 87:052104, May 2013.
- [21] Zheng-Hong Li, M. Al-Amri, and M. Suhail Zubairy. Comment on “past of a quantum particle”. *Physical Review A*, 88:046102, Oct 2013.
- [22] L. Vaidman. Reply to “comment on ‘past of a quantum particle’”. *Physical Review A*, 88:046103, Oct 2013.
- [23] Hatim Salih. Comment on "asking photons where they have been". arXiv:1401.4888v2 2014.
- [24] Pablo L. Saldanha. Interpreting a nested Mach-Zehnder interferometer with classical optics. *Physical Review A*, 89:033825, Mar 2014.
- [25] A. Danan, D. Farfurnik, S. Bar-Ad, and L. Vaidman. Reply to "comment on ‘asking photons where have they been’". arXiv:1401.5420v2 2014.
- [26] Jie-Hui Huang, Li-Yun Hu, Xue-Xiang Xu, Cun-Jin Liu, Qin Guo, Hao-Liang Zhang, and Shi-Yao Zhu. Comments on "asking photons where they have been". arXiv:1402.4581 2014.
- [27] Bengt E. Y. Svensson. Comments to asking photons where they have been (a danan et al, phys. rev. lett. 111, 240402 (2013)). arXiv:1402.4315v2 2014.
- [28] Marcin Wieśniak. Criticism of "asking photons where they have been". arXiv:1407.1739 2014.
- [29] Karol Bartkiewicz, Antonín Černoč, Dalibor Javůrek, Karel Lemr, Jan Soubusta, and Jiří Svozilík. One-state vector formalism for the evolution of a quantum state through nested Mach-Zehnder interferometers. *Physical Review A*, 91:012103, Jan 2015.
- [30] Yakir Aharonov, Peter G. Bergmann, and Joel L. Lebowitz. Time symmetry in the quantum process of measurement. *Physical Review*, 134:B1410–B1416, Jun 1964.
- [31] Miguel A. Bandres and Manuel Guizar-Sicairos. Paraxial group. *Optics Letters*, 34:13–15, 2009.
- [32] First Sensor. *Quad Sum and Difference Amplifier*, June 2012.
- [33] Luciana Pedrosa Salles and Davies William de Lima Monteiro. Designing the response of an optical quad-cell as position-sensitive detector. *IEEE Sensors Journal*, 10(2):286–293, 2010.
- [34] Les Allen, M. W. Beijersbergen, Spreeuw R. J. C., and Woerdman J. P. Orbital angular momentum of light and the transformation of Laguerre-Gaussian laser modes. *Physical Review A*, 45(11):8185–8189, 1992.
- [35] S. J. van Enk and G. Nienhuis. Spin and orbital angular momentum of photons. *Europhysics Letters*, 25(7):497–501, 1994.
- [36] S. J. van Enk and G. Nienhuis. Commutation rules and eigenvalues of spin and orbital angular momentum of radiation fields. *Journal of Modern Optics*, 41(5):963–977, 1994.
- [37] Robert P. Cameron, Fiona C Speirits, Claire R Gilson, Allen L., and Barnett Stephen M. The azimuthal component of poynting’s vector and the angular momentum of light. *Journal of Optics*, 17(12):125610, 2015.

- [38] Alison M. Yao and Miles Padgett. Orbital angular momentum: origins, behaviour and applications. *Advances in Optics and Photonics*, 3(2), 2011.
- [39] Les Allen and Padgett Miles. The orbital angular momentum of light: An introduction. In Juan P. Torres and Torner Lluís, editors, *Twisted Photons: Applications of Light with Orbital Angular Momentum*. Wiley-VHC, 2011.
- [40] G. N. Watson. *A Treatise of the Theory of Bessel Functions*. Cambridge University Press, 3rd edition, 1995.
- [41] H. He, M. E. Friese, N. R. Heckenberg, and H. Rubinsztein-Dunlop. Direct observation of angular momentum to absorptive particles from a laser beam with a phase singularity. *Physical Review Letters*, 75(5):826–829, 1995.
- [42] M. E. Friese, J. Enger, Rubinsztein-Dunlop, and N. R. Heckenberg. Optical angular-momentum transfer to trapped absorbing particles. *Physical Review A*, 54:1593–1596, 1996.
- [43] N. B. Simpson, K. Dholakia, L. Allen, and M. J. Padgett. Mechanical equivalence of spin and orbital angular momentum of light: an optical spanner. *Optics Express*, 22(1):52–54, 1997.
- [44] Anna T. O’Neil and Padgett Niles J. Three-dimensional optical confinement of micron-sized metal particles and the decoupling of the spin and orbital angular momentum within an optical spanner. *Optics Communications*, 185:139–142, 2000.
- [45] Stephen M. Barnett. *Quantum Information*. Oxford University Press, 2009.
- [46] Erwin Schrödinger. Discussion of probability relations between separated systems. *Mathematical Proceedings of the Cambridge Philosophical Society*, 31(4):555–563, 1935.
- [47] John S. Bell. On the Einstein Podolsky Rosen paradox. *Physics*, 1:195–200, 1964.
- [48] John F. Clauser, Horne Michael A., Abner Shimony, and Richard A. Holt. Proposed experiment to test local hidden-variable theories. *Physical Review Letters*, 23(15):880–884, 1969.
- [49] Stuart J. Freedman and John F. Clauser. Experimental test of local hidden-variable theories. *Physical Review Letters*, 28(14):938–941, 1972.
- [50] Alain Aspect, Jean Dalibard, and Gérard Roger. Experimental test of Bell’s inequalities using time-varying analyzers. *Physical Review Letters*, 49(25):1804–1807, 1982.
- [51] B. Hensen, H. Bernien, A. E. Dréau, A. Reiserer, N. Kalb, M. S. Blok, J. Ruitenberg, R. F. L. Vermeulen, R. N. Schouten, C. Abellán, W. Amaya, V. Pruneri, M. W. Mitchell, M. Markham, D. J. Twitchen, D. Elkouss, S. Wehner, T. H. Taminiou, and R. Hanson. Loophole-free Bell inequality violation using electron spins separated by 1.3 kilometres. *Nature*, 526:682–686, 2015.
- [52] Andrew Whitaker. *Einstein, Bohr and the Quantum Dilemma*. Cambridge University Press, 2nd edition, 2006.
- [53] C. G. Ghirardi, A. Rimini, and T. Weber. A general argument against superluminal transmission through the quantum mechanical measurement process. *Lettere al Nuovo Cimento*, 27(10):293–298, 1980.
- [54] Andreas Winter. The usefulness of uselessness. *Nature*, 446:1053–1054, 2010.

- [55] Charles H. Bennett, Gilles Brassard, Claude Crépeau, Richard Jozsa, Asher Peres, and William K. Wootters. Teleporting an unknown quantum state via dual classical Einstein-Podolsky-Rosen channels. *Physical Review Letters*, 70(13):1895–1899, 1993.
- [56] Dik Bouwmeester, Jian-Wei Pan, Klaus Mattle, Manfred Eibl, Harald Weinfurter, and Anton Zeilinger. Experimental quantum teleportation. *Nature*, 390, 1997.
- [57] Robert W. Boyd. *Nonlinear Optics*. Academic Press, 3rd edition, 2008.
- [58] B. E. Saleh and M. C. Teich. *Fundamentals of Photonics*. John Wiley & Sons, 2nd edition, 2007.
- [59] Paul G. Kwiat, Klaus Mattle, Harald Weinfurter, and Anton Zeilinder. New high-intensity source of polarisation-entangled photon pairs. *Physical Review Letters*, 75(24):4337–4342, 1995.
- [60] C. K. Hong and L. Mandel. Theory of parametric frequency down conversion of light. *Physical Review A*, 31, 1985.
- [61] Geraldo A. Barbosa. Wave function for spontaneous parametric down-conversion with orbital angular momentum. *Physical Review A*, 80, 2009.
- [62] Bart-Jan Pors. *Entangling light in high dimensions*. PhD thesis, University of Leiden, 2011.
- [63] Alison M. Yao. Angular momentum decomposition of entangled photons with an arbitrary pump. *New Journal of Physics*, 13, 2011.
- [64] Filippo M. Miatto, Alison M. Yao, and Stephen M. Barnett. Full characterization of the quantum spiral bandwidth of entangled biphotons. *Physical Review A*, 83, 2011.
- [65] Sonja Franke-Arnold, Stephen M. Barnett, Miles J. Padgett, and L. Allen. Two-photon entanglement of orbital angular momentum states. *Physical Review A*, 65, 2002.
- [66] L. Allen, Stephen M. Barnett, and Miles J. Padgett. *Optical Angular Momentum*. Institute of Physics Publishing, Bristol, 2003.
- [67] Alois Mair, Alipasha Vaziri, Gregor Weihs, and Anton Zeilinger. Entanglement of the orbital angular momentum states of photons. *Nature*, 412, 2001.
- [68] S. P. Walborn, A. N. de Oliveira, R. S. Thebaldi, and C. H. Monken. Entanglement and conservation of orbital angular momentum in spontaneous parametric down-conversion. *Physical Review A*, 69:023811, 2004.
- [69] Jonathan Leach, Barry Jack, Jacqui Romero, Anand K. Jha, Alison M. Yao, Sonja Franke-Arnold, David G. Ireland, Robert W. Boyd, Stephen M. Barnett, and Miles J. Padgett. Quantum correlations in optical angle-orbital angular momentum variables. *Science*, 329:662–665, 2010.
- [70] J. Leach, B. Jack, J. Romero, M. Ritsch-Marte, R. W. Boyd, A. K. Jha, S. M. Barnett, S. Franke-Arnold, and M. J. Padgett. Violation of a bell inequality in two-dimensional orbital angular momentum state-spaces. *Optics Express*, 17:8287–8293, 2009.
- [71] Alipasha Vaziri, Gregor Weihs, and Anton Zeilinger. Experimental two-photon, three-dimensional entanglement for quantum communication. *Physical Review Letters*, 98(24):240401, 2002.
- [72] B. C. Hiesmayr, M. J. A. de Dood, and W. Löffler. Observation of four-photon orbital angular momentum entanglement. *Physical Review Letters*, 116:073601.

- [73] Gergely Ferenczi, Václav Potoček, and Stephen M Barnett. Two-particle multi-mode interference. *Journal of Optics*, 16(10):105710, 2014.
- [74] Wolfgang Pauli. *General Principles of Quantum Mechanics*. Springer-Verlag, Berlin, 1980.
- [75] Malte C. Tichy. Interference of identical particles from entanglement to boson-sampling. *Journal of Physics B*, 47, 2014.
- [76] Alberto Peruzzo, Anthony Laing, Alberto Politi, Terry Rudolph, and Jeremy L. O’Brien. Multimode quantum interference of photons in multiport integrated devices. *Nature Communications*, 2, 2010.
- [77] Ebrahim Karimi, Daniel Giovannini, Eliot Bolduc, Nicolas Bent, Filippo M. Miatto, Miles J. Padgett, and Robert W. Boyd. Exploring the quantum nature of the radial degree of freedom of a photon via Hong-Ou-Mandel interference. *Physical Review A*, 89, 2014.
- [78] S. P. Walborn, A. N. de Oliveira, S. Pádua, and C. H. Monken. Multimode Hong-Ou-Mandel interference. *Physical Review Letters*, 90, 2003.
- [79] Anton Zeilinger. Quantum entanglement: A fundamental concept finding its applications. *Physica Scripta*, T76, 1997.
- [80] Jonathan Leach, Miles J. Padgett, Stephen M. Barnett, Sonja Franke-Arnold, and Johannes Courtial. Measuring the orbital angular momentum of a single photon. *Physical Review Letters*, 88, 2002.
- [81] Zhang Yingwen, Filippus S. Roux, Thomas Konrad, Megan Agnew, Jonathan Leach, and Forbes Andrew. High-dimensional Hong-Ou-Mandel interference with orbital angular momentum. *preprint*.
- [82] Amnon Yariv. *Quantum Electronics*. John Wiley & Sons, 3rd edition, 1988.
- [83] Simin Feng and Herbert G. Winful. Physical origin of the gouy phase shift. *Optics Letters*, 26:485–487, 2001.
- [84] Robert W. Boyd and Daniel J. Gauthier. Controlling the velocity of light pulses. *Science*, 326(5956):1074–1077, 2009.
- [85] J. E. Vornehm Jr. and R. W. Boyd. Slow and fast light. In M. A. Noginov, G. Dewar, M. W. McCall, and N. I. Zheludev, editors, *Tutorials in Complex Photonic Media*. SPIE, 2009.
- [86] I. S. Grant and W. R. Phillips. *Electromagnetism*. John Wiley & Sons, 2nd edition, 1980.
- [87] E.R. Nagelberg and J. Shefer. Mode conversion in circular waveguides. *Bell System Technical Journal*, 44:1321–1338, 1965.
- [88] S. Klewitz, S. Sogomonian, M. Herminghaus Woerner, and S. Stimulated raman scattering of femtosecond bessel pulses. *Optics Communications*, 154:186–190, 1998.
- [89] R. M. Herman and T. A. Wiggins. Production and uses of diffractionless beams. *Journal of the Optical Society of America A*, 8:932–942, 1991.
- [90] John H. McLeod. The axicon: A new type of optical element. *Journal of the Optical Society of America*, 44:592–592, 1954.
- [91] Antti Vasara, Jari Turunen, and Ari T. Friberg. Realization of general nondiffracting beams with computer-generated holograms. *Journal of the Optical Society of America A*, 6:1748–1754, 1989.

- [92] José Tadeu Lunardi. Remarks on bessel beams, signals and superluminality. *Physics Letters A*, 291:66–72, 2001.
- [93] D. Mugnai, A. Ranfagni, and R. Ruggeri. Observation of superluminal behaviors in wave propagation. *Physical Review Letters*, 84:4830–4833, May 2000.
- [94] K. B. Kuntz, B. Braverman, S. H. Youn, M. Lobino, E. M. Pessina, and A. I. Lvovsky. Spatial and temporal characterization of a bessel beam produced using a conical mirror. *Physical Review A*, 79:043802, Apr 2009.
- [95] I. Alexeev, K. Y. Kim, and H. M. Milchberg. Measurement of the superluminal group velocity of an ultrashort bessel beam pulse. *Physical Review Letters*, 88:073901, Jan 2002.
- [96] Peter W. Milonni. Controlling the speed of light pulses. *Journal of Physics B*, 35:R31–R56, 2002.
- [97] Rainer Kaltenbaek, Bibiane Blauensteiner, Marek Żukowski, Markus Aspelmeyer, and Anton Zeilinger. Experimental interference of independent photons. *Physical Review Letters*, 96:240502, Jun 2006.
- [98] Melanie McLaren, Jacqueline Romero, Miles J. Padgett, Filippus S. Roux, and Andrew Forbes. Two-photon optics of bessel-gaussian modes. *Physical Review A*, 88:033818, Sep 2013.
- [99] A. M. Steinberg, P. G. Kwiat, and R. Y. Chiao. Dispersion cancellation in a measurement of the single-photon propagation velocity in glass. *Physical Review Letters*, 68:2421–2424, Apr 1992.